DISSERTATION

DEVELOPMENT OF A NOVEL BLOCK COPOLYMER HYDROGEL FOR MENISCAL REPLACEMENT

Submitted by

Kristine Marie Fischenich

Graduate Degree Program in Bioengineering

In partial fulfillment of the requirements

For the Degree of Doctor of Philosophy

Colorado State University

Fort Collins, Colorado

Spring 2018

Doctoral Committee:

Advisor: Tammy Haut Donahue
Co-Advisor: Travis Bailey

Jeremiah Easley
Ross Palmer
Laurie Goodrich

ABSTRACT

DEVELOPMENT OF A NOVEL BLOCK COPOLYMER HYDROGEL FOR MENISCAL REPLACEMENT

Menisci are C-shaped fibrocartilaginous tissues responsible for distributing tibial-femoral contact pressure and are crucial for maintaining healthy joints and preventing osteoarthritis. Meniscal damage can be caused by age-related degradation, obesity, overuse from athletic activities, and trauma. Due to their primarily avascular nature, once damaged there is limited healing capacity and surgical intervention is often required. Limited technologies exist to replace damaged menisci, and standard treatment is to leave asymptomatic damage alone or perform partial meniscectomies, however, these treatment options lead to increased risk of OA. Attempts at tissue engineered meniscal scaffolds, and replacements have had mixed results due to design limitations and inability to recapitulate native tissue's material properties, shape, and pressure distribution.

This project strives to create an artificial meniscus from a polystyrene-polyethylene oxide diblock copolymer. It is hypothesized that this hydrogel can be tuned to have material properties similar to those of the native meniscus. Furthermore, it is hypothesized this hydrogel can be molded into a 3D meniscal construct, implanted into the joint, and have similar pressure distribution properties as the native meniscus. Thus, the aims of this project are:

1) Mechanical comparison of a polystyrene-polyethylene oxide diblock copolymer TPE hydrogel to native meniscal tissue.

2) Develop a 3D meniscal construct which can be implanted into an ovine model and assess load distribution properties including contact area, mean pressure, and max pressure in both the medial and lateral hemijoints.

If the goals of this project are met, there would exist a 3D TPE hydrogel construct that mimics the mechanical and functional properties of the native human meniscus. This meniscal replacement could provide a revolutionary addition to the field of osteoarthritis and meniscal injury.

ACKNOWLEDGMENTS

I would like to acknowledge my advisor, Dr. Tammy Haut Donahue, who has been influential in the completion of this work. I would also like to thank my co-advisor Dr. Travis Bailey. This project has been a marriage between two vastly different disciplines and without Dr. Bailey's and Dr. Haut Donahue's support, this work could not have come to fruition.

Additionally, I would like to thank all my various lab mates and committee members who have supported me directly with this work or otherwise. Lastly, I want to acknowledge both my parents Lisa and Craig Fischenich who have provided so much encouragement and love. Completing my doctorate has been a lifelong dream and this accomplishment is as much theirs as it is mine.

This work was supported by the National Institute of Arthritis and Musculoskeletal and Skin Diseases and the National Institutes of Health [R21 AR069826].

DEDICATION

John, you are the love of my life, and nothing makes me happier than finishing this with you by my side.

TABLE OF CONTENTS

CHAPTER 1:
INTRODUCTION

1.1 The Knee

The knee is a complex six degree of freedom joint and is usually divided into the patella femoral joint and the tibiofemoral joint. The patellofemoral joint consists of a sesamoid bone, the patella, which glides along the femoral groove to protect the articular surfaces throughout knee flexion[1]. The patella also increases the leverage that the patella tendon can exert on the femur. The tibiofemoral joint is composed of four major ligaments and two menisci which collectively work to stabilize the knee (Figure 1.1). The anterior cruciate ligament (ACL) and posterior cruciate ligament (PCL) are located in the center of the joint in what is known as the intercondylar fossa. The ACL primarily restricts anterior translation of the tibia with respect to the femur[2], while the PCL prevents posterior translation of the tibia[3]. The ACL extends from the anteromedial aspect of the tibia and inserts into the lateral femoral condyle toward the posterolateral aspect. The PCL inserts into the tibia in the posterior region and extends towards the anteromedial aspect inserting behind the ACL on the lateral surface of the medial femoral condyle. The medial and lateral collateral ligaments (MCL and LCL) are often described as longer broader bands of collagen fibers that connect the femur to the tibia and help to prevent excessive valgus and varus rotation respectively. The MCL extends from the medial femoral epicondyle to the anteromedial aspect of the tibia below the joint line[4]. The LCL attaches to the femur's lateral epicondyle in a more fanlike manner with the other attachment location being the lateral aspect of the fibular head[5]. The entirety of the knee is then also encased in a synovium membrane which helps to retain synovial fluid that acts as joint nourishment and lubricant[6,7].

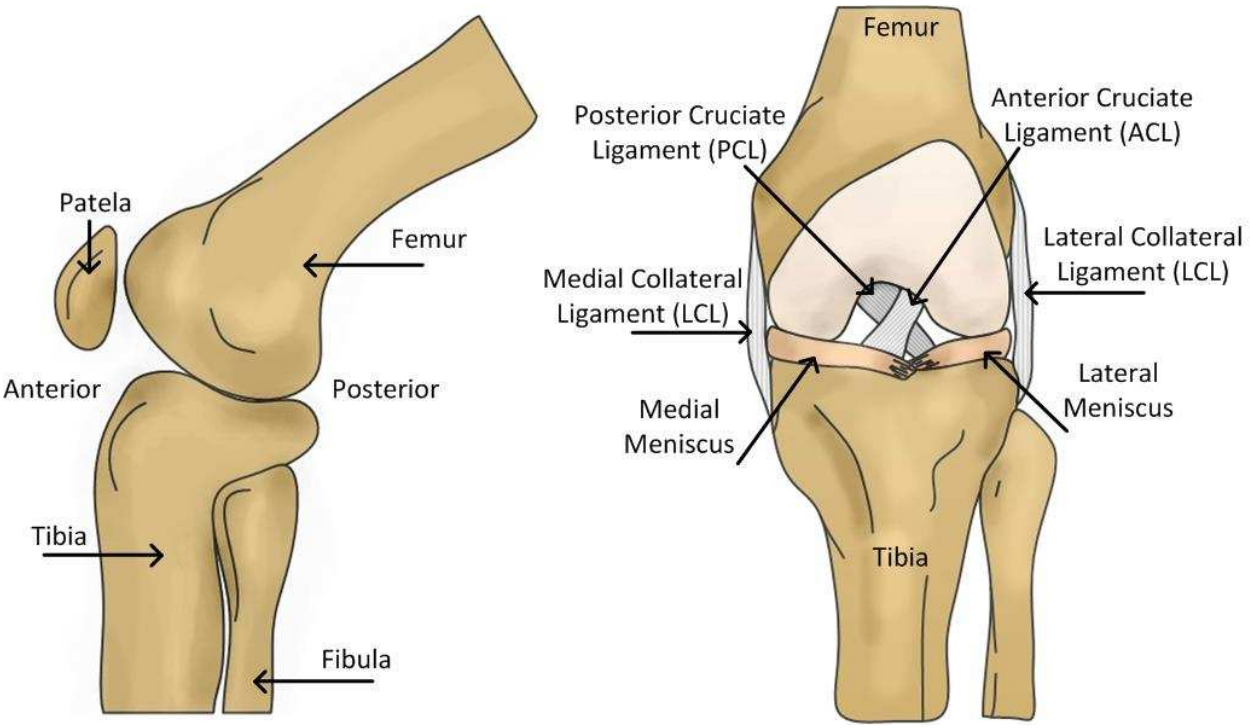

Figure 1-1: Knee anatomy

1.2 The Meniscus

Menisci are crescent-shaped biphasic tissues which lie between the femoral condyles and the tibial plateau (Figure 1.1). They are wedge-shaped in profile and attach to the joint capsule at the peripheral rim. When taking a superior view of the tibial plateau the menisci only partially cover the underlying articular cartilage (Figure 1.2). The primary function of the meniscus is to increase congruency and distribute load[8]. Previous studies have found that healthy menisci cover between 50-70% of the total contact area within the joint[9–11] and bear 45-75% of the load experienced in the knee joint[9,12]. Secondarily, the menisci aid in joint lubrication and protection of the underlying articular cartilage of the knee[9,13].

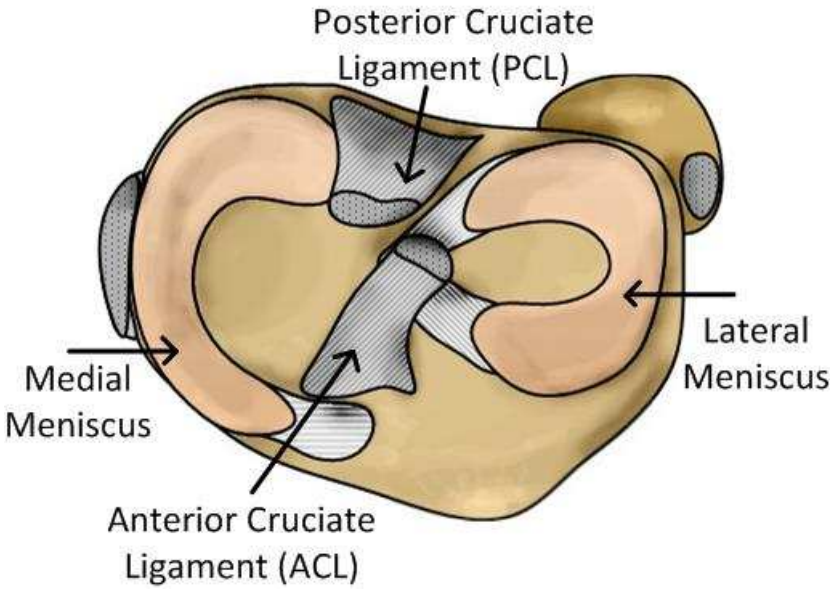

Figure 1-2: Superior view of the left knee

Normal human menisci are composed of approximately 72% water with the remaining constituents include collagen, proteoglycans, elastin, and other glycoproteins[14]. The meniscal matrix is primarily type I collagen fibrils with only small amounts of the other collagens (types II, III, V, and VI)[14]. The orientation of these fibers is highly variable on location and function (Figure 1-3). The primary orientation is in the circumferential direction parallel to the tibial plateau. This organization optimizes the high strength properties of collagen in tension by allowing for the bulk of the tissue to convert compressive loading to circumferential hoop stresses[15]. There are also radial tie fibers in the mid-zone of the meniscus which function to help hold the circumferential fibers together and prevent splitting. Lastly, the fibers making up the surface of the tissue tend to have a random composition which lends itself to reducing tear propagation and load distributing properties. In addition to collagen, meniscal tissue contains proteoglycans and glycoproteins which help to retain the interstitial fluid within the tissue, contributing to its biphasic nature[16]. One of the most common proteoglycans in meniscal tissue is glycosaminoglycan (GAG) which are negatively charged and help to retain the positively

charged interstitial fluid[17]. At birth, the meniscus is fully vascularized[18], but as the tissue develops there is a progressive loss of vascularization and in an adult only the outer one third, or the most peripheral region, remains vascularized[19] (Figure 1-3).

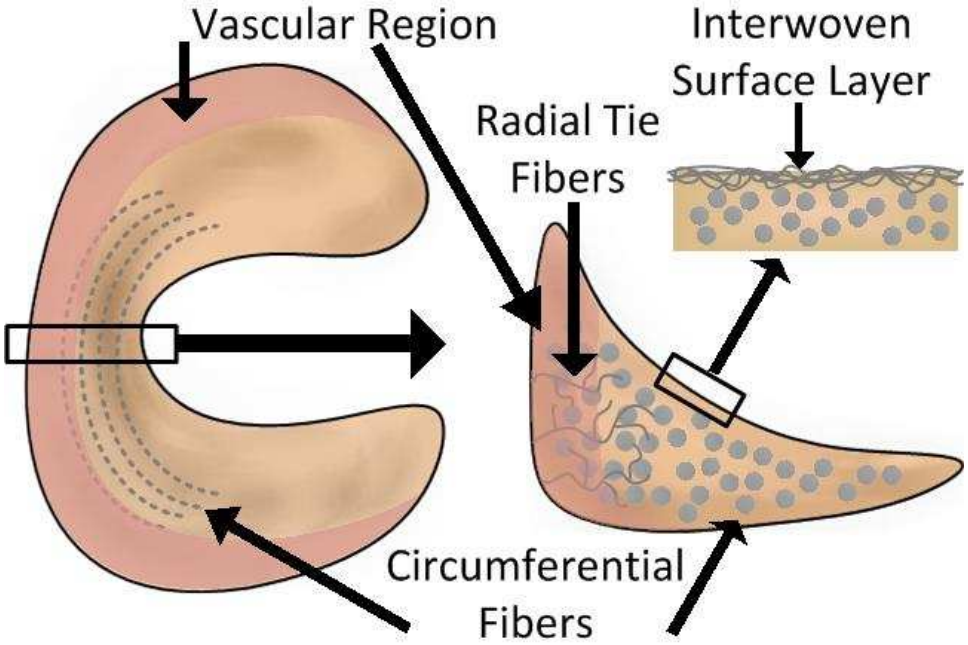

Figure 1-3: Meniscus with collagen fiber orientation and vascularization shaded in red

The primary anchoring means of the meniscus are the anterior and posterior insertions, or entheses, into the underlying tibial plateau. The circumferential collagen fibers that make up the fibrocartilaginous main body of the meniscus continue from the horns transitioning into a more ligamentous region then quickly to an uncalcified fibrocartilaginous region, to a calcified fibrocartilaginous region, and eventually subchondral bone[20]. This unique gradated structure allows for the soft tissue of the meniscus to insert into the hard underlying bone and reduces large stress concentrations that would otherwise be present[21]. The anterior horn and posterior horn of the medial meniscus are dissimilar in size with the anterior horn being slightly larger and more fan shaped[22]. The horns of the lateral meniscus are more similar in size. The medial

meniscus is less mobile than the lateral as the outer rim of the medial meniscus is connected to the joint capsule.

1.3 Meniscal Damage and Osteoarthritis

It is not well understood how meniscal tears initiate under various loading conditions, but it is widely believed that meniscal tears will progress in severity over time[23]. Meniscal tears can occur in both the medial and lateral meniscus, but medial meniscus tears seem to progress more rapidly than lateral tears[23]. Tears occur in three primary directions; longitudinally (circumferentially), horizontally, and radially and combinations of these tear orientations leads to bucket handle, flap, and complex tears. Meniscal damage as a result of trauma has been most frequently reported as longitudinal tears while horizontal and complex tears being more frequently associated with degenerative meniscal damage[24,25].

Once thought to be vestigial structures prior to the 1980's removal of the meniscus, or a meniscectomy, was a common treatment for damaged tissue. Since then, the important role menisci play in knee health and stabilization has been realized with studies concluding the removal, even in part, of the meniscus, leads to long-term degenerative effects including osteoarthritis (OA)[26–28]. Though traditionally thought of as simply loss of articular cartilage, osteoarthritis (OA) is now considered a "whole organ" disease where damage to one tissue influences other structures[29–31]. When the menisci become damaged and are unable to adequately distribute load, the articular cartilage can rapidly degrade[32,33]. Meniscal damage can be caused by age-related degradation[34,35], obesity[36,37], overuse from athletic activities and trauma[38,39], or worsen due to tear propagation[34,40]. Once damaged, the meniscus has little healing ability due to

its primarily avascular nature[14]. It is crucial for healthy joints to have intact and functional menisci to help to prevent osteoarthritis (OA)[27,41].

1.4 Meniscal Repairs and Replacements

There are limited clinical technologies to replace or repair damaged menisci, and standard treatment is to leave asymptomatic damage alone[42]. Treatment methods vary depending on location and severity of damage. When damage occurs in the vascular region of the tissue some success has been reported using suture repair techniques[43–46]. Although, failure and re-tear rates have been reported in 11% of cases at less than a 5 year follow-up[47]. In addition to suture repair techniques, various orthobiologics have been investigated including platelet-rich plasma, growth factors, stem cells, fibrin clot, and gene therapy. The primary strategy for treatment of tears in the avascular zone is a partial meniscectomy to limit tear propagation, however, partial meniscectomies have been shown to lead to an increased risk of OA[48–50].

Meniscal allograft, or meniscal transplantation, research has been investigated, but with mixed results and limited long-term data[51]. Originally, grafts were preserved by freezing methods, but it was shown that these freezing techniques led to a reduced number of fibrochondrocytes and lower cell activity resulting in 25-36% of patients reporting tears at an average follow-up time of fewer than six years[52,53]. Limited data exists on the importance of graft selection, sizing, and effectiveness of meniscal allografts in preventing osteoarthritis, leaving it a procedure that few surgeons perform[54,55].

Alternatives to meniscectomies and allografts include scaffolds and permanent replacements. Meniscal scaffolds have been utilized in attempts to tissue engineer new menisci. The scaffolds act as a template for cells to proliferate and lay down new extracellular matrix. As more and

more matrix material is produced the scaffold will degrade leaving behind a completely repaired or replaced meniscus. Common materials used for scaffolds include tissue-derived materials (acellular porcine meniscal tissue, decellularized tissue, etc.)[56–58], extracellular matrix components (collagen, proteoglycans, and elastin)[59–61], synthetic polymers (polyurethane, polyglycolic acid, polylactic-co-glycolic acid and polycaprolactone)[62–64], and hydrogels[65–67]. However, hydrophobicity, immune response, and inferior mechanical properties limit the application of these products. Permanent replacements are intended to not degrade with time and serve as alternatives to native tissue *in vivo*. The most popular material choice for permanent replacements is polycarbonate urethane (PCU)[68,69], with some preliminary investigations into the use of polyvinyl alcohol hydrogel [70,71].

Clinically there are two scaffolds and one permanent replacement on the market; the Menaflex CMI from ReGen Biologics, Inc. (ReGen Biologics, Inc., Cary, NC, USA), the Actifit® scaffold from Orteq Ltd. (Orteq Ltd., London, UK), and the NUsurface® Meniscus Implant from Active Implants (Active Implants, LLC., Memphis, TN, USA) (Figure1-4). The Menaflex CMI and Actifit® are considered partial meniscal scaffold replacements. They can be trimmed and used for defects[72] and full radial tears[73] or to replace the majority of the tissue so long as the meniscal rim is intact[74]. The Menaflex CMI is a collagen matrix scaffold while the Actifit is a polyurethane scaffold. These scaffolds have shown promising results with respect to histological, radiological, and clinical evaluations[72,74,75]; but have not been proven to protect from chondral degradation and prevention of osteoarthritis[76]. Previous studies have reported implant extrusion, scaffold tearing, and lack of tissue ingrowth[76–78]. A review of meniscus scaffolds reported a failure rate of 10.25% and a severe complication rate of 5.25%[79]. The NUsurface® is the only permanent replacement currently available and short-term clinical results

are promising. In an ovine model, no differences were found in cartilage condition between the NUsurface® and the contralateral control joints 6 months post operatively[80]. However, the implant geometry and fixation differ between the ovine model and the human condition. While the sheep implant was anatomically shaped and fixation bolts were used to secure the replacement within the joint, the human version is free floating and requires a healthy meniscal rim[68]. Human clinical results have found considerable pain relief with the NUsurface®; however, implant dislocation, fracturing, tearing, inflammation, and progression of osteoarthritis have been reported[81].

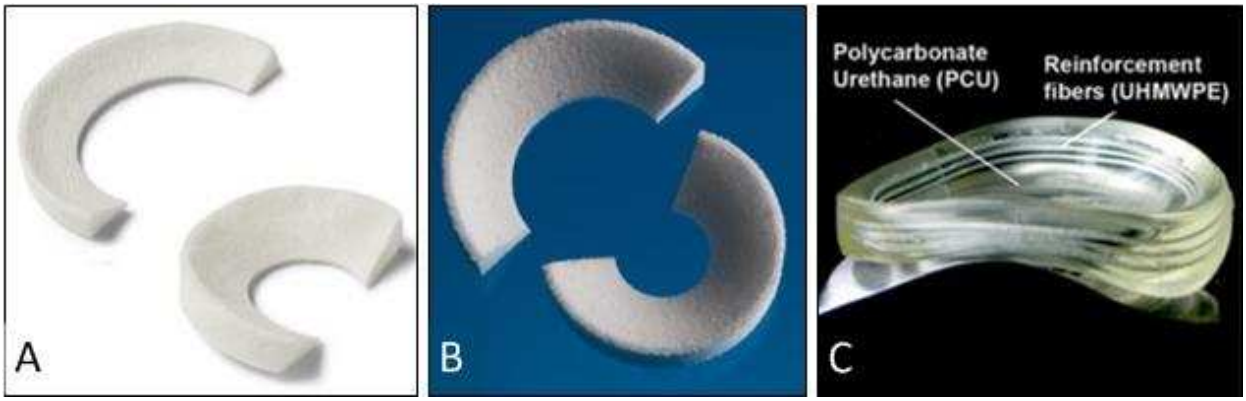

Figure 1-4: Meniscal scaffolds and replacements A) Menaflex CMI scaffold B) Actifit® scaffold C) NUsurface® Meniscus Implant

One of the primary limitations with all of the clinically available scaffolds and replacements is the necessity of a healthy meniscal rim. The two scaffolds are sutured into the meniscal rim while the NUsurface® uses the rim to help keep the free-floating implant in the joint. This almost certainly excludes patients with full radial tears, meniscal extrusion, and root avulsions which are common meniscal injuries. The failure rate, complications, and non-mimetic material properties that these existing systems have also impact the effectiveness of these treatment options. One of the investigated solutions is the use of hydrogel systems to more accurately mimic the anatomical and material properties of the native tissue.

1.5 Hydrogels

Hydrogels are composed of a network of polymer chains which are hydrophilic allowing them to absorb around 90% water by weight. The high water content of these systems and elastic properties of the polymer network result in a material that can behave similarly to biological soft tissues. Polyvinyl alcohol (PVA) hydrogels have been previously explored for meniscal replacements[70,82]. PVA hydrogels are formed by physically crosslinking chains through repeated freeze/thaw cycles or chemically crosslinking though glutaraldehyde or epichlorohydrin. Based on crosslinking density, the elastic properties of these PVA hydrogels can be manipulated to have a tensile strength from 0.066-1.018 MPa and compressive moduli ranging from 0.0012-.85 MPa[83]. While the tensile properties are far lower than reported values for human meniscal tissue the compressive properties are similar. Limitations with PVA hydrogels include poor durability and biocompatibility[82,84]. Furthermore, when used in a large animal model the PVA hydrogel implant caused severe damage to articular cartilage, along with full thickness radial tearing of the implant itself[85]. Mechanical characterization of other hydrogels has typically resulted in hydrogel systems with significantly poorer mechanical compressive properties compared to native tissues at physiological strains[71,86].

In recent years there have been advances in creating more robust hydrogel systems that can overcome the limitations of traditional hydrogels. Many conventional hydrogel systems are brittle in nature in part due to heterogeneous crosslinking. More densely crossed linked systems improve toughness by increasing the number of network chains per unit cross-sectional area but at the expense of swelling and viscoelastic behavior. One approach being explored is the use of AB diblock and ABA triblock copolymer hydrogel systems to create thermoplastic elastomer (TPE) hydrogels[87,88]. By applying a TPE approach the hydrogel system is formed from swelling

vitrified melt-phase blends of these two copolymers. Using specific AB blends, the dry polymers adopt a spherical morphology with vitrified cores and soluble coronas organized into a homogeneous body-centered cubic sturcture[87–90]. With the addition of the ABA triblock copolymer, these spherical micellar domains become physically tethered together and provide the system with mechanical integrity (Figure 1-5).

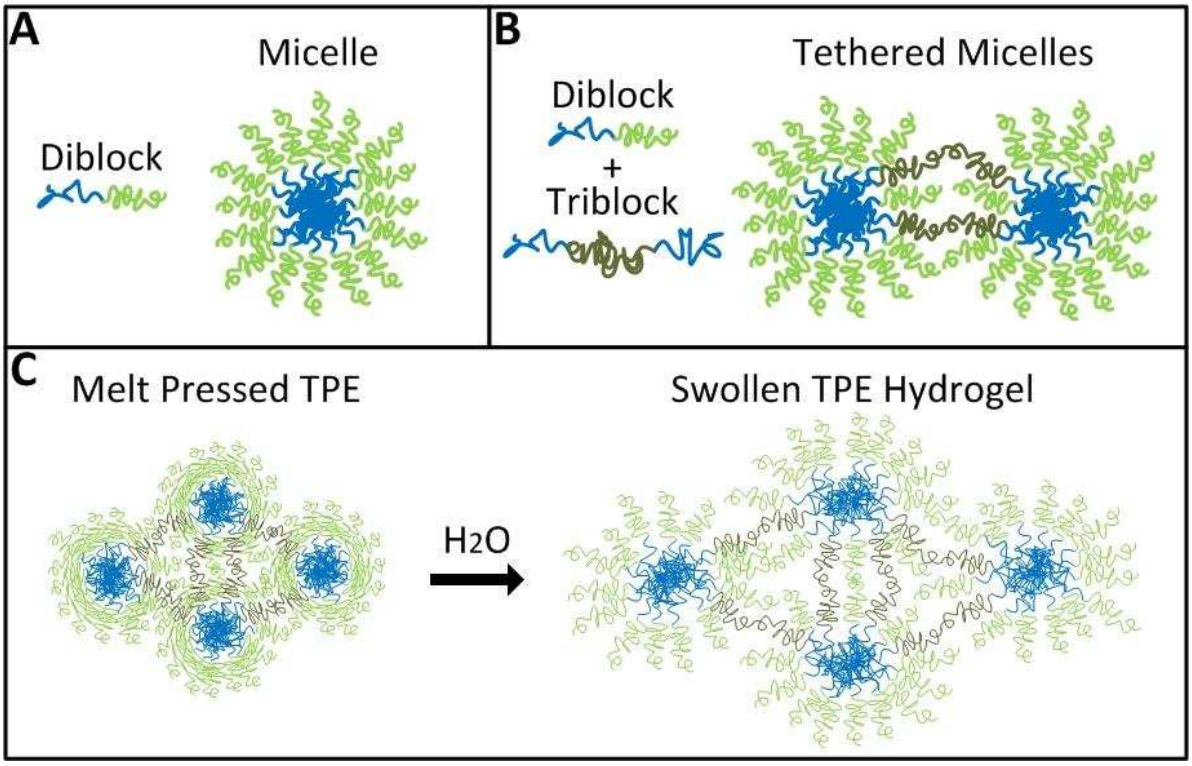

Figure 1-5: AB diblock and ABA triblock copolymer hydrogel system A) AB diblock forms micelle during melt phase B) incorporation of ABA triblock created physical tethers between micelles C) melt pressed TPE dry polymer system has dense packing of tethered micelles that when added to water will retain their lattice structure but imbibe water.

An advantage of the melt phase assembly method described above is that it is solvent free. Many other micelle assembly methods use solvents which can result in micelle cores which are less stable and unable to adequately distribute stress[91–93]. Self-assembly during the melt phase allows for pre-structuring and prevents retention of solvents and plasticizing of the micelle cores. The vitrification process used in TPE hydrogels fixes the network structure before any swelling

takes place which allows a greater volume of diblock copolymer compared to triblock copolymer while still achieving an infinitely tethered network. The TPE hydrogel of interest for a meniscal replacement is a polystyrene-poly (ethylene oxide) (PS-PEO, SO) diblock and a PS-PEO-PS (SOS) triblock copolymer blend. This blend has been reported to have a mean aggregation of over 200 PS chains[88]. The mol% triblock content of these blends can be controlled resulting in a hydrogel system with a range of tunable mechanical properties. The method used for processing these hydrogels in the melt phase also provides an opportunity to assign shape and structure which is then retained during swelling. These unique characteristics make this TPE hydrogel material a candidate for potential meniscal replacements.

1.6 Research Aims

There exists a clear need for a meniscal replacement that is more mimetic of the native tissue and can be implemented regardless of the degree of meniscal damage, specifically without the need for a meniscal rim. In order to address the aforementioned criteria, the following specific aims are proposed:

Aim 1: Mechanical comparison of SOS72 TPE hydrogel to native tissue. Aim 1 will expand upon the preliminary data, using a SOS72 blend as this is hypothesized to be similar in mechanical properties to the native human tissue. Comparisons will primarily be made to human soft tissues as the end application of this TPE hydrogel replacement is for the human condition.

Aim 1A: Perform a mechanical work up of SOS72 TPE hydrogel in simple compression (relaxation and dynamic compression), tension, and shear and compared to literature values for human soft tissue including the knee meniscus, articular cartilage, and intervertebral discs.

Aim 1B: Assess the response of SOS72 TPE hydrogel, human meniscal tissue, and ovine meniscal tissue to repeated compressive cyclical loading. Data currently does not exist for meniscal tissue tested in compression at high cycles and is thus being determined experimentally. In addition to the comparisons of the TPE hydrogel to native human meniscal tissue, ovine meniscal tissue will be tested to assess the appropriateness of the ovine model for future *in vivo* work.

Aim 2: Develop a 3D meniscal construct and assess load distribution properties in an ovine model. A meniscal replacement will need to have geometry mimetic of the native tissue to properly distribute load from the femoral condyles to the tibial plateau. Aim 2 will focus on creating a more unique 3D meniscal construct and assessing in situ load distribution.

Aim 2A: Create a 3D meniscal construct that can be implanted into an ovine knee. Using negative molding techniques a 3D TPE construct will be created based on a μCT image of an ovine medial meniscus. Construct design will account for surgical techniques and feasibility along with the use of existing instrumentation.

Aim 2B: Elucidate the load distribution properties of the 3D TPE construct *in situ*. An ovine model will be used to determine the contact area, mean pressure, and peak pressure of the native joint compared to the 3D TPE construct as well as other treatment conditions including a meniscectomy, suture repair, and allograft.

CHAPTER 2:
TPE HYDROGEL SYNTHESIS[1]

2.1 Materials and characterization

Styrene (99%, 4-tert-butylcatechol inhibitor, Aldrich) and ethylene oxide (99.5+%, compressed gas, Aldrich) monomer were each purified by successive vacuum distillations (10–20mTorr) from dried di-n-butylmagnesium (1.0M solution in heptane, Aldrich) before use. Both purified styrene and ethylene oxide monomer were stored in glass burettes in the dark, at room temperature (styrene) and 3 °C (ethylene oxide), respectively, before use (typically less than 24h). Argon degassed cyclohexane (CHX) was purified by passing the solvent over activated alumina followed by Q-5-like supported copper catalyst (Glass Contour, proprietary). Argon degassed tetrahydrofuran (THF) was purified by passing the solvent over activated alumina. High-purity argon (99.998%, Airgas) was passed through additional oxygen and moisture traps prior to use. Glassware and polymerization reactors were flamed under vacuum and backfilled with argon multiple times. All other reagents were used as received. 1H NMR spectra were collected at room temperature in CDCl3 on a Varian Inova 400MHz Spectrometer (n = 32, delay = 30s). Size exclusion chromatography (SEC) was performed on a Viscotek GPC-Max chromatography system fitted with three 7.5 x 340mm PolyporeTM (Polymer Laboratories) columns in series, an Alltech external column oven, and a Viscotek differential refractive index (RI) detector. Measurements were performed using a DMF (55°C) mobile phase (1mL/min) with PS standards (Polymer Laboratories). Final SO/SOS compositions were confirmed via relative peak integrations in the SEC chromatograms of these blends.

[1] *All TPE hydrogel synthesis and chemical characterization for the entirety of this dissertation work was performed by Jackson T. Lewis from Dr. Travis Bailey's lab as part of this collaborative project. The following chapter summarized that synthesis process*

2.2 ω-Hydroxy-polystyrene (S-OH)

Purified styrene monomer (120g, 1.14mol, 20°C) was added to a stirring solution of sec-butyllithium (10.23mL, 1.3M in cyclohexane, Aldrich) and dry, air-free cyclohexane (1L, 20°C) in a 2L reaction vessel. The solution was then raised to 40°C and stirred continuously for 8 hours. At a reduced pressure of 1 psig, purified ethylene oxide (6.6g, 0.15mol, 0°C, liquid) was added to the reaction vessel. The reaction was held at 40°C for an additional 24 hours, after which all excess ethylene oxide was removed from the reactor under a constant argon flow. The reaction was terminated by acidic methanol (50mL). The polymer was precipitated in methanol (5L total), producing a fluffy white solid, and dried under vacuum at room temperature over a 48h period (yield 116 g, 97%, Mn= 8370g/mol, PDI = 1.03).

2. 3 ω-Hydroxy-polystyrene-b-poly(ethylene oxide) (SO)

S-OH (7g, 0.836mmol) was added to a 2L reaction vessel containing a glass coated magnetic stir bar. The reactor was evacuated and backfilled with purified argon before adding 1L of dry, air-free tetrahydrofuran (THF). Concentrated potassium naphthalenide in THF was added to the polymer solution via cannula until a light green color persisted for 30 minutes. The temperature of the reaction mixture was raised to 40°C and purified ethylene oxide monomer (78.7g, 1.78mol, 0°C) was added under argon (1psi) to the stirring solution for 48 hours. The reaction was terminated by methanol (50mL) and the polymer was precipitated in 4L of pentane, producing a fluffy white solid. The polymer was dried under vacuum at room temperature for 48 hours. (Mn= 107,000g/mol, PDI = 1.07, fPS = 0.085).

2. 4 Polystyrene-b-poly(ethylene oxide)-b-polystyrene (SOS)

SO (29g, 0.271mmol) was placed into a 2L round bottom reactor vessel that was evacuated and backfilled with purified argon. The SO was allowed to dry under vacuum overnight. The SO was then dissolved in dry THF. A concentrated potassium naphthalenide solution in dry THF was titrated into the reactor until the solution maintained a green color for 30 minutes. α,α′-dibromo-p-xylene (35.8mg, 0.136mmol, 0.5 eq) in THF (1.5mL) was then injected into the reactor over a 12 hour period at a rate of 0.125mL/hr using a syringe pump and a 2.5mL glass syringe. The coupled polymer was recovered through precipitation in 5L of pentane followed by vacuum filtration. The precipitated polymer was dried overnight under vacuum to produce a fluffy white solid as a blend of coupled (SOS) and uncoupled (SO) block copolymer (52mol% SOS).

2.5 SO/SOS fractionation

To achieve higher SOS concentrations than the 52mol% produced during the SO coupling reaction, fractionation was performed. Dry SO/SOS polymer (4g) was dissolved in chloroform (400ml) and heated to 45°C. N-hexane (920ml) was added slowly, keeping the temperature above 40°C. The SOS precipitated and the solution turned cloudy. Upon cooling to room temperature, the solution turned transparent. The solution contained the majority of the SO while the SOS existed as a precipitate. The SOS precipitate was recovered and allowed to dry under vacuum overnight, while the SO in solution was recovered through rotary evaporation. Even higher SOS concentrations were achieved through successive fractionations of precipitated SOS.

CHAPTER 3:
PRELIMINARY CHARACTERIZATION OF A THERMOPLASTIC ELASTOMER HYDROGEL[2]

3.1 Introduction

With a biphasic composition reminiscent of biological tissues, synthetic hydrogel networks have been embraced as a foundation from which biomechanically accurate musculoskeletal soft tissue surrogates might be engineered. The most prominent advances in hydrogel design have employed the inclusion of interpenetrating networks[94], hydrophobic interactions[95,96], ionic interactions[97] tough[97,98], deformable domain structures[99], sliding junction points[100,101], and multifunctional macromers of prescribed structure[95,102,103] to produce intriguing network designs pushing the boundaries of mechanical achievement. These designs are responsible for stunning demonstrations of modulus[97], stretchability[96,98,100,101], ultimate strength[94,95,102], and overall toughness[96,98,100,101] that were inconceivable less than two decades ago. However, most of these systems are plagued by combinations of limited moduli at small strain, unacceptably high levels of energy dissipation and fatigue or slow and incomplete elastic recovery that are incompatible with the cyclic biomechanical loading profiles of most musculoskeletal soft tissues. Intrinsic susceptibility to permanent covalent bond rupture and significant plastic deformation[104–108] preclude a network from returning elastically to its original configuration, while recovery dynamics in the minutes to hours range[98] preclude it from doing so at physiologically relevant (often sub-second) time scales. Unfortunately, none of these advanced systems would yet be acceptable, for example, as substitutes for the fibrocartilage comprising

[2] *Text within this chapter is part of a joint manuscript effort by both Jackson T. Lewis and the author. All mechanical characterization presented within this chapter was conducted and analyzed by the author. Collaborator Jackson T. Lewis performed all gel permeation chromatography*

menisci of the knee, the annulus fibrosis of the intervertebral disc, or connective tissue of the cardiovascular system, which rely on high levels of elasticity to rapidly absorb and transfer (not dissipate) strain energy into efficient body movement or pulsatile blood flow[104,105].

Fatigue in typical non-swollen elastomeric polymers often considered for biomaterials applications tends to begin after hundreds of thousands of cycles[106–109]. Swollen systems, in contrast, tend to be rather brittle and have not been able to produce a comparable benchmark[110]. The brittleness derives from both the reduced areal density of polymer chains compared with their non-swollen counterparts, and the tendency of swelling to exaggerate strand length heterogeneity and localized stress concentrations, facilitating bond rupture[111]. Unfortunately, the development of higher modulus, fatigue-free hydrogel systems that can demonstrate a sustained ability to absorb and store energy elastically have not received the attention that tough dissipative systems have been afforded[110,112]. Two important contributions, however, have come from the groups of Sakai[102,103] and Ito[101], who have pioneered synthetic approaches for removing strand heterogeneity and promoting uniformity in the dispersal of stress. Sakai and coworkers used exact reaction stoichiometry and monodisperse tetra-arm macromonomers[95,102,103] to produce materials supporting very large compressive strains (99+%), which they attribute to the near absence of "spatial inhomogeneities and trapped entanglements" in the network[102]. In a somewhat contrary approach, Ito used topologically trapped but freely movable junctions to form "slide-ring gels", which allow the network to autonomously adjust strand lengths and use a "pulley effect" to redistribute local stress concentrations[100,101]. Notably, while each of these innovative networks has the potential to enhance elasticity while minimizing hysteresis, the specific materials synthesized in these examples were generally quite soft (compressive moduli in the tens of kPa). That is, they were not necessarily designed to produce a biomechanically

appropriate modulus, particularly over the small strain ranges relevant during standard physiological compression of many musculoskeletal soft tissues (e.g., meniscus ~ 12%[113–115], intervertebral disc ~ 10%[116,117], articular cartilage ~ 5 to 30%[118,119]). Regardless, these groundbreaking studies demonstrate the importance of utilizing network architectures that promote homogenization of the stress field, if elasticity without fatigue is to be achieved.

In that vein, the objective of this work was to assess the mechanical properties of a simple two-component block copolymer hydrogel, synthetically designed to be conveniently processable as a thermoplastic prior to swelling[87,88,120,121], and characterized by a network nanostructure that imparts both a physiologically relevant modulus and an unprecedented ability to distribute stress, resist fatigue, rapidly recover, and avoid catastrophic failure even under extreme degrees of compressive strain. The ability to control material properties of this polystyrene-poly(ethylene oxide) (PS-PEO, SO) diblock and a PS-PEO-PS (SOS) triblock copolymer blend will be assessed at various triblock copolymer concentrations.

3.2 Methods

3.2.1 Preparation of SO/SOS hydrogel samples

Dry polymer for the different SOS blend compositions (22 - 87mol%) was compacted into circular steel washers (8mm diameter, 0.73mm deep) or rectangular steel cutouts (assorted dimensions, 0.1mm deep) and sandwiched between two sheets of Teflon coated Kapton™. These assemblies were then placed into a Carver Press and heated to 150°C under an applied pressure of ~500psi for 5 minutes. In some cases, multiple compressions were used to remove visible bubbles. Samples were allowed to cool to room temperature before swelling. Samples taken from circular washer molds were used for indentation relaxation testing and swelling analysis.

Samples taken from the rectangular cutouts were used for fatigue and overloading compressions tests. In all cases, 8 mm or 6 mm diameter testing plugs were punched from swollen rectangular hydrogels using a biopsy punch.

3.2.2 Indentation Relaxation Testing of SO/SOS hydrogels.

Specimens were kept hydrated in DI water or PBS before and during indentation relaxation tests, which were run on an MTS Bionic Model 370.02 servohydraulic test system (MTS Corp, Eden Prairie, MN). The water or PBS bath containing the sample was attached to a multi-degree of freedom camera mount, and an x-y plate fixture allowing for the indentation surface to be oriented normal to the indenter and centered on the specimen respectively. A spherical tip with a diameter of 1.59 mm was used as an indenter, and loads were recorded using a 2lb load cell (Futek LSB200, Irvine, California). Due to the time-dependent nature of the compressive properties of hydrated materials both the equilibrium and instantaneous moduli were computed. All samples were preloaded with 20mN, and preliminary tests determined a relaxation time of 300 seconds resulted in near-equilibrium conditions. Specimens were indented to a strain of 12%/s. A Hertzian contact model was applied and used to determine both the instantaneous and equilibrium moduli (Equation 1 and 2). The contact equation assumes contact between an elastic half-space and a sphere where F is the force, R is the radius of the indenter, d is the indentation depth, $E1$ and υ1 are the elastic modulus and Poisson's ratio of the hydrogel respectively, and $E2$ and υ2 are the elastic modulus and Poisson's ratio of the indenter. The indenter tip had an elastic modulus and Poisson's ratio of 210GPa and 0.3, respectively. The elastic modulus of the hydrogel was calculated assuming the Poisson's ratio of the hydrogel was approximately 0.5 at small strains.

Equation 3-1: $$E_1 = \frac{(1-{v_1}^2)}{\frac{4R^{\frac{1}{2}}d^{\frac{3}{2}}}{3F} - \frac{(1-{v_2}^2)}{E_2}}$$

3.2.3 Cyclical Fatigue testing of SO/SOS hydrogels

Fatigue tests were initially run on hydrogels fabricated using three concentrations of SOS triblock copolymer (22, 46, and 72 mol% SOS). The three disk-shaped samples (SOS 22, SOS 46, and SOS 72) were swollen in DI water (8 mm diameter x 2.4, 2.2, and 1.9 mm, respectively), mounted (Loctite Super Glue Ultragel Control, Henkel Corporation, Rocky Hill, CT) on one side to a polished aluminum platen, submerged in a DI bath, and compressed using a secondary aluminum plate. The sample was preloaded to 200mN and then compressed to 12% strain at a frequency of 1Hz for 1,000 cycles using an MTS Bionic Model 370.02 (MTS Corp, Eden Prairie, MN) configured with a 2lb load cell (Futek LSB200, Irvine, California). The sample was then unloaded and left submerged in DI for one hour before being retested under the same conditions for four additional sets of 1,000 cycles.

An extended fatigue test was subsequently run on a disk-shaped hydrogel sample containing 61mol% SOS triblock copolymer. The SOS61 sample was swollen in PBS (6mm diameter x 1.8mm), mounted (Loctite Super Glue Ultragel Control, Henkel Corporation, Rocky Hill, CT) on one side to a polished aluminum platen, submerged in a PBS bath, and compressed with a secondary aluminum plate. The sample was preloaded to 200mN and then compressed to 12% strain at a frequency of 1 Hz for 10,000 cycles using an MTS Bionic Model 370.02 (MTS Corp, Eden Prairie, MN) configured with a 2lb load cell (Futek LSB200, Irvine, California). The hydrogel was then unloaded and left submerged in PBS for the balance of 24 hours before being retested under the same conditions for four additional sets of 10,000 cycles.

Lastly, five 6mm diameter disk-shaped plugs of SOS61 swollen in PBS with an average 1.6mm thickness were used to assess the mechanical integrity of the hydrogel over 500,000 cycles. Due to the extended duration of the experiment, the applied loading was performed in a

custom built material testing system designed to allow simultaneous axial displacements of up to six samples while the mechanical measurements were performed using an MTS Bionic Model 370.02 (MTS Corp, Eden Prairie, MN) configured with a 2lb load cell (Futek LSB200, Irvine, California). The first of the five samples was used to establish the baseline mechanical performance over the initial 1000 cycles. This sample was mounted (Loctite Super Glue Ultragel Control, Henkel Corporation, Rocky Hill, CT) on one side to a polished aluminum platen, submerged in a PBS bath, and compressed with a secondary aluminum plate. The sample was preloaded to 200mN and compressed to 12% strain at a frequency of 1Hz for 1,000 cycles. The remaining four samples were simultaneously and collectively subjected to 500,000 consecutive compression cycles over a nearly six-day period. At the conclusion of the 499,000 cycles, one of the four samples was immediately removed and transferred to the MTS to establish the baseline mechanical performance over the final 1000 cycles. The remaining three samples completed their final 1000 cycles in the home built system, after which they were evaluated on the MTS using an additional 1000 cycle test following rest periods of 3, 12, and 27 hours, respectively. Samples tested on the MTS were all mounted on one side during testing.

3.2.4 Overloading and ramp to failure of SO/SOS hydrogels

Overloading and ramp-to-failure experiments were performed on SOS61 disk-shaped hydrogel samples swollen in PBS (8mm diameter x 1.5mm). The overloading sample was mounted (Loctite Super Glue Ultragel Control, Henkel Corporation, Rocky Hill, CT) on one side to a polished aluminum platen, submerged in a PBS bath, and compressed using a secondary aluminum plate. A preload of 200mN was then applied to ensure contact with the sample. The hydrogel was compressed to 12% strain at 1Hz for 10 cycles followed by 1 cycle of 50% strain at 1Hz. This 11-cycle regiment was repeated 10 times using a Bionic Model 370.02 servohydraulic

testing system (MTS Corp, Eden Prairie, MN) configured with a 2lb load cell (Futek LSB200, Irvine, California). The ramp-to-failure experiment was performed on a SOS61 hydrogel disk swollen in PBS (6mm diameter x 1.6mm). The swollen sample was placed unfixed between the two platens, preloaded to 200mN, and submerged in a PBS bath. Compression was ramped at 2%/s up to 99% strain and unloaded at the same rate using an MTS Bionic Model 370.02 (MTS Corp, Eden Prairie, MN) configured with a 2lb load cell (Futek LSB200, Irvine, California). The sample was then inspected for defects and rerun under the same conditions a second time, after which it was stained with India ink for better visualization of possible microcracks formation.

3.2.5 Analysis

MATLAB (Mathworks, Natick, MA) was used to analyze the resulting data. Maximum and minimum compressive force and displacement for each cycle were determined and a linear fit between strains nearest 2-10% was used to ascertain the compressive modulus. For the overloading experiment, the same method was used to fit a linear function across the 2-10% strain range of all cycles as well as the 40-48% strain range for the overloading cycles. For the 500,000-cycle experiment, the modulus of each cycle recorded was determined, and then averaged across the 1000 cycles recorded.

3.3 Results

3.3.1 Indentation testing

Indentation testing was performed on four of the hydrogel blends to develop a complete picture of osmotic movement during compression and its effect on mechanical properties (Figure 3-1). In indentation testing of hydrated materials, there is a well-documented effect of instantaneous modulus attributed to trapped water generating a reactionary force followed by an

equilibrium or aggregate modulus after water has had sufficient time to move from the indentation site. The equilibrium moduli were 14.9 ± 5.3% lower than the instantaneous moduli, implying a significant effect of water movement on modulus. Testing showed increasing SOS content increases both the instantaneous and equilibrium modulus in indentation.

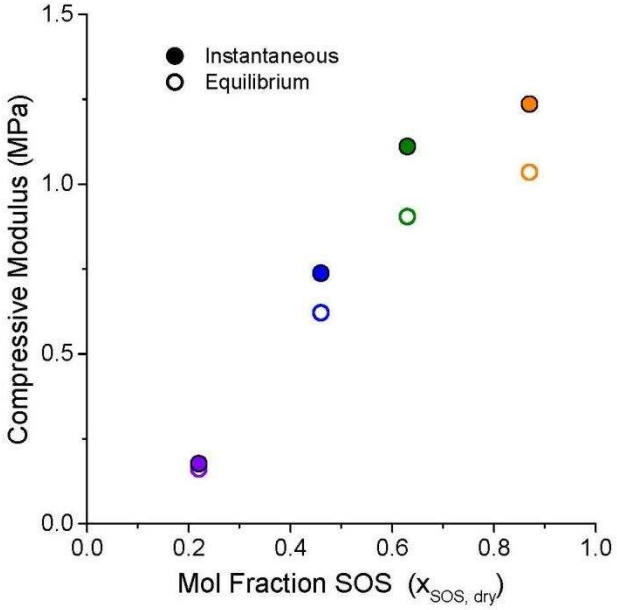

Figure 3-1: Indentation relaxation testing of swollen hydrogels showing the dependence of both instantaneous and equilibrium compressive modulus on SOS content of four distinct SOS blends

3.3.2 Fatigue

In order to gain a more complete picture of the materials fatigue resistance, three SOS content hydrogels were all strained to 12% at a strain rate of 12%/sec for 5 consecutive 1000 cycle runs (Figure 3-2). Though there is an average relaxation of 14.7 ± 0.5% in the modulus throughout each of the 1000 cycles, the original modulus of the prior run is largely recovered (98 ± 4.5%) following a 1 hour period of no loading for all of the SOS content hydrogels. Figure 3-2B shows that the standard deviation between the five runs is minimal. This implies that there is very little to no damage occurring to the underlying polymer network upon these loading cycles.

In fact, this decay is likely due to the movement of water within the hydrogel as it is completely recoverable.

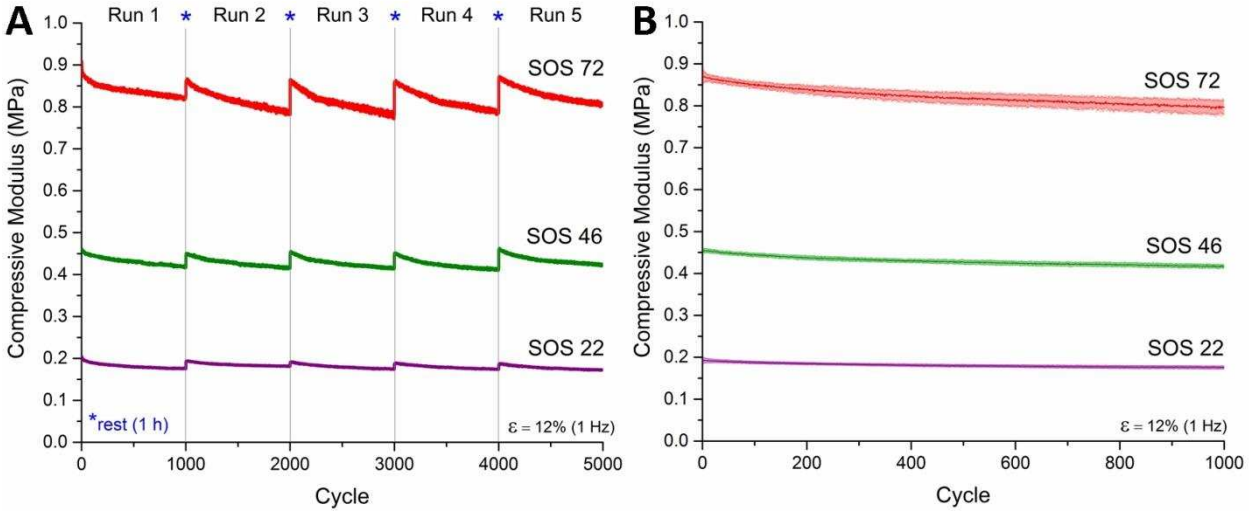

Figure 3-2: Modulus vs cycle results of three distinct SOS blends A) individual data from 5 runs of 1000 cycles with 1 hr rest between runs B) average and std of the 5 runs of four distinct SOS blends

Aditional testing was performed on a SOS61 blend to assess fatigue at longer time points of 10,000 cycles for 5 runs with at 24 hr rest period between runs (Figure 3-3). Again, the hydrogel shows a clear relaxation of modulus, with a mean final relaxation of about 22.1%. However, after each run, the hydrogel regained its original configuration, producing a pooled mean modulus over the first ten cycles of each run that is extremely narrowly distributed (0.614 ± 0.012 MPa). The SEC data comparing tested and untested samples also confirm that even after 50,000 cycles, there is no detectable difference in the molecular weight distribution in the loaded hydrogel.

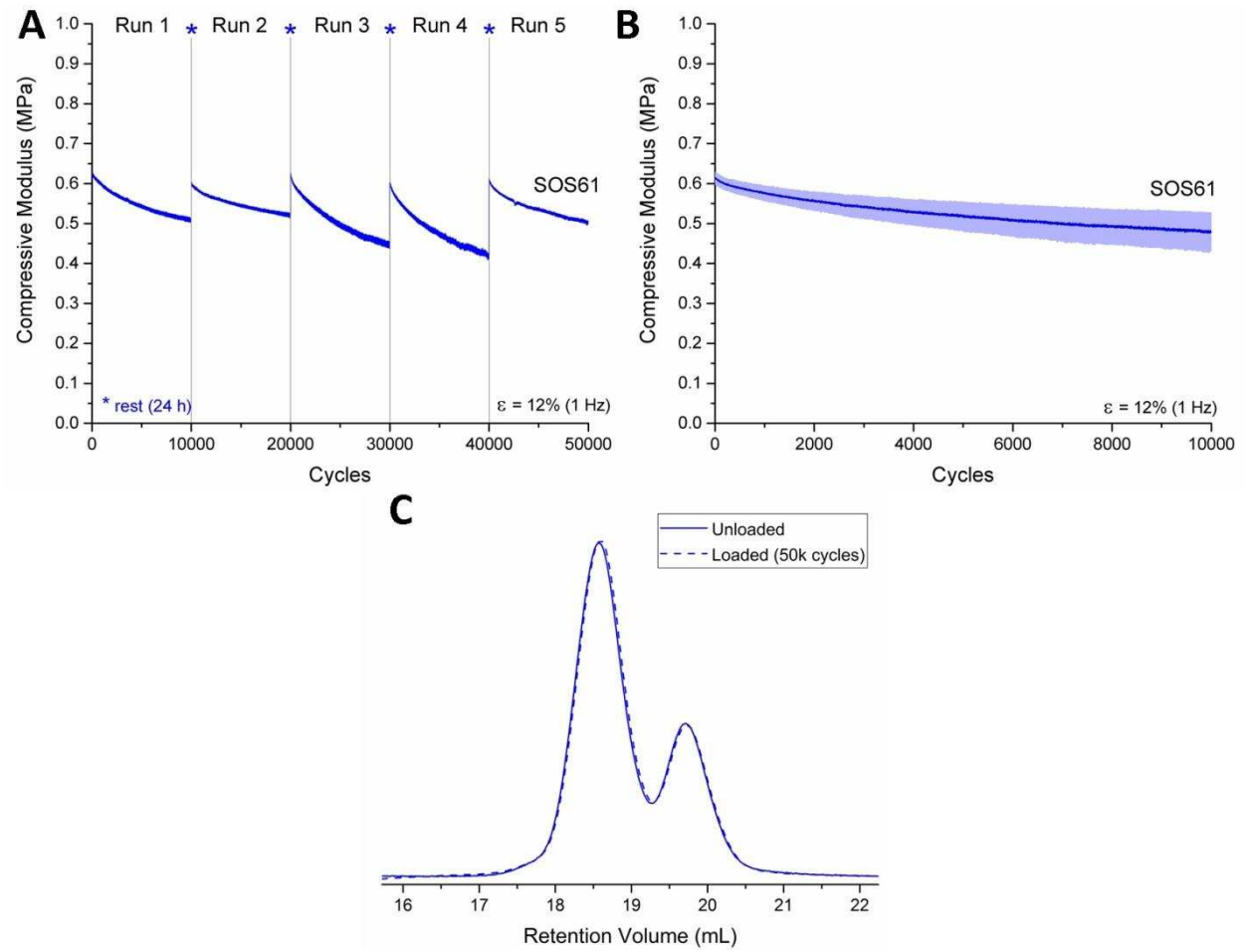

Figure 3-3: Modulus vs cycle results for SOS61 A) individual data from 5 runs of 10,000 cycles with 24 hr rest between runs B) average and std of the 5 runs C) GPC from a sample that was processed but unloaded and from a sample that experienced 50,000 cycles

In a final test designed to challenge the limit of fatigue resistance in these hydrogels, the SOS61 blend was subjected to 500,000 consecutive compression cycles (Figure 3-4) without rest. The immediate effect following the conclusion of the 500,000 compression cycles was a net 32.2% decay in mean modulus between the initial and final 1000 cycles of the run. Following 27 hours of rest, the cycled hydrogel produced an instantaneous modulus (measured over the first few cycles) equal to 94.8% of that measured for the pristine hydrogel, and a mean modulus over 1000 cycles equivalent to 92.3% of the initial 1000 cycle mean value. Despite these apparent

indicators signifying the onset of fatigue, the SEC data before and after loading continues to show limited to no observable change in molecular weight distribution.

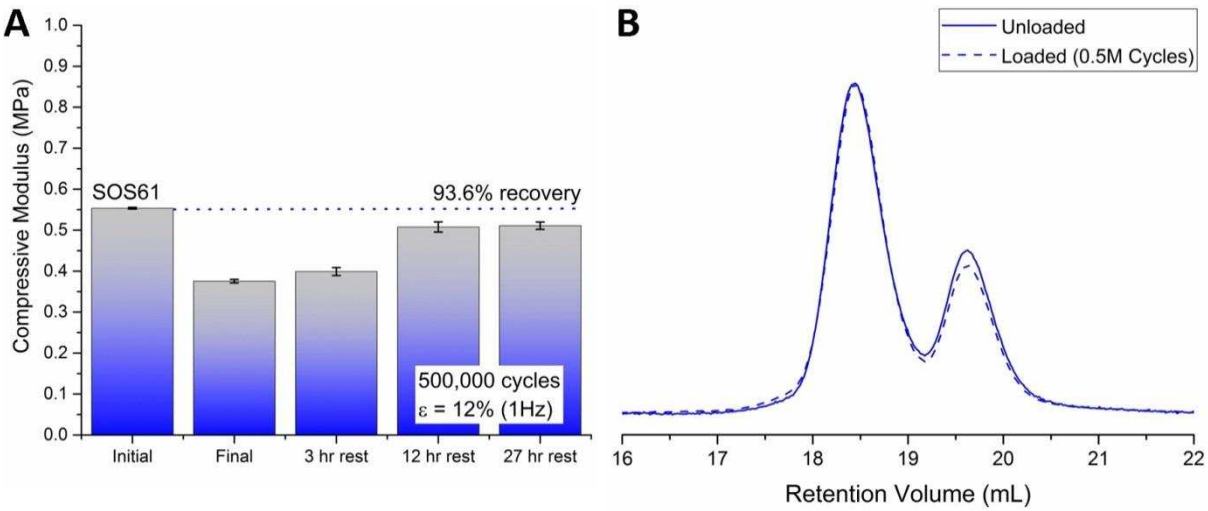

Figure 3-4: Modulus vs cycle results for SOS61 A) individual data average and std of 1000 cycles B) GPC from a sample that was processed but unloaded and from a sample that experienced 500,000 cycles

3.3.3 Overloading and ramp to failure

When subjected to a series of physiological compressions in addition to a compressive overloading cycle of 50% strain the hydrogel behaved in a similar manner to previous tests (Figure 3-5). The mean compressive modulus between 2-10% was found to be 0.54 ± 0.003MPa while the modulus for the 40-48% strain region of the data was found to be 1.2 ± 0.008MPa. The hydrogel system was able to recover to its original configuration following an overloading cycle. The stress-strain graph shows very little hysteresis between the loading and unloading legs indicative of minimal energy dissipation. GPC results from this experiment suggest no change in polymer chain lengths following repeated overloading cycles.

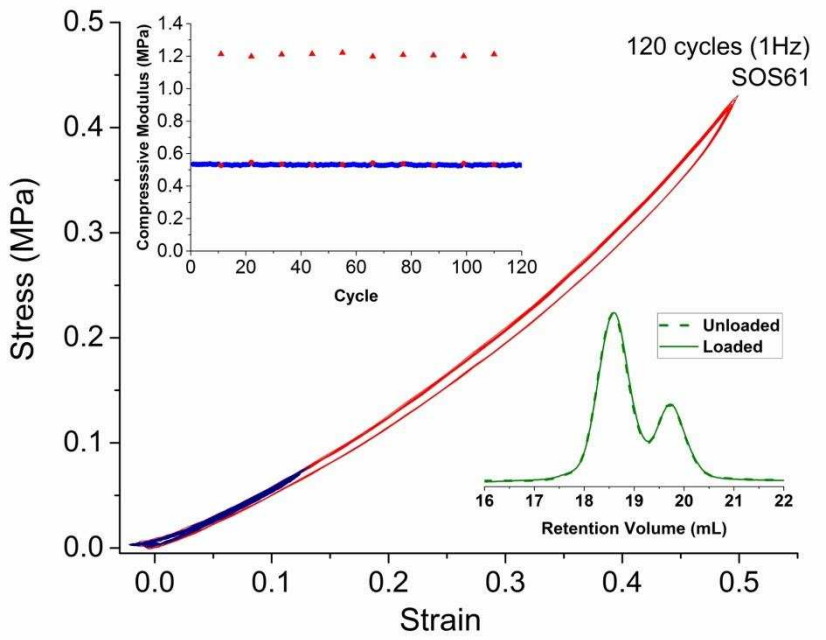

Figure 3-5: Stress-strain data from overloading experiment. Blue data highlights cycles from 0-12% strain and red highlights overloading cycle up to 50% strain. Upper inset denotes compressive modulus vs cycle and lower inset shows GPC of both a sample that was processed but unloaded and a sample that experienced the 120 cycles of compression

The final test performed was a ramp to failure test where a SOS61 sample was strained to 99% in two consecutive cycles (Figure 3-6). This data underscores the exceptional ability of the hydrogel nanostructure to absorb and distribute strain energy. For this testing strain rate was reduced compared to previous tests to reduce surface stress at the hydrogel-platen interface. The overlap of the two consecutive cycles confirms the ability of the network to accommodate extreme degrees of strain without plastic deformation. Video stills from the second cycle visually capture the full shape recovery, and photographs of the disc before and after the second cycle compression confirm the absence of visible fracture. The minimal hysteresis following this extreme compression suggests that the dissipation that does occur is primarily the result of transient phenomena like strain-induced convective flow, bond rotation, and/or chain repetition (in the diblock copolymer population) that have no permanent impact on the network architecture and subsequent mechanical performance. Consistently, GPC data confirm the

molecular weight distributions of the SO diblock and SOS triblock copolymer remain detectably unchanged following even this extreme compressive test.

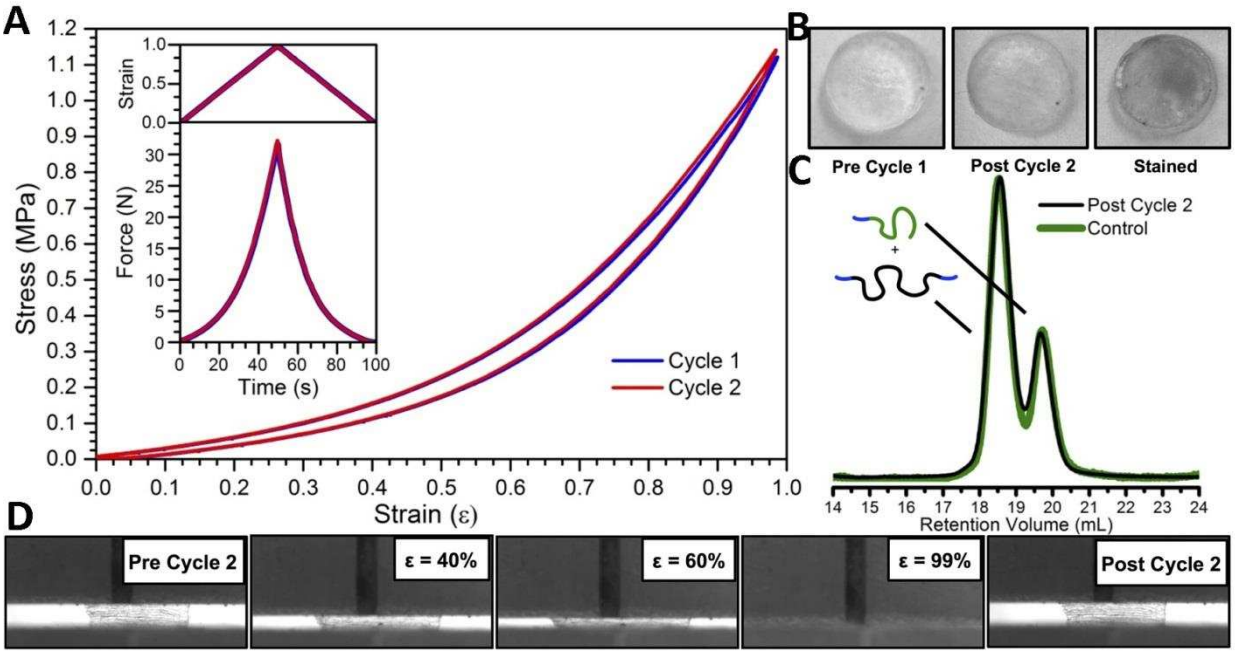

Figure 3-6: Ramp data of SOS61 A) stress vs strain data for both runs to 99% strain with insets of strain and force vs time B) photographs showing no visible damage to the surface of the sample following two cycles (India ink was used to stain the sample and highlight any defects) C) GPC of control processed but unloaded sample and the sample following the second cycle of 99% strain D) images taken during the second cycle test

3.4 Discussion

This work has shown that the TPE hydrogel material is mechanically tunable, highly elastic, and fatigue resistant. From indentation testing we found the equilibrium moduli were 14.9 ± 5.3% lower than the instantaneous moduli, implying a significant effect of water movement on modulus. Testing showed increasing SOS content increases both the instantaneous and equilibrium modulus in indentation. This increase in compressive modulus in higher triblock systems is largely due to a higher level of coronal overlap of the micelles. As the triblock copolymer content increases the physical cross-links between micelles increases as well. This leads to increased levels of topological entanglements limiting micelle separation and increasing

coronal overlap thus stiffening the material. The increased level of topological entanglements in higher SOS content hydrogels yielded a greater relaxation in modulus due to an increased restriction to fluid flow producing a higher relative instantaneous force and was evidenced in both the indentation testing and the unconfined testing.

Table 1 shows the average modulus results and decay results across the 5 runs of unconfined cyclical testing to 1000cycles with one hour rest between runs. The decay across the various SOS content is nearly identical for the full 1,000 cycles as well as the final 500 cycles suggesting a similar mechanism. Traditionally in high cycle fatigue testing, damage from cycle to cycle is due to stress concentrations leading to microcrack formations resulting in mechanical failure of the material. Due to the minimal amount of fixed juncture points in the TPE hydrogel system, there is a large amount of chain mobility. This ability to absorb energy through recoverable means allows the system to minimize stress concentrations, thus reducing micro crack formations, increasing the mechanical longevity of the material.

Table 1: Average initial modulus (MPa), Average modulus over full 100 cycle run (MPa), Average decay in modulus throughout the full run (%), and average decay over the second half of the 1000 cycle run (%) for three SOS content hydrogels (22,46, and 72).

Sample	Initial Modulus (MPa)	Mean Run Modulus (MPa)	Full Run Decay (%)	Second Half Run Decay (%)
Average SOS 22	0.19 ± 0.008	0.17 ± 0.009	14.4 ± 4.3	4.2 ± 1.2
Average SOS 46	0.46 ± 0.01	0.41 ± 0.007	15.2 ± 1.9	4.4 ± 1.1
Average SOS 72	0.85 ± 0.015	0.76 ± 0.024	14.6 ± 2.0	4.2 ± 2.0

Results from the 5000 repeated cyclical test along with the 500,000 cycle test suggest that under extended continuous loading some residual fatigue occurs in the mechanical properties of the TPE hydrogel. However, SEC data before and after loading continues to show limited to no observable change in molecular weight distribution. This may indicate that physical mechanisms such as chain pullout and not chemical bond rupture are largely responsible for the small, yet

emergent decline in mechanical performance. While the extent to which this decline will progress with continued cycling is currently unknown, post-assembly crosslinking of the hydrophobic core domains could offer an opportunity to push suppression of fatigue to even more extreme limits.

The rapid recovery rate and minimal hysteresis intrinsic to the network under more moderate, physiological strains was captured with the overloading study. The mean compressive modulus of the SOS61 blend was found to be 0.54MPa for each of the 120 cycles between strains of 2-10% strain while the modulus at higher strains between 40-48% was found to be 1.2MPa on average. In the 0.5 s interval in which the unloading leg of each cycle is performed, the network demonstrates a clear ability to fully recover its original configuration, and reproduce the stress-strain behavior identically in the next cycle, even after experiencing the overload to 50% strain. It is also notable that each cycle is accompanied by an extremely small degree of hysteresis between the loading and unloading legs, indicative that minimal energy is dissipated[110]. This result, in combination with cycle repeatability, suggests that the dissipation that does occur is primarily the result of transient phenomena like strain-induced convective flow, bond rotation, and/or chain repetition (in the diblock copolymer population) that have no permanent impact on the network architecture and subsequent mechanical performance. Consistently, SEC data confirm the molecular weight distributions of the SO diblock and SOS triblock copolymer remain detectably unchanged following the 120-cycle compression test. The ability of the TPE hydrogel to recover following 99% strain highlights the thermoplastic nature of the system and emphasizes the ability of the network nanostructure to dictate mechanical properties in the absence of permanent chemical cross-links. Furthermore, the SEC data, in combination with the coincident stress-strain data, supports the hypothesis that the prescribed

network architecture is able to efficiently absorb and distribute extreme degrees of compressive strain without succumbing to permanent chain pullout or mid-chain bond rupture.

Through a more comprehensive mechanical analysis of the TPE hydrogel in compression, shear, and tension is necessary, these hydrogels may be an ideal candidate for many high cycle applications. This system has been able to demonstrate a tunable elastic modulus appropriate for fibrocartilage-like applications (0.1-1MPa) while being extraordinary resistant to fatigue even after 500000 compressive cycles. The results from this study suggest a TPE hydrogel with an SOS concentration of ~70-80mol% triblock would behave similarly to native human meniscal tissue. For this reason, all future work will focus on an SOS blend in this range.

CHAPTER 4:
MECHANICAL VIABILITY OF A THERMOPLASTIC ELASTOMER HYDROGEL AS A SOFT TISSUE REPLACEMENT MATERIAL[3]

4.1. Introduction

Osteoarthritis (OA) is one of the leading causes of pain and disability among adults. Some of the most common joints affected are the large load-bearing joints of the knee, hip, and spine [122,123]. Joints are typically lined with articular cartilage to provide a smooth lubricated surface for articulation and protecting the underlying bone. Articular cartilage break down results in exposed bone and eventually both chronic and intermediate pain [124]. This cartilage breakdown can be a result of either trauma or natural degradation due to aging and can occur directly in the cartilage or indirectly in the case of damage to other neighboring soft tissues. For example, within the knee joint, the loss of meniscal tissue has been shown to lead to altered joint biomechanics and the early onset of OA [125]. Similarly, intervertebral disc degeneration usually occurs prior to facet joint OA [126].

The reason soft tissue injuries are of such a concern is that these tissues have poor cellularity and vascularization and thus a very limited capacity to regenerate or heal [14,127,128]. Currently, there are minimal therapies and few surgical options once these avascular tissues are damaged. The gold standard for articular cartilage damage is the removal of damaged tissue by way of debridement or a microfracture to promote blood flow and some healing, or a sometimes a mosaicplasty is performed where osteochondral plugs from non-weight bearing regions are grafted, though typically a total or partial joint replacement is eventually necessary [129]. Similarly,

[3] *This chapter is published as a Research Paper in the Journal of Mechanical Behavior of Biomedical Materials (volume 79, 2018). All content has been adapted with permission from John Wiley and Sons.*

if the knee meniscus is damaged, portions can be removed via meniscectomy or the entire tissue replaced with an allograft transplant but these treatments inevitably still lead to early OA [50,130]. Degradation of the annulus fibrosus or herniation leads to degenerative disc disease where the most common surgical intervention is a spinal fusion [131]. Fusions result in reduced mobility and have been associated with accelerated degradation of adjacent disc [132,133].

Soft tissue replacements are often broadly characterized as resorbable or non-resorbable. Resorbable scaffolds or tissue engineered constructs suffer from resorption rates that do not necessarily match the rate of matrix deposition leading to inferior mechanics and scaffold collapse under the complex loading regimes these tissues experience [76]. Conversely, non-resorbable replacements, as in the case of spinal fusion bracing, or the ultra-high molecular weight polyethylene, metals and ceramics used as part of knee and hip replacements, tend to have mechanical properties in excess of their native counterparts and result in high risk of stress shielding to neighboring tissues. It is for this reason that it is important to investigate material options that are more mimetic of the native soft tissues they wish to replace.

Hydrogels have been broadly investigated for both resorbable and non-resorbable replacement due to their ability to mimic the viscoelasticity of native soft tissues [66,71,86,134–136]. Thus, the objective of this study was to fully characterize a unique thermoplastic elastomer (TPE) hydrogel and assess its viability for use as a potential soft tissue replacement. This hydrogel is unique such that it is a block copolymer that is processable in the melt phase but forms a physically cross-linked network of glassy, spherical polystyrene (PS) domains within a matrix of covalently bound polyethylene oxide (PEO) chains [87]. These trillions of physically tethered spherical domains per milligram of polymer in turn are responsible for a network structure that is highly elastic, able to distribute stress, and resist fatigue. It is hypothesized that

this system will have mechanical properties similar to those of other native soft tissues, specifically articular cartilage, the knee meniscus, and the intervertebral disc.

4.2. Methods

4.2.1 Synthesis and preparation

Polystyrene-b-poly(ethylene oxide) block copolymer was synthesized as previously described [87,88]. Briefly, purified styrene monomer was added to an air-free solution of sec-butyllithium in cyclohexane and stirred for approximately 8 hours at 40 ˚C. Under a positive pressure of ~6895 Pa, while maintaining a solution temperature of 40 °C, ethylene oxide was added as a terminal capping agent. After a 24 hour period, the reaction was terminated by acidic methanol and the polymer precipitated in methanol, filtered, and dried under vacuum. Once dry, the ω-hydroxy-polystyrene (SO-H) was redissolved in dry tetrahydrofuran (THF) and titrated with concentrated potassium naphthalenide. The solution was raised to 40 °C and ethylene oxide monomer was added and allowed to react for 48 hours. The solution was terminated with methanol and the resulting ω-hydroxy-polystyrene-b-poly(ethylene oxide) (SO) was precipitated in pentane. The SO was dried under vacuum overnight, redissolved in dry THF and re-titrated once again with concentrated potassium naphthalenide. α,α′-Dibromo-p-xylene was added to this solution to induce partial coupling of the SO chains. The coupled polymer product, a blend of unreacted SO and coupled polystyrene-b-poly(ethylene oxide)-b-polystyrene (SOS), was precipitated using pentane and dried overnight. Lastly, the dry SO/SOS polymer was fractionated using chloroform/n-hexane mixtures until the desired 72 mol% concentration of SOS was achieved (SOS72). This blend was chosen based on preliminary data suggesting the SOS72 mechanical properties would be most similar to the soft tissues of interest.

4.2.2 Sample fabrication

Dry SOS72 polymer was compacted into cylindrical molds (2.5 mm in diameter x 1.5 mm thick) or rectangular cutouts (2.5 mm x 5 mm x 0.5 mm thick), lined with two Teflon coated Kapton™ sheets, and melt pressed at 150° C and 3.45 MPa for 5 minutes. Cylindrical plugs were used for all compression and shear testing while rectangular samples were used for tension testing. Following the melt press procedure, the molds were removed and allowed to cool to room temperature. The rectangular sheet was cut down into strips and then all polymer samples were swollen in 1x phosphate buffered saline (PBS) solution (11.9 mM phosphates, 137 mM sodium Chloride and 2.7 mM potassium chloride in DI water, diluted from 10x PBS, Fisher Scientific) for 24 hours. PBS was chosen as a dispersion medium as it more closely mimics the interstitial fluid found in the knee joint and spine compared to DI water. Samples were measured in their swollen state just prior to testing so strain based displacements could be appropriately determined for each individual sample as well as the cross-sectional area could be measured.

4.2.3 Testing Fixtures

All mechanical testing was performed using a servohydraulic test system (MTS Bionic Model 370.02, MTS Corp, Eden Prairie, MN) equipped with an 8.9 N load cell (Futek LSB200, Irvine, California). Compression testing was performed in a heated (35-37 °C) 1x PBS bath while shear and tension testing were performed in open air. A total of n= 12 plugs were used for indentation, compression, and shear tests. Due to the non-destructive nature of the compression tests, each plug underwent indentation, unconfined compression, and finally destructive shear testing sequentially. Performing all tests on the same plug increased statistical power by allowing for paired comparisons. The instantaneous response, or the response of the TPE hydrogel to the loading or ramp phase of the stress relaxation tests, as well as equilibrium response, or the

response at the end of the stress relaxation test hold period, were of interest. Twelve separate strips were used for the tension testing. In addition to using the internal linear variable differential transformer (LVDT) of the servohydraulic test system, digital image correlation (DIC) was utilized to assess local strain during lap shear and tension testing. Samples were blotted dry and speckled coated with graphite powder. As the graphite powder would shift and disperse if submerged in fluid, thereby preventing accurate strain tracking, lap shear and tension tests were performed in open air. To minimize any effects of this testing modality, samples were tested within 60 sec of being removed from fluid and all testing was concluded within 120 sec. Images were collected using a video camera (Point Grey Flea3 FW-14S3M-C, Richmond, BC, Canada) with a 25mm f/1.4 2/3″ fixed focal machine vision lens (Fujinon HF25HA-1B). The acquisition of load cell and video data were synchronized and collected at a rate of 10 frames per second. Acquired images were processed with an open sourced MATLAB based digital image correlation code which has been previously described[137]. For this analysis, the region of interest which was used during analysis was the central 50% of the sample.

4.2.4 Indentation Relaxation

Samples were first indented, while submerged in a heated PBS bath, at three locations using a spherical non-porous indenter. Indentation relaxation testing was performed to an indentation depth equivalent to 12% engineering strain and as such, each indentation depth was sample dependent, however, all samples were ramped over 1 second. Preliminary work determined a 180 second relaxation period was necessary for the material to reach equilibrium. Hertzian contact (Equation 4-1) was used to determine elastic modulus of the hydrogel where F is the force, R is the radius of the indenter (0.59 mm), d is the indentation depth, $E1$ and $\nu 1$ are the elastic modulus and Poisson's ratio of the hydrogel respectively, and $E2$ and $\nu 2$ are the elastic

modulus and Poisson's ratio of the indenter (210 GPa and 0.3 respectively). Poisson's ratio of the hydrogel was approximated at 0.5 for the small strains tested. Modulus values were reported for the instantaneous response and equilibrium response of the relaxation test.

Equation 4-1: $$E_1 = \frac{(1-{v_1}^2)}{\frac{4d^{\frac{3}{2}}R^{\frac{1}{2}}}{3F} - \frac{(1-{v_2}^2)}{E_2}}$$

4.2.5 Unconfined Relaxation and Dynamic Mechanical Analysis

Once all three indentation sites were tested, the indenter was removed and replaced with a polished aluminum plate. Samples were then subjected to two unconfined compression stress relaxation tests. The first stress relaxation test matched the parameters of the indentation testing: 12% engineering strain, 1 sec ramp, 180 sec relaxation. The second relaxation test began after a 3 minute rest period and was to 12% engineering strain, 5ms ramp, and 180 sec relaxation. Similar to the indentation relaxation tests, the elastic modulus was determined for the instantaneous and equilibrium portion of the loading regime. Tangent fits of the stress-strain data were assessed from the point at which the ramp was completed and from the data point immediately preceding the 180 sec relaxation. Additionally, an elastic modulus value was calculated from a linear fit of the 2-10% strain region of the stress-strain curve during the ramp loading. Following all relaxation tests the samples were subjected to a sinusoidal frequency sweep with 5% engineering strain amplitude at 0.1, 1, and 10 Hz with 5, 10, and 20 cycles per frequency. Storage (G') and loss moduli (G'') were determined by analysis of the third cycle of each sweep allowing for the material to be preconditioned by the initial cycles.

4.2.6 Lap Shear

Following all compressive testing, samples were tested in simple shear utilizing a fixture similar to that previously described [138]. Cyanoacrylate was applied to both ends of the sample and the sample adhered to the parallel plates of the shearing fixture. Preliminary work found the cyanoacrylate had limited penetration into the sample as it can be peeled from the hydrogel surface following testing. Samples were subjected to a pull to failure at a rate of 0.1 mm/s, minimizing any potential fluid effects, and any samples determined to fail as a result of the adhesive bond to the plates were discarded. Elastic modulus values were determined using a linear fit of the stress-strain values from both the LVDT and DIC methods. In the case of DIC strain values, the average strain across the entire region of interest was used and force data was downsampled to match the acquisition rate of the image capturing system. Two regions of interest were assessed; 2-10% strain region of the stress-strain curve and the middle 50% of the stress-strain curve till failure. Image J (NIH, Bethesda, MD) with FIJI package was used to assess failure angle determined from the change in angle between the first image and the image just prior to failure (Figure 4-1).

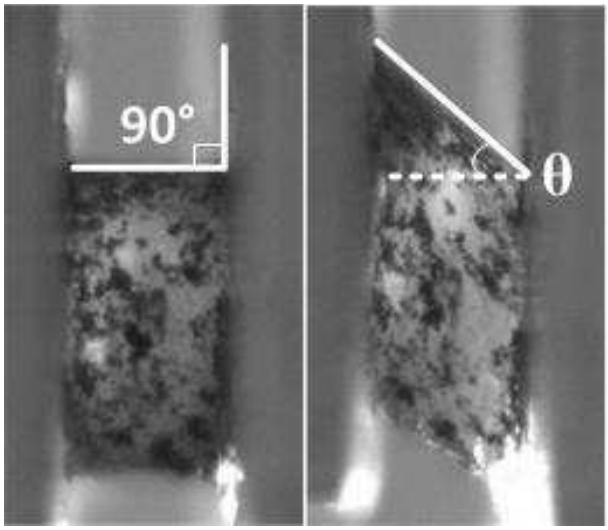

Figure 4-1: Example images from lap shear testing left) initial unloaded image right) final image before failure with θ denoting the failure angle

4.2.7 Tension

Rectangular strips of swollen hydrogel were dusted with graphite powder and placed in thin film grips (Imada FC-20). Similar to the lap shear testing, a displacement of 0.1 mm/s was applied to the samples until the samples reached an overall strain of 100%. Elastic modulus values were determined using a linear fit of the stress-strain values from both the LVDT and DIC methods. Again two regions were assessed; the 2-10% strain region of the stress-strain curve and the middle 50% of the stress-strain curve.

4.2.8 Statistics

All statistical analyses were performed with Minitab statistical software (Minitab15, State College, PA). Paired t-tests were used to evaluate differences between the instantaneous and equilibrium elastic modulus calculated within each compression stress relaxation testing regime. The differences between instantaneous and equilibrium elastic modulus values were assessed across both indentation relaxation vs unconfined compression stress relaxation with a 1 sec ramp and compression stress relaxation with 1 sec ramp vs the compression stress relaxation with 5ms ramp using a paired t-test. A paired t-test was also used to evaluate differences between instantaneous elastic modulus determined by the tangent fit vs the linear fit method for both unconfined compressive relaxation tests. A one-way analysis of variance (ANOVA) with post hoc Tukey's test was conducted to assess the differences in G' and G'' across the three frequencies tested. Paired t-tests were used to evaluate the differences between the elastic modulus values calculated using the strain determined by the LVDT and DIC. Finally, a one-way analysis of variance (ANOVA) with post hoc Tukey's test was used to evaluate the differences between all modulus values calculated from a linear fit of the 2-10% strain region of the

unconfined compression stress relaxation with a 1s ramp, shear, and tension tests. Significance was taken to be $p<0.05$ for all metrics.

4.3. Results

Following a 24 hour swelling period, swollen sample dimensions were taken immediately prior to testing. The average measured swollen plug thickness was found to be 2.87 ± 0.09 mm with a nominal diameter of 5 mm based on mold dimensions. The rectangular strips had an average width of 2.1 ± 0.3 mm, thickness of 1.7 ± 0.03 mm, and overall length of 10 mm based on mold dimensions. The elastic modulus calculations for the three indentation locations had a small deviation within each plug so values were averaged.

4.3.1 Stress Relaxation

Equilibrium elastic moduli values for all stress relaxation testing (indentation, unconfined with a 1sec ramp, and unconfined with a 5ms ramp) were found to be significantly lower (all with $p < 0.001$) than instantaneous elastic moduli values (Figure 4-2). The average difference within a single plug between the instantaneous and equilibrium elastic modulus was 12.6 ± 2.9%. The hydrogel was also found to be strain rate dependent with the modulus between the unconfined stress relaxation with a 1 sec ramp and a 5 ms ramp being significantly different in both the instantaneous ($p < 0.001$) and equilibrium responses ($p < 0.001$). No significant differences were seen between the indentation moduli and the unconfined 1s ramp moduli at either the instantaneous or equilibrium response ($p = 0.067$ and $p = 0.61$ respectively). An exponential time constant was determined from the unconfined stress relaxation with 1 sec ramp tests (assessing the average stress vs time) and found to be 2055 sec. While this value far exceeds

the testing time of 180 sec, on average stress decreased only 0.13% in the final 10 seconds of the 180 sec testing regime suggesting the TPE hydrogel has a limited and slow relaxation.

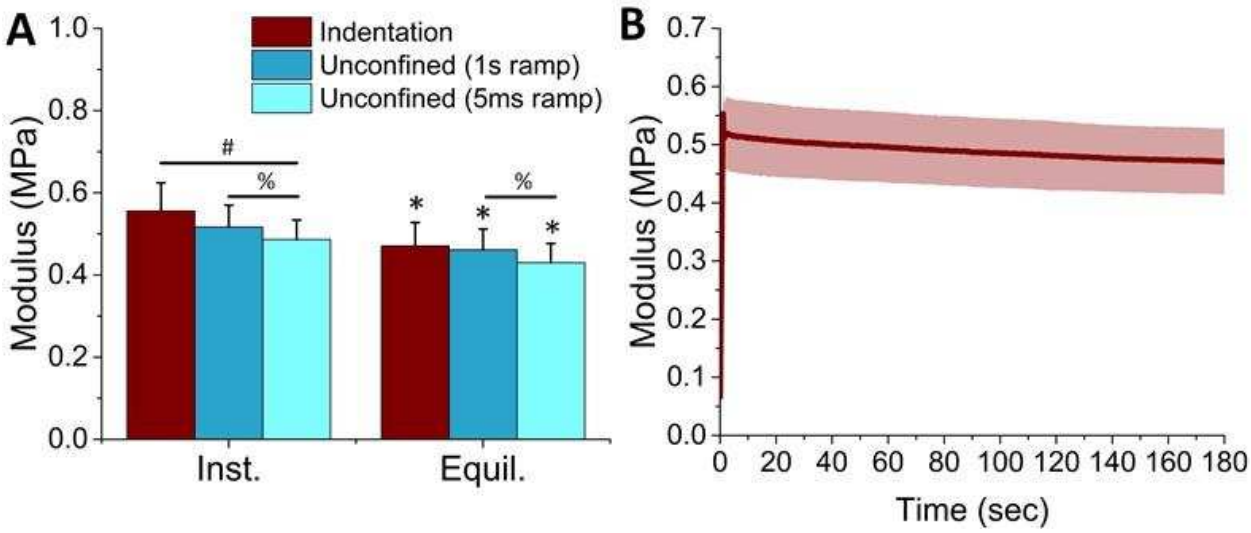

Figure 4-2: Stress relaxation test results. A) comparisons across three relaxation tests *denotes a significant difference between instantaneous and equilibrium moduli within testing regimes % denotes a significant difference between moduli values across unconfined 1s ramp and unconfined 5ms ramp B) average ± std of modulus vs time from all indentation tests

4.3.2 DMA

The average complex modulus at a frequency of 0.1 Hz, 1 Hz, and 10 Hz was found to be 0.59 ± 0.05 MPa, 0.58 ± 0.06 MPa, and 0.63 ± 0.13 MPa respectively. Storage and loss moduli were found to be frequency dependent (Figure 4-3). No differences were found between the storage or loss moduli across 0.1 Hz and 1 Hz ($p = 0.89$ and $p = 0.99$ respectively). However, both the storage and loss moduli at 10 Hz were found to be significantly lower than those found at 0.1Hz ($p < 0.003$ for both) and 1Hz ($p < 0.005$ for both).

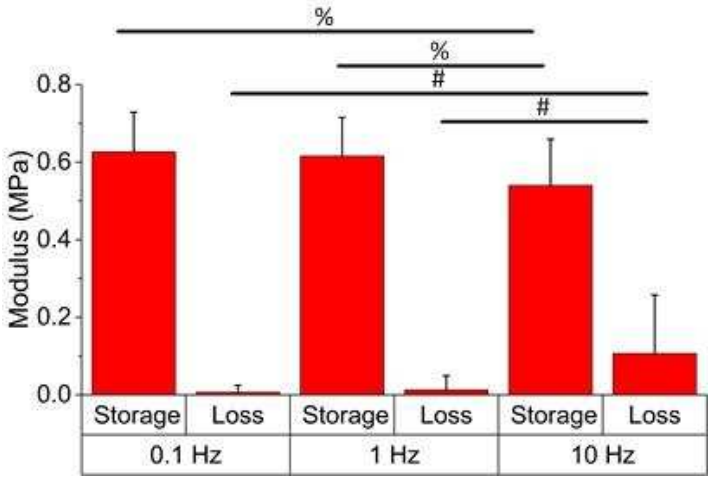

Figure 4-3: DMA test results. % denotes a significant difference between storage moduli; # denotes a significant difference between loss moduli

4.3.3 Lap Shear

The average failure strain across all 12 samples was found to be 0.5 ± 0.13 and the average failure angle was 37.8 ± 5.8°. No statistical differences were found between the modulus values calculated using the LVDT strain values vs the DIC strain values for either the data from the 2-10% strain or the 25-75% failure ($p = 0.231$ and $p = 0.401$). The data from DIC strain calculations were used for analysis as this represents local strains rather than global in that the middle 50% of the sample was used for a region of interest and thus is unlikely to be affected by potential sample slippage at the grips. The modulus calculated from the lower strain levels, 2-10% was found to be minimally but statistically ($p = 0.048$) higher than the modulus calculated for the mid 50% strain to failure modulus (Figure 4-4).

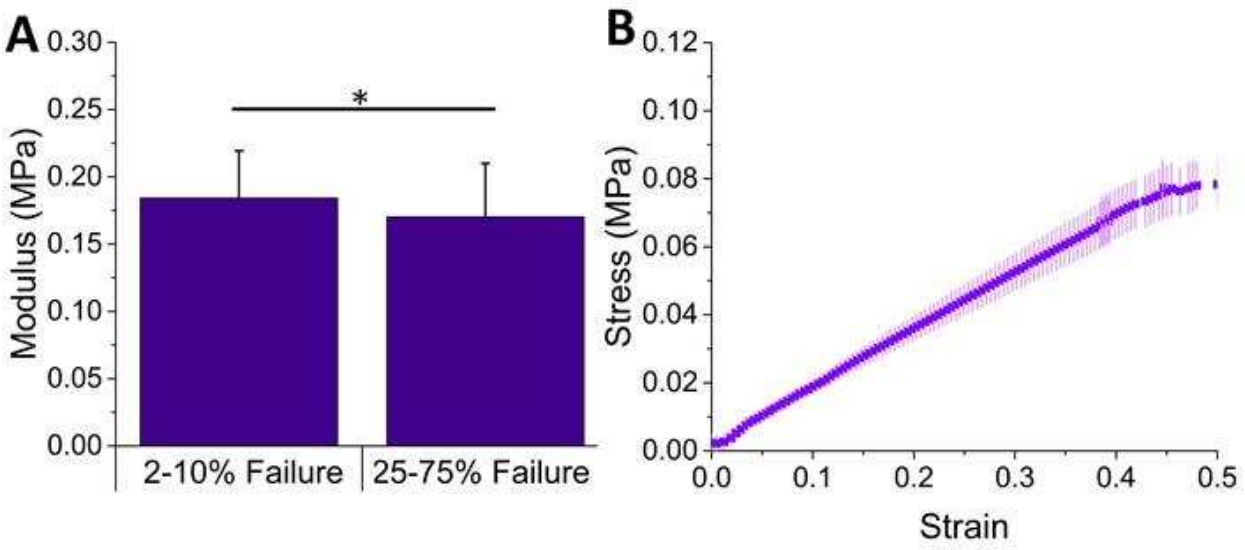

Figure 4-4: Results from the lap shear testing A) modulus from two regions of interest *denotes a significant difference B) stress vs. strain (average ± std) from all samples

4.3.4 Tension

Similar to the lap shear testing only the data from the DIC measured strain is presented. Modulus values were calculated from the 2-10% strain region and the 25-75% strain region (Figure 4-5). The moduli calculated from these two regions of the data sets were found to be statistically different ($p < 0.01$). In addition to elastic modulus, Poisson's ratio was calculated from the images captured during tension testing and was found to be 0.38 ± 0.07 for this SOS72 TPE hydrogel blend.

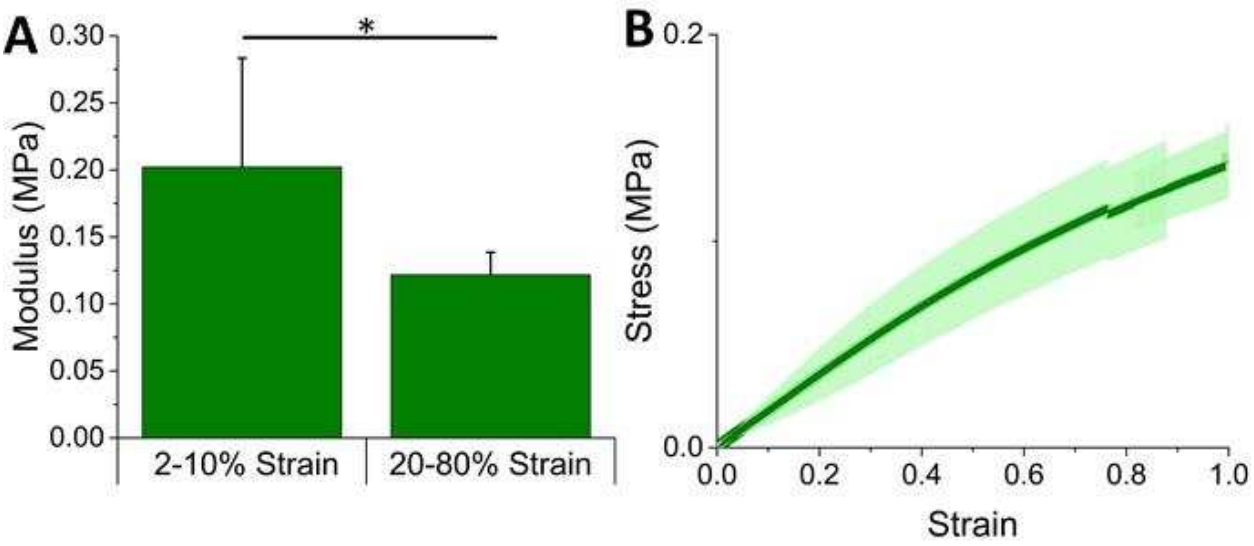

Figure 4-5: Results from the tension testing A) modulus at two regions of interest *denotes a significant difference B) stress vs. strain (average ± std) from all samples

4.3.5 Comparison

Neither the modulus values from the unconfined stress relaxation tests with a 1 sec ramp nor the 5 ms were found to be significantly different when assessed using the tangent modulus approach vs the linear modulus approach. Thus, when assessing tension-compression asymmetry the unconfined stress relaxation test with 1 sec ramp and modulus determined from the linear fit of the 2-10% strain region was used to represent the compressive modulus as this is most similar to the method for ascertaining the modulus from the tension and shear tests (Figure 4-6). Statistical differences were found between the compressive modulus and both the tensile and shear moduli ($p < 0.001$ in both cases). No statistical difference was found between the tensile and shear modulus ($p = 0.75$).

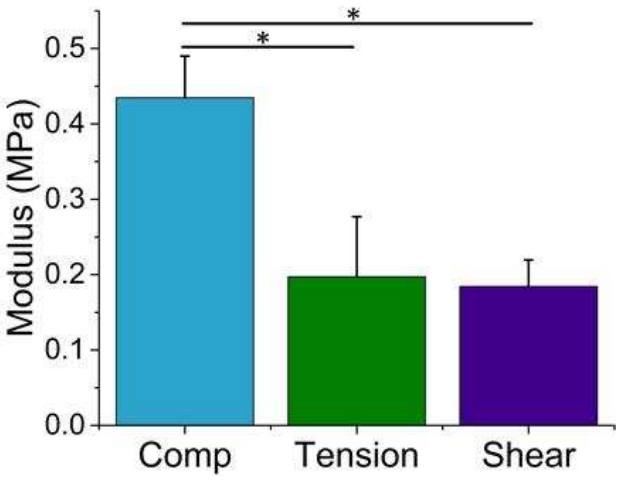

Figure 4-6: Modulus results across the three testing types * denotes significant differences

4.4. Discussion

The goals of the present work were to assess the mechanical response of a unique TPE hydrogel material and assess its viability as a soft tissue replacement material. Based on the assessments made within the scope of this study the TPE hydrogel tested performs similarly in its viscoelastic response, compressive modulus, and shear modulus compared to reported literature values of articular cartilage, the knee meniscus, and the intervertebral disc. It is, however, lacking significantly when it comes to a comparable tensile modulus.

The elastic moduli, determined at equilibrium from 3 separate relaxation tests, were significantly lower than the instantaneous response (Figure 4-2) with the average relaxation across all samples being 12.6%. While the soft tissues of meniscus and articular cartilage display a similar property, the magnitude of relaxation is greater [139]. Meniscal tissue has been found to relax 50-90% [140–142] and articular cartilage has been reported to relax 40-80% [143–145]. The nucleus pulposus of the spine has a similarly high degree of relaxation of 66% [146]. The role this relaxation plays in the function and health of the tissues of interest, as well as neighboring

tissues, is not fully characterized. Our TPE replacement may not have to perfectly replicate this drastic relaxation seeing as our inert replacement would not require fluid flow for nutrient transfer and matrix health.

When comparing the compressive properties of the TPE hydrogel to other soft tissues it has a comparable equilibrium elastic modulus, but an inferior instantaneous elastic modulus. The TPE equilibrium modulus average was 0.45 ± 0.05 MPa. The compressive aggregate modulus of annulus fibrosus has been reported to range from 0.1 - 0.5 MPa [147–150] and the nucleus pulposus even softer with an average less than 0.001MPa [146] depending on the testing condition and orientation of the tissue. Likewise, for meniscus and cartilage, numerous tests in various orientations have been conducted and a large range of reported elastic modulus values exists. However, direct comparisons to literature values is challenging due to differences in testing modalities (confined vs. unconfined vs. indentation), testing procedures (creep vs. stress relaxation) as well as differences in data processing. For meniscal tissue combining reported values of elastic modulus at equilibrium, average equilibrium responses have been reported at 0.68 MPa [140,141,151–153] with a range from 0.05-1.6 MPa while the average reported aggregate modulus is 0.08 with a range from 0.06-0.22 [154–156]. The equilibrium elastic response of articular cartilage have ranged from 0.58-0.7 MPa [157,158] and an aggregate modulus of 0.84 MPa has been reported [157].

The compressive instantaneous response of this TPE hydrogel was found to be 0.52 ± 0.06 MPa which is substantially lower than reported values for soft tissues. Although there is no consensus on what merits "instantaneous" numerous studies including both confined and unconfined testing setups the reported values that represent data acquired at a high loading rate, at the beginning of the loading phase, or immediately following the loading phase. For general

comparison, the reported average elastic response across these varying studies was found to be 1.8 MPa with a range from 0.7-3.7 MPa [140,151,152] and 5.65 MPa [158,159] for the meniscus and knee articular cartilage respectively. However, because biological tissue relaxes, it is difficult to state what the functional range is between instantaneous and equilibrium modulus, as the tissues likely function between these two extremes.

As with most viscoelastic materials, the TPE hydrogel material properties were found to be dependent on strain rate. Both the instantaneous and equilibrium moduli were found to be significantly lower in the samples strained to 12% over the 5 ms ramp compared to the 1 sec ramp (Figure 4-2). Typically at higher loading rates, the modulus would be expected to increase due to the contribution from the fluid components. One explanation for the opposite effect seen in this study is perhaps the rest period between stress relaxation steps was insufficient to allow the TPE hydrogel to fully rehydrate. Another reason could be the effect of the longer time (1 sec), causing visco non-elastic creep, as per the Maxwell-Voigt viscoelastic model. Future work should be done to determine the necessary recovery time for this material.

Under dynamic loading conditions, the storage and loss moduli were found to be similar across the frequencies of 0.1 Hz and 1 Hz but significantly different at 10 Hz (Figure 4-3). At a frequency of 10 Hz, the TPE hydrogel had a decreased storage modulus and an increased loss modulus suggesting that it has some energy damping capabilities at higher frequencies. Limited damping was seen at lower more physiological frequencies of 0.1 Hz and 1 Hz as evidenced by an average damping ratio of 0.022 across the two frequencies. The TPE hydrogel tested had a dissimilar trend compared to typical soft tissues which have been reported to have increasing storage moduli with frequency and decreased damping [153,160,161]. Nevertheless, the limited contribution of viscous dissipation was similar between our TPE hydrogel compared to menisci

samples tested at similar physiological frequencies of 0.1 and 1 Hz [153]. In a study testing the dynamic properties of human tibial articular cartilage at a frequency of 1 Hz the damping coefficient was found to be approximately 0.028 and compared to our hydrogel damping coefficient of 0.026 at the same frequency [161].

No significant differences were seen between compressive moduli values determined using indentation vs unconfined testing methods (Figure 4-2). This suggests that the surface and bulk material properties are not significantly different which follows the expected results since this TPE hydrogel material is homogeneous. However, this is in contrast to most soft tissues where the collagen architecture often provides both depth-dependent properties as well as zonal differences [153,162–165].

The average shear modulus for the TPE hydrogel was found to be 0.18 MPa which is comparable to the intervertebral disc, knee meniscus, and articular cartilage. The nucleus pulposus has a low shear modulus of 0.01 - 0.05 MPa in the axial direction [166]. While this TPE hydrogel exceeded the shear modulus of nucleus pulposus, the TPE hydrogel is similar to the annulus fibrosus and knee meniscus, 0.06 - 0.15 MPa [167,168] and 0.121 MPa [8] respectively. Previous studies have investigated the shear properties of articular cartilage and some report it in a very similar range of 0.17-0.27 MPa [169,170], while others have reported values as high as 0.4 - 0.7 MPa [8,143]. Shear modulus an important material property, but ultimately the addition of a wear study would be beneficial in assessing the ability of this TPE hydrogel to succeed in the complex loading environment it would experience if used as a soft tissue joint replacement.

The greatest insufficiency of the current TPE hydrogel as a potential soft tissue replacement is likely its limited tensile modulus compared to native musculoskeletal soft tissues. The tensile modulus of our hydrogel material is approximately 0.2 MPa while the native soft

tissues have moduli values an order to two orders of magnitude greater both along and perpendicular to the primary collagen fiber direction. The collagen that runs in the circumferential direction of the knee meniscus and the annulus fibrosus gives the native tissue an advantage compared to our homogenous hydrogel material. Tensile modulus values have been reported in the order of 50 - 100 MPa [171,172] for the annulus fibrosus and 80-120MPa [8,115,173] for the knee meniscus when tested along the fiber direction. Testing along the fiber direction in articular cartilage is more challenging due to the architecture, however, values reported for tensile modulus of samples parallel to the surface have been in the 2 - 6 MPa range [8,162,174] which is still more than an order of magnitude greater than our TPE hydrogel. If greater tensile elastic modulus is found to be necessary for specific soft tissue replacements, it will need to be incorporated into our current hydrogel system. This could potentially be accomplished by incorporation of fibers or selective crosslinking but would need to be further investigated.

There are a number of limitations to the current study that should be noted. Firstly, all hydrogel samples were pressed from a single synthetic batch. Future work should assess batch to batch variance as this could be of importance for large-scale manufacturing. Additionally, all samples were created under pressure but not under vacuum. Care was taken to discard samples with any visible defects or bubbles, but removal through vacuum this could have a significant effect on material properties obtained, particularly those from indentation and tensile tests. For both loading conditions in unconfined stress relaxation testing, 1 sec and 5 ms, the relaxation period was maintained at 180 seconds and it is possible that pure equilibrium was not achieved. Lastly, lap shear and tension tests were performed in open air and although testing did not occur over an extended period of time the use of an alternative speckle patterning procedure which would allow for testing in a bath should be considered in future work.

Conclusions

Based on the results of this study, this TPE hydrogel blend is a viable material for potential use as a soft tissue replacement. It has a modulus greater in magnitude to the nucleus pulposus in compression and shear. The equilibrium modulus and shear modulus of the hydrogel are very similar to that the annulus fibrosus, knee meniscus, and articular cartilage. It also responds damping ratio under physiological dynamic loading. A limitation of this material as synthesized and tested in this study is the low tensile modulus compared to native tissues. Thus, further incorporation of supporting fibrous zones may be necessary. However, this is still a positive step in trying to develop a soft tissue mimetic material.

CHAPTER 5:
DYNAMIC COMPRESSION OF HUMAN AND OVINE MENISCAL TISSUE COMPARED TO A POTENTIAL THERMOPLASTIC ELASTOMER HYDROGEL REPLACEMENT[4]

5.1 Introduction

The menisci are wedged fibrocartilaginous tissues housed within the knee joint located between the femoral condyle and the tibial plateau. The structure of the menisci allows for stabilization of the knee and load distribution within the joint[11,175]. The menisci are biphasic tissues composed of approximately 75% interstitial fluid and a ground matrix composed of predominantly circumferential collagen fibers and glycosaminoglycan rich proteoglycans[14,176,177]. A number of studies have investigated the compressive mechanical properties of human menisci under confined[154,155] and unconfined environments[58,140,141,151,156,178] as well as indentation relaxation[151,156,179]. Little investigation of the dynamic properties of the tissue has been performed, and that which has been done has assessed the tissue under a limited number of cycles[153]. Understanding how the tissue responds to loading regimes more mimetic of daily life is necessary if we wish to succeed in ultimately replicating the meniscus with a functionally accurate synthetic surrogate or scaffold.

Meniscal tissue is primarily avascular in nature[14] limiting its ability to heal when damaged, which is common as a result of both athletic injuries as well as degenerative changes[180]. The National Survey of Ambulatory Surgery in 2006 identified more than 364,000 knee arthroscopies performed due to a diagnosis of a tear to the medial cartilage or meniscus[181], and meniscal arthroscopic treatment is one of the most common orthopaedic surgical procedures

[4] *This chapter has been published as a Research Paper in the Journal of Biomedical Materials Research Part A (volume 105 issue 10, 2017). All content has been adapted with permission from Elsevier.*

accounting for up to 20% of all surgeries[182]. Currently, there are few technologies to replace damaged menisci, and standard treatment is to leave asymptomatic damage alone or perform partial meniscectomies[42]. However, both of these solutions lead to an increased risk of osteoarthritis (OA) development[48–50].

Ultimately, the functionality of both the material used as a replacement or scaffold, as well as the large animal model used for in vivo testing should be considered carefully. A number of synthetic materials have been investigated for meniscal replacements[68,70,80,183–186]. Limitations with previously reported materials include poor durability, mechanics, and biocompatibility[82,84,187]. Degradable scaffolds have also been investigated to serve as temporary meniscal replacements but have been shown to have limited mechanical integrity and lead to cartilage damage once tested *in vivo*[76,77,188–190]. Large animal models, such as the ovine model, are often used for in vivo studies of potential meniscal replacements[72,77,80,191] for their similarity to human menisci both with respect to size[192], single compression mechanical data[154] and structural composition[193]. However, while these tissues are very similar in many aspects, comparisons thus far are limited and their differences are important to consider when designing a translational implant.

The objective of this study was to test human meniscal tissue across 5000 compressive cycles and compare findings to ovine menisci and a recently developed thermoplastic elastomer (TPE) hydrogel[87] engineered for its potential as a meniscal replacement. The TPE hydrogel evaluated in this study has been previously shown to possess high elasticity, fatigue resistance, and compressive moduli tunable within the range of that exhibited by native meniscal tissue. This study will be one of the first to evaluate native meniscal tissue across a high number of compressive cycles. Previous work has only assessed strain rate dependency at low frequencies

and a limited number of cycles[153]. Modulus values will be compared as well as a model fit of the modulus vs cycle data. It is hypothesized that the human and ovine modulus values and cyclic relaxation profile will be similar given the physiological and compositional similarity between these tissues[154]. Preliminary work suggests the TPE hydrogel material will exhibit modulus values within the range of the native tissues but is not expected to have the same magnitude of cycle to cycle relaxation due to its much faster fluid transfer and limited hysteresis compared to native menisci.

5.2 Materials and Methods

5.2.1 Sample Harvesting

Human specimens were de-identified and obtained from a tissue bank (National Disease Research Interchange, Philadelphia, PA, USA), and ovine knees were collected from other terminal studies. NIH guidelines for the care and use of laboratory animals (NIH publication #85-23 Rev. 1985) have been observed. Menisci, identified as healthy, from a total of seven human cadaveric specimens (ages 60±21) and 8 mature ovine (*Ovis aris* Rambouillet X Columbia breed) cadaveric specimens were sectioned into medial and lateral, anterior and posterior segments and slowly thawed in 1x phosphate buffer saline (PBS) solution. Samples were created using a five-millimeter diameter biopsy punch taken from the proximal to distal ends with the number of samples dictated by the tissue available; usually, 4 samples were taken from each meniscus but individual meniscus shapes and thicknesses sometimes limited sample collection. Samples were then stored at 1.6°C in 1x PBS for 24 hours to allow equilibrium swelling to occur. A sizing apparatus was used to cut the samples 3 mm thick from the mid-belly of the biopsy (Figure 5-1). A total of 10 samples for all regions were tested for both human

and ovine groups with the exception of the medial posterior region in human where only 9 samples were tested due to tissue availability.

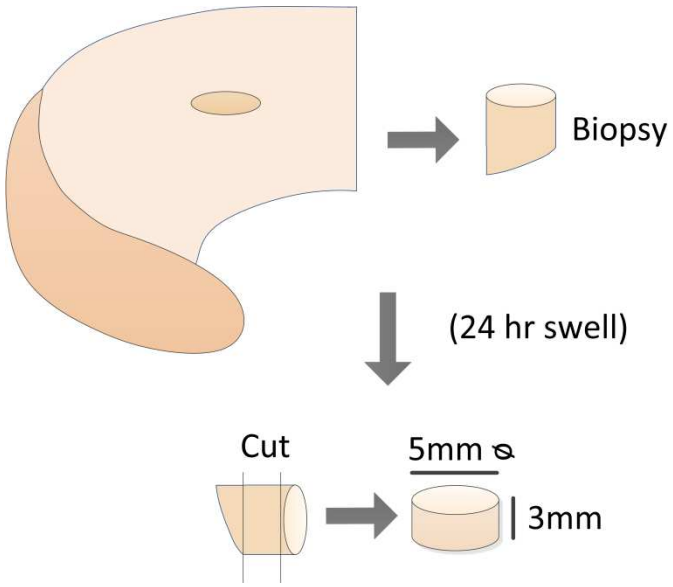

Figure 5-1: Meniscus harvesting and cutting

TPE Hydrogels where created using custom aluminum cylindrical molds. A blend of polystyrene-polyethylene oxide (PS-PEO) and polystyrene-polyethylene oxide polystyrene (PS-PEO-PS) were synthesized as previously described[87], packed between two Kapton sheets, melt pressed in a Carver Press (150°C, 500psi, 10 minutes), allowed to cool to room temperature, and then swollen in 1x PBS for 24 hours prior to testing. Mold dimensions were created such that the swollen cylindrical samples were 3 mm thick and 5mm in diameter. A total of 10 TPE hydrogel samples were used for testing.

5.2.2 Testing Protocol

Samples were mounted with the femoral aspect of the plug exposed using a cyanoacrylate glue between two polished aluminum platens in a heated 1x PBS bath (96-99°F) and tested using a servohydraulic testing system (Bionic Model 370.02 MTS) equipped with a 2lb load cell (Futek LSB200) for measuring axial force. The average thickness was measured using calipers,

and following a 200mN preload, samples were compressed to 12% strain in a sinusoidal waveform for 5000 cycles at 1 Hz representing physiological strains, frequency, and the average daily steps taken by Americans[115,194]. After initial testing, all samples were again stored at 1.6°C in 1x PBS for 24 hours after which the testing protocol was repeated resulting in two tests for each sample.

5.2.3 Data Analysis

A customized MATLAB (Mathworks, Natick, MA) script was used to analyze the data. Modulus values were determined from a linear fit of the 2-10% stress-strain data of each loading cycle. This portion of the data was found to be linear and avoided inconsistencies in data points resulting from a change of direction in loading. A second order power law fit of the modulus vs cycle graph was used to fit the relaxation curve, as has been previously done for biological tissues[195–197]. A one-way analysis of variance (ANOVA) with a post hoc Tukey's test was used to assess differences between the two tests across all regions of interest. If no differences between the two tests were found, samples were averaged. A one way ANOVA was also used to assess differences between regions with values of interest including cycle 1, cycle 10, cycle 25, cycle 50, and the final 5000th cycle as well as the three coefficients from the power law fit (coefficients A, B, and C from Equation 5.1 where x is equal to the cycle and y is equal to the modulus). If no statistical differences were observed across regions, all regions were averaged. Once averaged an ANOVA was used to determine differences across cycles of interest within groups (human, ovine, and TPE hydrogel) as well as differences across groups for both modulus values and coefficients of the power law fit. Significance was set at $p<0.05$.

Equation 5.1: $y = Ax^B + C$.

5.3 Results

The average thickness of the human, ovine, and TPE hydrogel samples was 3.02±0.29, 2.68±1.38, and 2.83±0.06 respectively. The smaller meniscal size of the ovine samples resulted in a number of biopsies not producing a cylindrical sample with a thickness greater than 3mm. In this case, samples were leveled on the proximal and distal aspects to create a uniform sample thickness and still tested to 12% strain accounting for the tissue height. Using a second order power law, the average curve fit had a R^2 value of 0.96±0.04, 0.87±0.1, and 0.99±0.003 for human, ovine, and the TPE hydrogel respectively. No statistical differences were found between the test one and test two, so the two tests were averaged. After averaging the initial and repeat tests, statistical comparisons were performed to ascertain differences between regions for the human and ovine menisci. No statistical differences were found between regions, with respect to modulus (Figure 5-2), or the coefficients from the second order power law fit (Figure 5-3) for human and ovine tissue.

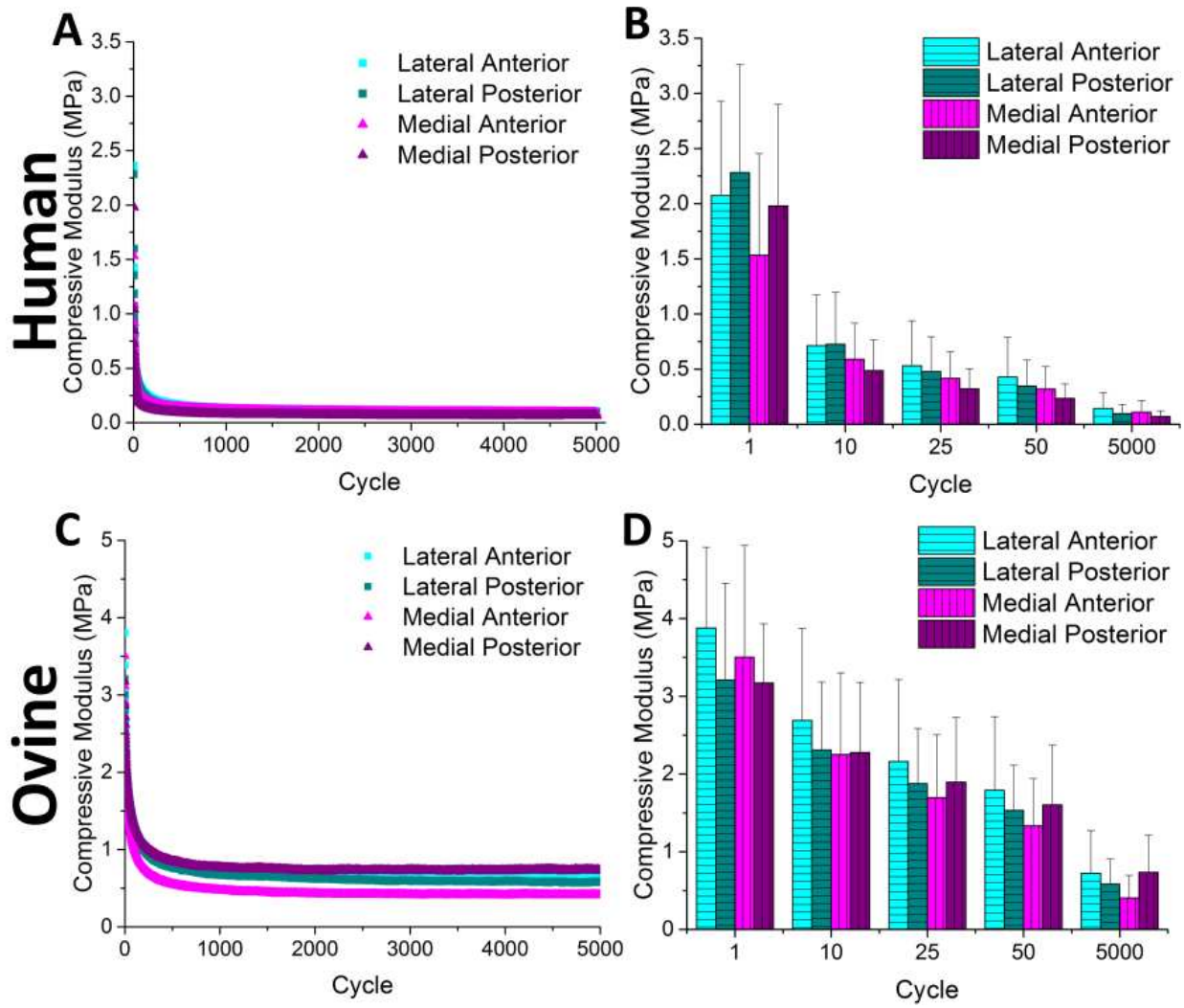

Figure 5-2: Regional compressive modulus vs cycle for human (A, B) and ovine (C, D) meniscal tissue. B and D show compressive moduli (average ± std) after selected numbers of completed cycles (1, 10, 25, 50, and 5000) used for statistical analysis

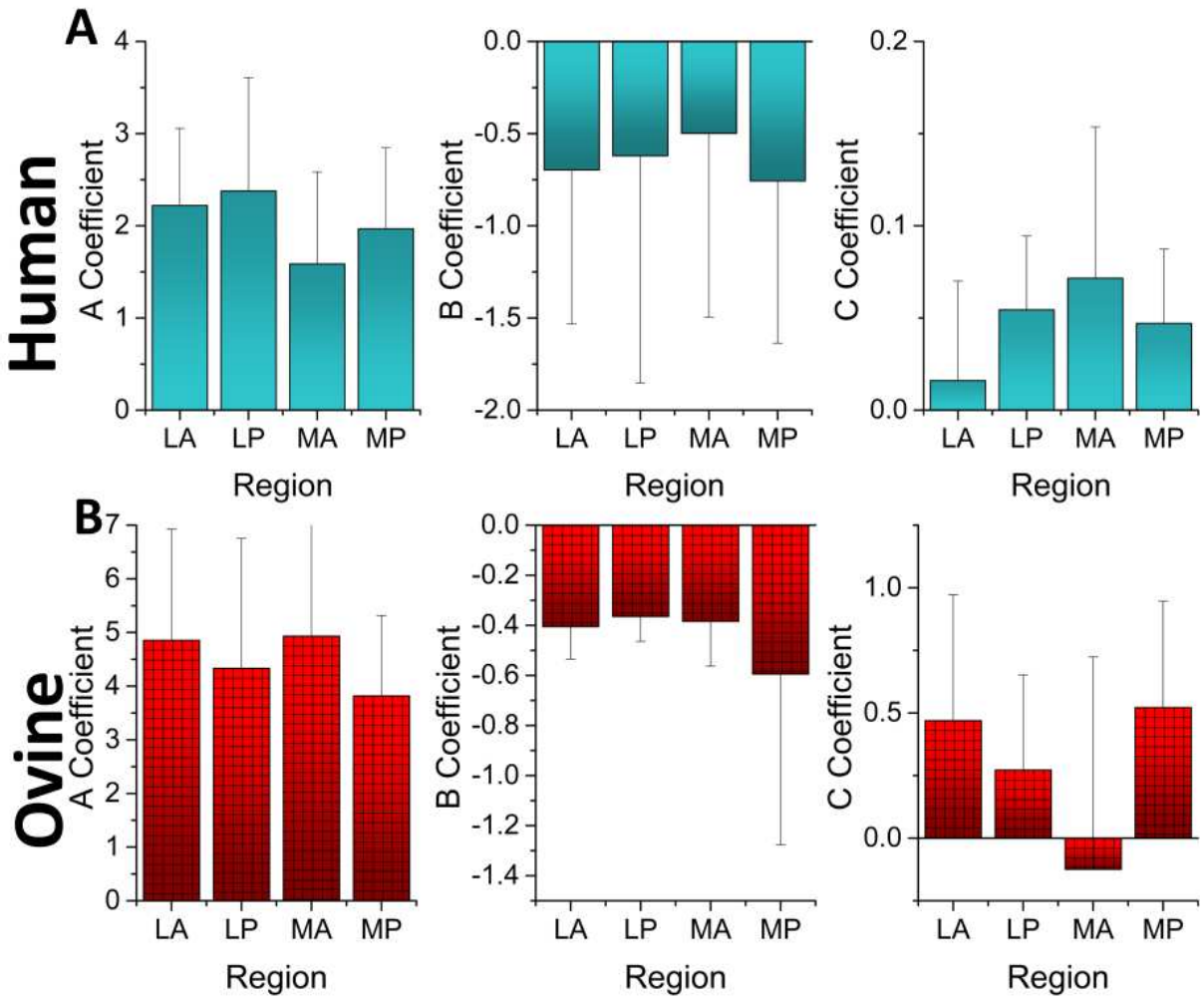

Figure 5-3: Coefficients of power law fit for all regions of human (A) and ovine (B) meniscal tissue. Data shown as an average ± std

Since no regional differences were found in the native human or ovine meniscal tissue, all regions were combined for comparison with the TPE hydrogel samples (Figure 5-4). Rapid relaxation occurred in both the human and ovine menisci with equilibrium typically reached prior to 1000 cycles. With all regions averaged, statistical differences were assessed within groups (human, ovine, and TPE hydrogel) as well as across groups at specific cycles including cycle 1, 10, 25, 50 and 5000. Significant differences were found, with the ovine meniscus having a higher modulus value than both human and the TPE hydrogel at all cycles of interest (Figure 5-5).

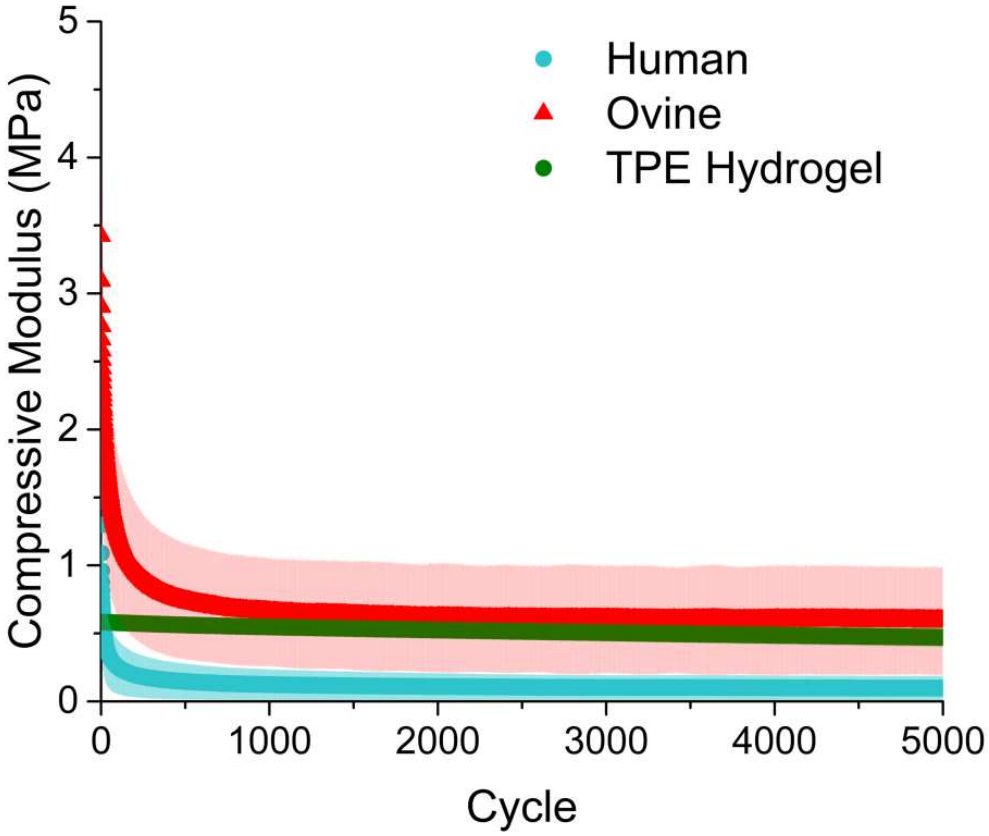

Figure 5-4: Modulus values and relaxation profile across all 5000 cycles (average ± std)

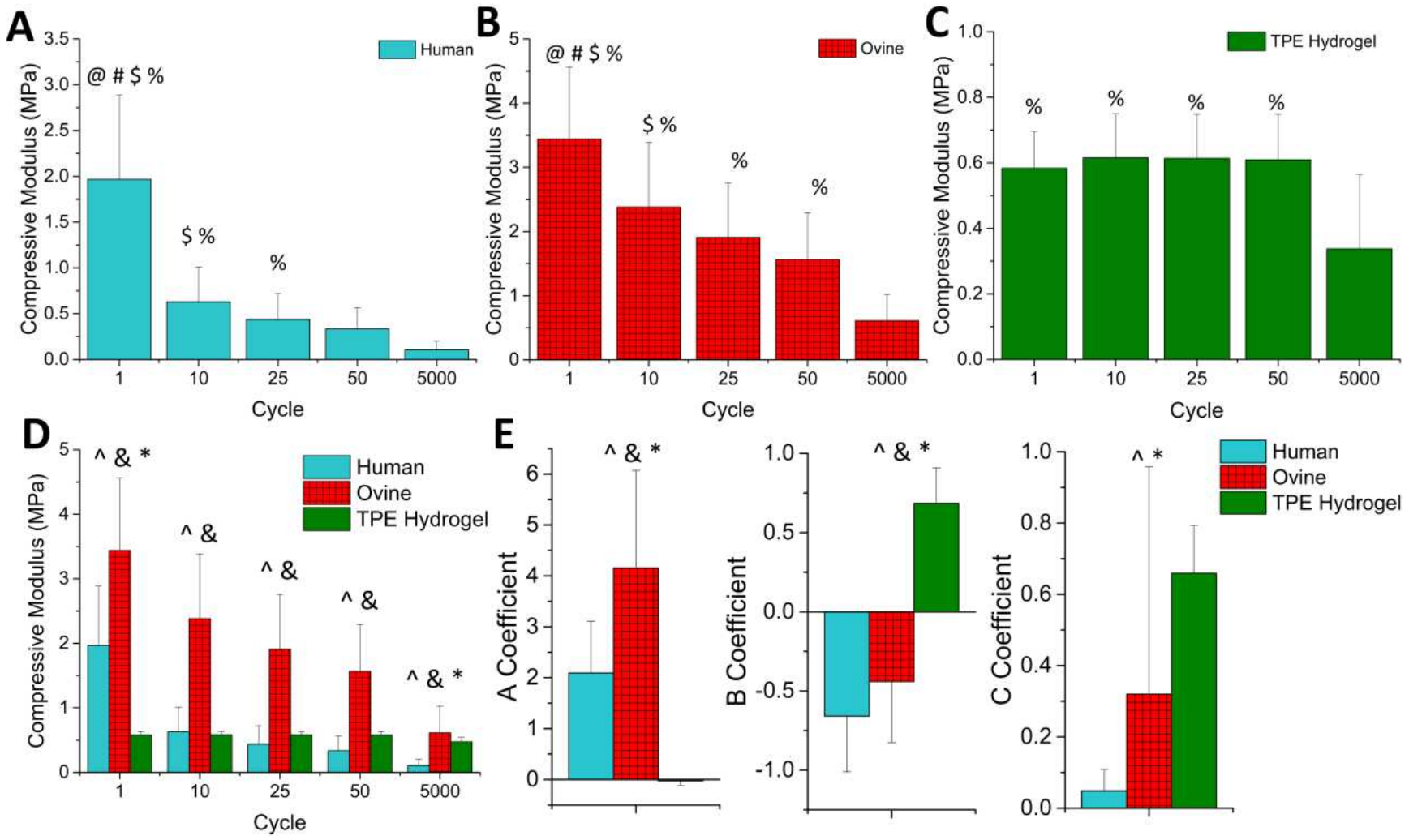

Figure 5-5: Modulus values (average ± std) for cycles of interest for human (A) ovine (B) and TPE hydrogel (C) as well as a comparison of all three groups (D). Coefficients from power law fit (average ± std) for all groups (E). Statistical significance denoted as the following: @ sig diff from cycle 10, # sig diff from 25, $ sig diff from 50, % sig diff from 5000, ^ sig diff between human and ovine, & sig diff between ovine and TPE hydrogel, * sig diff between human and TPE hydrogel

5.4 Discussion

This study is one of the first to investigate the mechanical response of multiple meniscal tissues as well as a potential replacement material under repeated cyclic compression similar to what is experienced *in vivo* over the course of multiple days. It was found that when allowed to rest for 24 hours between cyclic tests, no significant differences were seen in any of the samples with respect to the initial response, relaxation profile, and equilibrium response. Human and ovine menisci were found to be similar in response, but the magnitude of the modulus values for the ovine tissue was greater. The TPE hydrogel material, although often found to be statistically different, had a modulus value between that of the human and ovine for the majority of the 5000 cycle test. The greatest difference between the TPE hydrogel and the two native meniscal tissues was the limited relaxation observed in the TPE hydrogel.

Previous research has reported significant differences between the anterior and posterior regions of meniscal tissue[140], which was not observed in this study. However, a previous report by Leslie et al. reported no significant differences between posterior and anterior values[178], and although our data was not found to be statistically different, it does follow the trend of the anterior region being stiffer than the posterior region as others have shown[152,156]. In the current study, samples were sectioned into anterior and posterior regions, and when possible multiple samples were excised from a single region. While the biochemical constituents responsible for compressive and tensile mechanics have been suggested to be proteoglycans and collagen respectively, it is unclear how the tissue supports cyclic compressive loading.

Modulus values obtained in this study are similar to those previously reported for human and ovine meniscal tissue under alternative compressive testing methods. In a stepped relaxation followed by dynamic sweep study, instantaneous modulus values for human tissue was reported to be ~1MPa and equilibrium values ~0.2MPa with dynamic modulus values in the 0.7-0.8MPa

range, all of which is in agreement with the current study[152]. In a similar study by Bursac et al. the dynamic modulus at 0.2% strain and 1Hz was found to be 1.03MPa which is lower than that seen for the first few cycles in the current study but can be attributed to the lower strain level. In a stress relaxation test of human tissue Chia et al. found instantaneous modulus values of approximately 0.7MPa and equilibrium values approximately 0.08MPa[140] at 12% strain. Less work has been performed to characterize the instantaneous or dynamic response of ovine menisci, but the average 0.6MPa value reported here for the 5000th cycle (representing equilibrium) are similar to existing studies with aggregate moduli ranging 0.2-0.5MPa[154,198]. This leads the authors to believe that although continuous cyclic loading is important to understanding the temporal effects on the tissues and potential replacements, the more conventional single-cycle compressive testing and relaxation testing could stand as a proxy for characterizing the initial and final cycles of such a test. These more conventional tests require far less time allowing for larger sample groups.

It has been well documented meniscal tissue has an initial response vastly different from the equilibrium response likely due to the fluid flow and/or inherent viscoelasticity within the tissue when compressed. It is unknown how much time the tissue requires to return to its fully hydrated, uncompressed state following a compressive cycle. In the current study, a rest period of 24 hours was chosen and the meniscal tissue for both species was able to recover within this time frame. Additional work is necessary to determine the minimal time required and this time frame is likely dependent on the environment. Samples were tested and allowed to re-equilibrate in an unconfined and unpressurized environment which is not totally mimetic of the *in vivo* condition. Future work in this area would benefit from including histological analysis along with mechanical assessments. Comparisons between the relaxation profile of the tissue and the

biochemical composition, specifically glycosaminoglycan (GAG) content, may provide a stronger correlation than purely comparing GAG content to the equilibrium response of the tissue as has been previously done[199].

The current study shows that while ovine meniscal tissue under certain loading conditions is mimetic of human meniscal tissue, there is a statistically significant difference in the cyclic compressive load response. As shown in Figure 5 the human and ovine menisci were found to be significantly different in all areas assessed including modulus values at 5 different cycles throughout the 5000 cycle test as well as all three coefficients from the power law fit. From this data, ovine menisci appear to be stiffer and relax slightly slower than human tissue. Nevertheless, the apparent response across all 5000 cycles shown in Figure 4 is comparable. For this reason the ovine model is still a valid animal model for meniscal work; however, researchers should consider these stiffer properties when assessing translational therapies and replacements. In the case of a meniscal replacement restoring contact mechanics and pressure distribution is likely more vital than precisely mimicking the native tissue mechanics.

Our TPE hydrogel material did not achieve modulus values of the same magnitude as the initial few cycles of either native tissue but relaxed much less than the native tissues as over 5000 cycles. The TPE hydrogel only lost 19% of the initial response compared to the human and ovine tissues which experienced a drop of 95% and 82% respectively. Compressive mechanical deterioration of the menisci has been shown to occur in patients with osteoarthritis and increase with the severity of osteoarthritis[179]. The pathogenesis of the disease and subsequent relationship to the mechanical integrity of the surrounding tissues is still not fully understood. It may be advantageous to design a replacement material that still exhibits some viscoelasticity but does not relax to the extent of the native tissue. The importance of the native tissue's vastly greater

initial modulus compared to the equilibrium modulus as well as the rapid relaxation of the tissue has not been investigated. For this reason, the TPE hydrogel tested in this study may still be a viable material option for future meniscal replacements. The nature of this TPE hydrogel sets it apart from previous materials as it allows for long-term shape preservation and tunable swelling[87] while more closely matching native meniscal properties compared to other replacement technologies which often exceed the native tissues compressive mechanics[68,82].

All TPE hydrogel samples used within the scope of this study were produced from a single batch polymerization and as such the variance from sample to sample was extremely low. In contrast, meniscal samples were taken from a range of donors leading to greater sample to sample variance. Ultimately, if this material is to be considered for potential meniscal replacement a more thorough assessment of mechanical properties should be conducted as well as an evaluation of batch to batch variance and cytocompatibility. Another limitation of the current study is human samples were healthy but were collected from a more elderly population. A clear link has yet to be discovered between tissue age and mechanics, as it is difficult to divorce joint changes resulting from age, genetics, obesity, and altered joint kinematics. However, increased severity of visual tissue degradation associated with OA has been shown to result in decreased compressive properties of human meniscal tissue[179], and tissue degradation along with OA prevalence is more common in elderly populations[200].

In conclusion, this study found that although ovine menisci are statistically different from human they do have similar relaxation trends when comparing cyclic compressive mechanic properties. This, in combination with previous literature, supports the use of ovine as a large animal model for the human meniscus condition. However, researchers should bear in mind the modulus differences between the two species when choosing to use an ovine model for meniscal

studies. The TPE hydrogel material tested had a similar average modulus to the human tissue and ovine tissue but did not experience the same rate or degree of relaxation across the 5000 cycles tested. Without a clear understanding of the importance of this relaxation phenomenon, it is hard to conclude if the TPE hydrogels lack of relaxation would prove disadvantageous or not. Implanting the TPE hydrogel in the ovine joint and evaluating the long-term effects of joint protection is necessary to determine its viability as a material option for meniscal replacement.

CHAPTER 6:
3D CONSTRUCT CREATION AND IMPLANTATION

6.1 Introduction

Menisci are fibrocartilaginous tissues which sit between the femur and tibia and function primarily as load distributors within the knee[14]. Meniscal damage has been shown as a result of trauma as well as age-related degradation so it affects individuals of all ages[180]. Since the majority of the meniscus is avascular and will not heal following injury, the most common surgical procedure to address meniscal damage remains a partial meniscectomy. This treatment method can temporarily relieve the patient from pain, but individuals are at a higher risk for later development of osteoarthritis (OA) [201,202]. Therapies and surgical strategies for meniscal repair are being investigated[203], but there remains a need for additional research into the development of a meniscal replacement.

Any potential meniscal replacement has a number of design requirements that must be met in order for it to be successful in vivo. The first issue is finding a material that has similar enough material properties that it can withstand the loading regime of the knee. This becomes a balance between a material that can withstand the loading environment and prevent neighboring tissue damage but also is not over-engineered to the point where the replacement causes stress shielding. The second design aspect to consider is recreating the proper 3D geometry of the meniscus. Donahue et. al. has previously shown the importance of geometric and shape factors in maintaining tibio-femoral contact pressures[204,205]. Once an appropriate material is selected and molded to the shape of the native meniscus it is important to consider the role of the meniscal attachments and how the replacement will be implanted into the joint. In the native tissue the meniscal entheses are important in transferring hoop stresses of the native tissues into the

underlying tibial plateau[20], and while the importance of replicating this exact gradual transition from soft to hard tissues may or may not be necessary implantation method of the replacement is important. Lastly, once implanted into the joint the replacement needs to be able to withstand physiological loading and properly distribute load within the knee joint.

This study aims to investigate the feasibility of a number of the aforementioned design requirements. Preliminary work suggests that one material worth investigation as a potential meniscal replacement is a thermoplastic elastomer (TPE) hydrogel created from a polystyrene-poly (ethylene oxide) (PS-PEO, SO) diblock and a PS-PEO-PS (SOS) triblock copolymer blend at a concentration of 72 mol% triblock[139,206]. This material to date has only been created in relatively simple flat shapes, so the ability to create a more complex meniscus-shaped construct will be explored. Once a 3D meniscal construct is created, techniques for implanting the construct into an ovine joint will be investigated. It is hypothesized that a geometrically memetic medial meniscus can be created using imaging and negative molding techniques and this construct can be implanted and fixed into an ovine stifle joint.

6.2 Methods and Results

6.2.1 Simplified Proof-of-Concept

Initially, the native meniscus geometry was dramatically simplified to a crescent wedge shape (Figure 6-1A). While accounting for hydrogel swelling, a preliminary negative mold was created. Simulated Polypropylene material (Durus RGD430, Stratasys Ltd., United States) was used in conjunction with a 3D printer with polyjet technology (Objet30 Pro, Stratasys Ltd., United States) to create the negative mold (Figure 6-1A). The mold was designed such that the meniscus would have a dry height of 3 mm and a cross-sectional width of 5 mm. The mold was

packed with SOS46, melt pressed at 75°C under 10psi for 30 minutes, and then cooled in a freezer. Once the mold was cool to the touch, the dry polymer meniscus was removed and swollen in DI water overnight. The resulting hydrogel was approximately three times the size of the dry polymer with a size and shape similar to the sheep meniscus (Figure 6-1B and C).

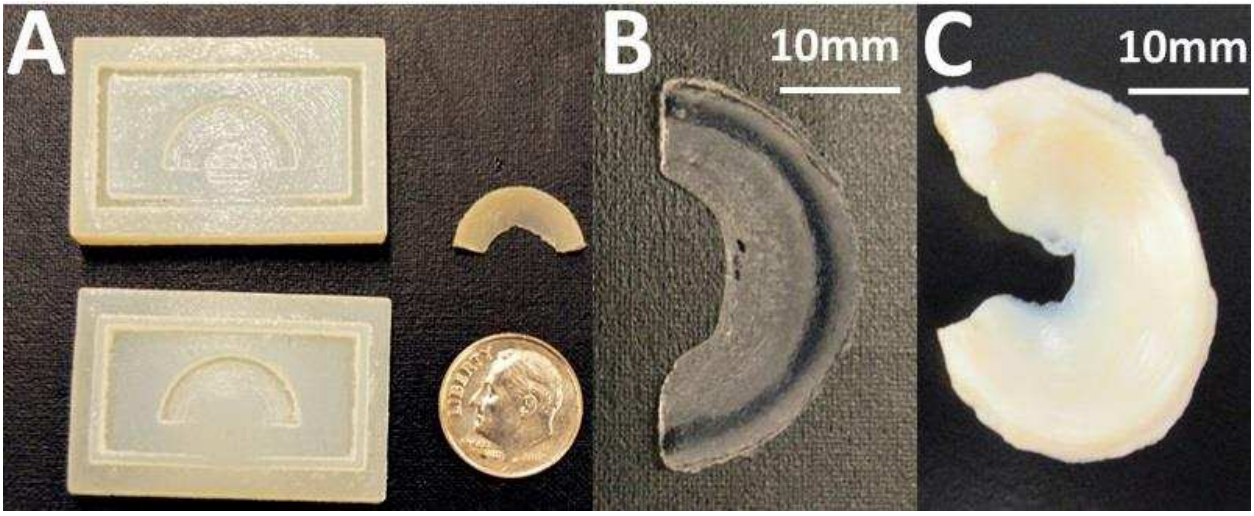

Figure 6-1: Initial proof of concept compression molding experiments validating the ability of the hydrogel polymer to be molded into a crescent shape and swollen to match the size of actual meniscal tissue A) 3D printed negative mold and melt pressed TPE dry polymer construct B) swollen TPE hydrogel construct C) ovine medial meniscus

While the simplified crescent-shaped construct was a good proof of concept and preliminary step, a more accurate replica of the shape of the native meniscus is necessary to properly distribute load from the femoral condyles to the tibial plateau. This will overcome a significant limitation to existing scaffolds which is their non-unique and non-mimetic geometry. Advances in image technologies enable us to better capture the true shape of the tissue.

6.2.2 Negative mold creation

Imaging software was implemented to create a more accurate meniscal construct. The medial meniscus of an *Ovis aris* Rambouillet X Columbia breed stifle joint was excised and scanned via micro-computed tomography (µCT) (Scanco mCT 80, Scanco Medical AG, Brüttisellen, Switzerland) with a voxel size of 18µm, voltage of 70kV, and integration time of

500ms. 3DSlicer (Slicer v4.8) was used to convert the DICOM images to a 3D-rendered surface. A mesh of that surface was prepared in open source software MeshLab and using the built-in quadratic edge collapse decimation. The number of faces was reduced from over 10,000 to 200 bringing the resolution down to a 3D printable range (Figure6-2). A Laplacian smoothing function with three smoothing steps, one-dimensional boundary smoothing, and cotangent weighting removed all small artifacts. Internal structures and overhangs were adjusted by hand using open source software MeshMixer (MeshLab v2) and Blender (Blender Foundation v2.7.7), respectively.

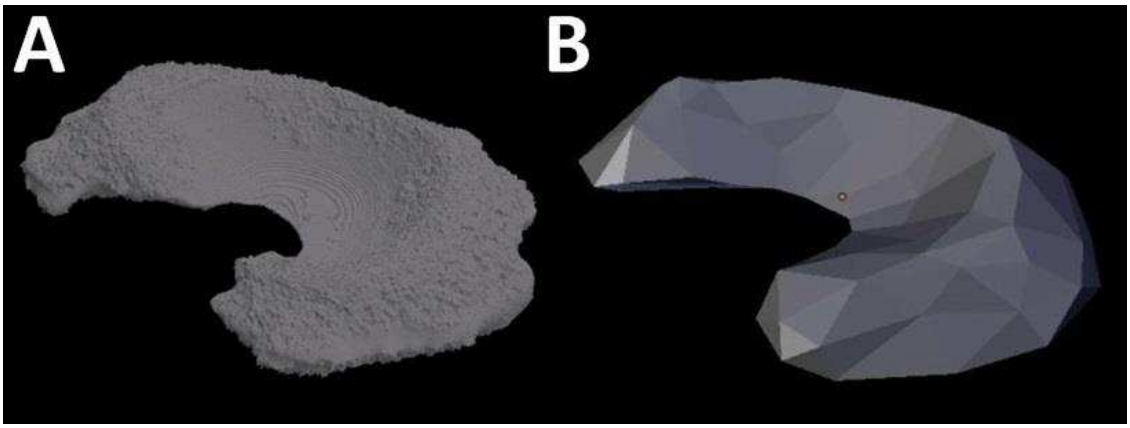

Figure 6-2: μCT of medial ovine meniscus A) original 3D rendered surface B) 3D rendered surface after processing

Once reduction, smoothing, and shaping were complete, SolidWorks (Dassault Systems, SolidWorks Corporation, USA) was used for creating the actual negative molds. First, a parting surface was created which allowed a positive and negative draft of the 3D rendered surface. Original molds were two-part molds which included voids for cylindrical plugs that would later be used for construct implantation (Figure 6-3). All molds were printed using a Prusia i3 maker select 3D printer (Monoprice, Brea, CA model 15.01) and 1.75mm diameter filament. Open source slicing software Cura 3D (v 2.1.3) was used for g-code generation.

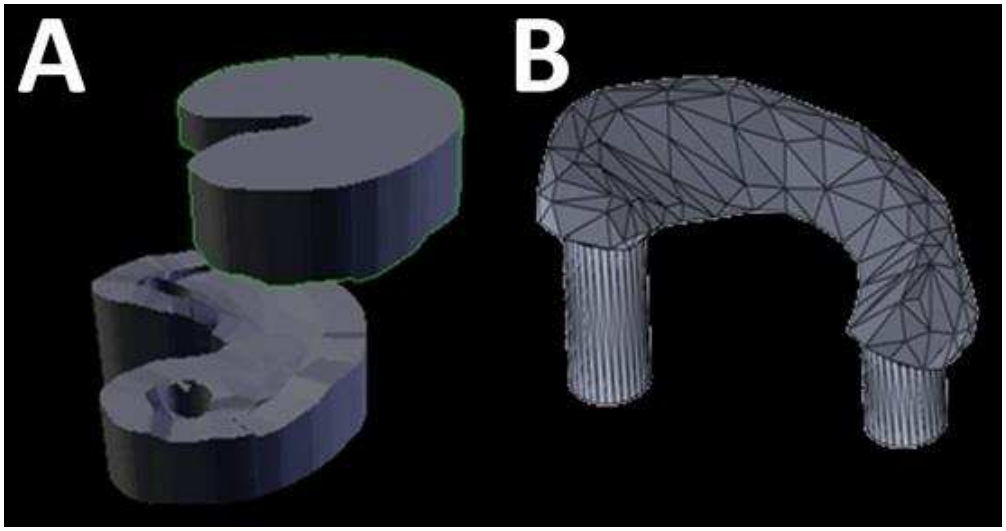

Figure 6-3: Molding A) original negative mold B) positive mold shape

The first molds created were two-part molds printed from polylactic acid (PLA) with an infill density of 75% and printing temperatures of 200°C and 50°C for the extruder and bed respectively. PLA was the initially chosen material for ease of printing and smoother finished surface. However, the glass transition temperature of PLA is ~65°C which limited the melt pressing processes. At temperatures lower than 65°C the mold withstood processing but the TPE polymer material did not melt. When temperatures were raised, the mold deformed and collapsed (Figure 6-4A). The second material used was acrylonitrile butadiene styrene (ABS) which has a much higher glass transition temperature of 105°C (Figure 6-4B). ABS molds were printed with an 85% infill density with a base plate temperature of 70°C and an extruder temperature of 250°C. Molds from this iteration maintained their shape during processing, but the TPE polymer material did not easily release from the mold resulting in rough and distorted edges. To avoid the TPE polymer material from adhering to the mold, all molds were coated with an aerosol dry wax lubricant (DuPont Teflon multi-use lubricant, Dupont)

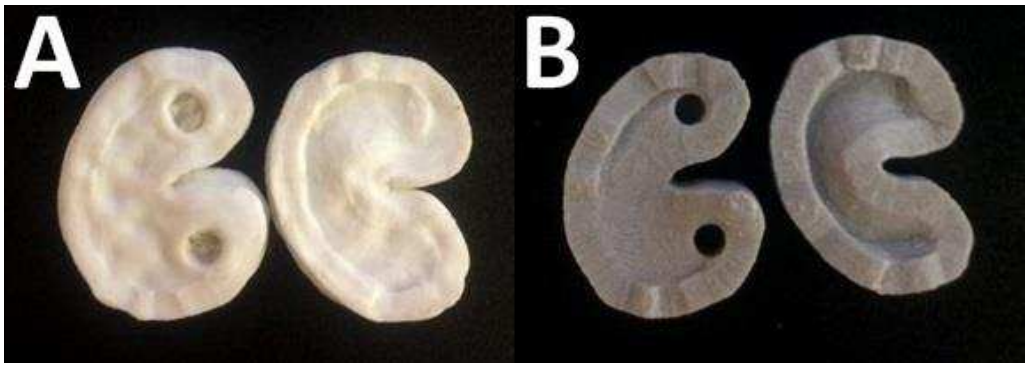

Figure 6-4: Molding A) original negative mold B) positive mold shape

Finally, the parting surface was extended to provide a larger plane and a raised/recessed feature which helped to prevent mold slippage during processing. To aid in the removal of the melt-pressed TPE construct, with intact anterior and posterior tabs, the distal half of the mold was split along a plane which bisected the two tab voids resulting in a three-part mold (Figure 6-5). This three-part mold was composed of part one, the proximal or top halves of the construct, part two, the distal interior portion of the mold, and part three, the distal periphery mold portion. To better align the two distal halves, three pegs sized 4mm in diameter and extruded 4 mm normal to the split plane were added to the left, center, and right of part two. In corresponding locations on part three, 5mm in diameter and 5mm deep holes were created allowing the two parts to fit together. A full list of printing parameters can be found in Table 6-1.

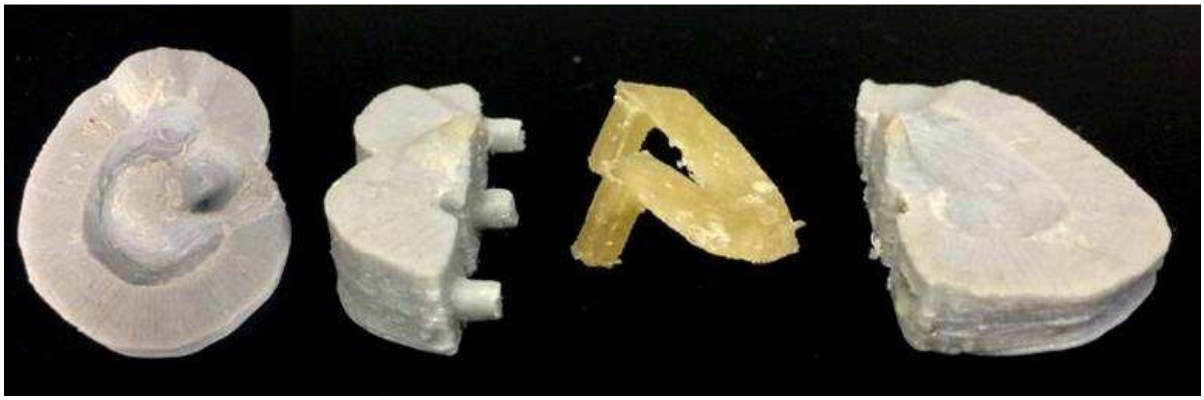
Figure 6-5: 3 part mold (left to right) part one proximal half, part two distal interior, melt pressed TPE construct, part three distal periphery.

Table 6-1: 3D printing parameters

Shell	Wall Thickness	0.8 mm
	Top/Bottom Thickness	0.8 mm
Infill	Density	85%
Material	Layer Height	0.06 mm
	Printing Temperature	250°C
	Bed Temperature	70°C
	Diameter	1.75 mm
	Flow	107%
Speed	Print Speed	60 mm/s
	Infill Speed	80 mm/s
	Outer Wall Speed	30 mm/s
	Inner Wall Speed	60 mm/s
	Top/Bottom Speed	15 mm/s
	Travel Speed	120 mm/s
Support	Placement	Everywhere
Raft Adhesion	Air gap	0.3 mm
	Initial Layer Z Overlap	0.15 mm
	Raft Top Layers	2

Although this method of mold creation could be implemented for patient-specific molds, production time and cost may be inhibiting. Thus, to reduce production time and cost, specific measures were implemented to accommodate joints of differing limbs and sizes. Blender was used to create a mirror image of the mold which provided a right and left medial meniscus option. Molds were also scaled to 50% to accommodate the swelling ration of the SOS72 TPE polymer material and printed in 3 sizes, a small, average, and large. Swollen these sizes scaled to 90%, 100%, and 110% the size of the originally imaged meniscus to accommodate variation in knee joint sizes. Finally, to prevent distortion of the molds from melt processing, molds were used for a maximum of two rounds of processing.

6.3 Implantation

The implantation approach mimicked the double bone plug technique common to meniscal allografts[207]. In native tissue, this approach allows for the native attachments and the soft to hard tissue gradation to be maintained while sutures are used to pass the plugs through bone tunnels created in the tibia. While the 3D TPE construct has no material gradation, a similar approach is still useful. If sutures were used to pass the soft TPE hydrogel through bone tunnels, the sutures would likely pull through the hydrogel construct. To circumvent this, PLA tabs were 3D printed and used as an outer shell for the TPE hydrogel plugs. With the TPE plugs encased in these hard PLA tabs, sutures could be passed through the tabs rather than the TPE plugs and used to aid in inserting the construct into the joint space. The inner diameter of the PLA tabs were designed to be 5 mm and equal to the swollen size of the TPE plugs with the outer diameter being 6mm and equal to the bone tunnel diameter. This design allowed for the TPE plugs to be swollen into the tabs and the tabs to be press fit into the bone tunnels, thus requiring little tensioning of sutures through the bone tunnels in order to maintain the position of the main body of the 3D TPE construct.

Preliminary implantation was performed on disarticulated ovine joints with excess musculature removed. The medial meniscus was excised and transosseous tunnels were created at the former insertion sites using an inside-out anterior approach for the anterior insertion and an inside-out posterior approach for the posterior insertion. A 3mm drill bit was used to create a pilot hole, followed by a 6mm bit to expand the tunnel. Tunnels were initially oriented such that the exit of the anterior tunnel was on the antero-medial tibia while the posterior tunnel exited at the postero-medial tibia. This orientation was selected to reduce strain on the plugs which were extending from the meniscal main body at 90° angles (Figure 6-6). Visually the 3D TPE

construct appeared similar in size and location to the native medial meniscus (Figure 6-6). However, when attempting this implantation with the collateral and cruciate ligaments intact, or in a non-disarticulated joint, it was challenging to create the bone tunnels in this orientation even with all excess musculature removed.

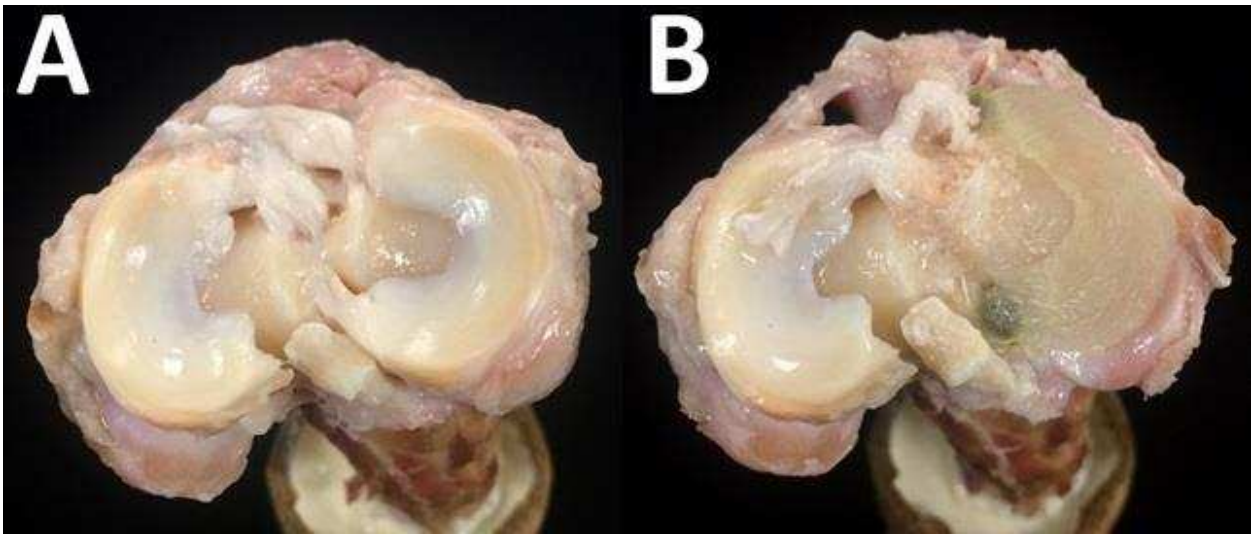

Figure 6-6: Superior view of ovine tibial plateau A) intact native menisci B) medial meniscus replaced with 3D TPE construct (tabs were created with a bright yellow/green PLA which can be seen in the image).

Molds were redesigned to accommodate a posterior tab which extended from the main body of the meniscus at a 45° angle as compared to the previous 90° angle while the anterior plug was maintained at the 90° angle. This adjustment allowed the bone tunnel orientations to be adjusted so they were more similar to a common surgical technique for bone anchors on allografts[208,209]. Tunnels were created in the same manner as previously described; however, the posterior tunnel now originated from near the native attachment site (PCL restricted exact overlap) and exited in the antero-medial tibia (Figure 6-7C). The 3D TPE constructs were swollen to equilibrium and then inserted into the joint along the periphery from the posterior aspect of the joint. The anterior tabs were initially threaded through the space between the MCL and the condyle with the interior of the rim of the construct angled downward and the main body

wrapped around the posterior aspect of the condyle. This insertion approach was made possible by placing the knee joint in high flexion (between 120-140° flexion) and creating the largest gap between the MCL and articulating surfaces. The posterior tab was then inserted into the posterior bone tunnel and the anterior tab was lightly tensioned to pull the entire construct into place and secured by anchoring into the anterior bone tunnel. The primary means of anchoring was accomplished through friction of the plugs/tabs within the bone tunnels, but light tensioning of the sutures was applied and the two sets of sutures (anterior and posterior) were tied together on the antero-medial tibia. Once the meniscal replacements were inserted into the joint, the knees were able to go through an extension-flexion range of motion.

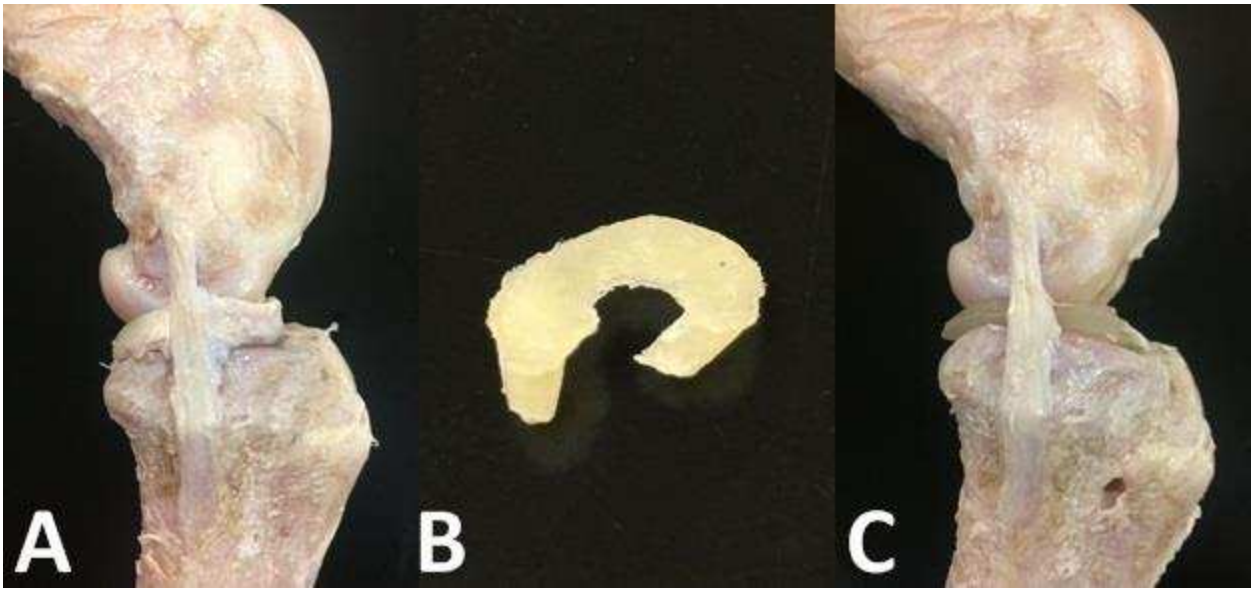

Figure 6-7: A) left ovine stifle with native medial meniscus B) dry 3D TPE construct with a 45 posterior plug and a 90 anterior plug C) Swollen 3D TPE construct implanted into ovine joint (antero-medial tibia exit location of posterior tunnel visible).

6.4 Discussion

This study clearly showed that our TPE hydrogel can be molded into a shape that is mimetic to the native medial meniscus and can be implanted into an ovine joint. Furthermore, this molding process allows for scalability so constructs can be created in a variety of sizes to

accommodate variance in limb sizes. The user has a great deal of control over the final construct geometry and size which is advantageous from a customization and optimization standpoint. Standards and protocols can easily be written for face reductions, smoothing, and sizing, but it is more challenging to standardize the elimination of overhangs and the precise location of tab extensions to reliably be able to have two users create identical molds. No optimization or repeatability studies were conducted on the creation of molds.

A benefit to using an ABS based mold is the rapid and inexpensive prototyping which can be done. If these molds were to be metal or ceramic cast, that would allow for more stable molds, but would also increase the time and financial cost of creating slight variations for either patient specific molds or for creating a variety of molds for an optimization study. The materials and 3D printer used were commercially available and represent low-cost printing options. It may be beneficial for future work to investigate the overall loss in volume due to the reduction of faces and smoothing. If a significant loss is occurring a more precise, but still commercially available and cost-effective, 3D printer could address some of these issues.

There are a number of limitations to this implantation approach, which will need to be addressed prior to transitioning to an *in vivo* animal study. Most significant is the amount of musculature which was removed to allow access to the joint. Images from Figure 6-7 were taken from pilot work where all musculature was removed, but subsequent *in situ* studies were still performed with large portions of muscle tissue excised. Most of the flexor and extensor muscles of the tarsus and the digit which attached to the tibia were retained up to ~60 mm from the stifle joint line and portions of the M. vastus medialis, specifically where it intersects with the patella, were also retained; but otherwise the majority of musculature was removed and the joint capsule was opened. For the purpose of the *in situ* studies, this approach was considered acceptable in an

effort to retain the native attachments of the MCL. However, implantation in an in vivo setting will require additional consideration. Furthermore, to create enough space within the joint to remove the native meniscus sand implant the 3D TPE construct the joint was flexed beyond that which is possible in an *in vivo* animal model. Moving into an *in vivo* model it is likely that the MCL will need to be released with a bone block to open up the medial compartment similarly to what has been previously reported for ovine allograft and replacement studies[80,208,210]. Lastly, the surgical instrumentation that would be used would likely dictate an outside-in approach for the posterior bone tunnel.

This study represents one of the first studies where a geometrically accurate full meniscal construct was created from a hydrogel material and implanted into a joint. Previous studies have opted for a simplified crescent, wedge shape similar to what was presented as a proof of concept in the current study, but have not identified ways to successfully create more mimetic replacements[211,212]. Similarly, more complex memetic meniscal constructs have been created but means of attachment and implantation methods have not been investigated[213,214]. Our construct was created using primarily all open source software and off the shelf, cost-effective materials and 3D printer. Others have directly printed a 3D hydrogel menisci, but they have had to modify printers to have a syringe pump for dispensing their solution based hydrogel material[214]. Our material has the added benefit of being a thermoplastic elastomer and could potentially be directly 3D printed in the dry state. Additionally, this method for utilizing imaging software to create a solid model of the meniscus as well as the methods used for negative mold creation could also be implemented for the creation of other soft tissue structures.

CHAPTER 7:
HOW A NOVEL HYDROGEL MENISCAL REPLACEMENT RESTORES KNEE JOINT PRESSURE AND DISTRIBIBUTION IN AN OVINE MODEL COMPARED TO THE NATIVE MENISCUS

7.1 Introduction

The menisci play a vital role in knee biomechanics and distribution of pressure during both stance and locomotion. Removal of meniscal tissue has consistently been shown to increase peak and mean contact pressures and decrease contact area[215–217]. These pressure distribution changes can, in turn, lead to osteoarthritis, a degenerative disease of the underlying articular cartilage, which is why total meniscectomies are no longer common clinical practice[27,218]. Rather than simply removing the entire meniscus, efforts have been made to repair or replace the damaged tissue[219,220].

One of the more common replacement approaches includes tissue engineering and the use of scaffold material as a base for new tissue deposition[221–223]. Menaflex CMI (Collagen Meniscus Implant, ReGen Biologics Inc., Cary, NC, USA) and Actifit® (Orteq Bioengineering, London, UK) are two clinically available scaffolds. The Menaflex CMI is a collagen matrix scaffold and the Actifit® is a polyurethane scaffold, but both are porous crescent-shaped wedges allowing for ingrowth of fibrovascular tissue before ultimately degrading themselves. However due to the limited blood supply, researchers have found it challenging to achieve a tissue-engineered replacement which maintains its mechanical integrity within the joint over time and scaffold collapse, lack of tissue ingrowth, and scaffold tearing have all been reported[76–78]. Thus, others have investigated inert replacements for the meniscus.

The only clinically available inert replacement is the NuSurface® (Active Implants, LLC., Memphis, TN, USA). Short-term clinical results are promising, however, this

polycarbonate-urethane implant has material properties that are very different from the native tissue and it is a free-floating replacement thus requiring a healthy meniscal rim for implantation[68]. For this reason, it could be advantageous to develop an inert meniscal replacement material which is mimetic of the native meniscus, and upon implantation results in a similar pressure distribution to the underlying articular cartilage as the native meniscus delivers.

Contact mechanics and pressure distribution have been widely studied in the human cadaveric knee[9,11,224–228]. However, when developing replacement technologies, an *in vivo* large animal model is necessary for evaluation prior to clinical trials. Ovine models have been found to have a similar anatomy[192,193,229,230] and similar meniscal material properties to those of humans[139,154]. For this reason, the ovine model has been used frequently when studying meniscal replacements and scaffolds[72,77,80,191,216]. Two technologies commonly used to measure tibiofemoral pressure distribution include prescale pressure sensitive films and electronic sensors. Pressure sensitive films such as Fuji® film is advantageous from a shape perspective since the film can be cut to fit the unique shape of the knee joint but only provides singular static readings so the film must be replaced between load and angle changes. Electronic sensors such as Tekscan® have the ability to take dynamic measurements and do not need to be replaced during knee motion and loading. Tekscan® has also been reported to be more reproducible and reliable and is now commonly used in the biomechanics community[231].

One material of interest as a meniscal replacement is a thermoplastic elastomer (TPE) hydrogel that has been mechanically characterized in prior studies and has some similar material properties to the native meniscus as well as the ovine meniscus[139,206]. Due to its thermoplastic nature not only can this material be molded into a meniscus-like shape during the melt phase and retain that shape after swelling, it also has greater fatigue resistance compared to traditional

hydrogels which tend to be very brittle at low strains[110]. Although the bulk compressive and shear properties are comparable, ultimately any meniscal replacement needs to be able to successfully transfer load and distribute pressure to the underlying articular cartilage when implanted into the knee joint. The objective of this study was to assess the native pressure distribution of the ovine knee meniscus and compare mean and max pressures as well as contact area from the native condition to a medial meniscectomy and three treatment conditions including a novel TPE hydrogel construct. Specifically, the three treatment conditions will include a suture repair of the native meniscus, an allograft from a donor limb, and the TPE hydrogel construct. It is hypothesized that a medial meniscectomy will result in increased contact pressures and decreased contact areas primarily in the medial hemijoint and that all three treatment conditions will improve upon the meniscectomy condition and restore contact area and pressures to that of the native intact condition.

7.2 Methods

7.2.1 Dissection

Seven female ovine (*Ovis aris* Rambouillet X Columbia breed) limbs were harvested from animals euthanized as part of unrelated studies which were approved by the local animal use ethics committee. Animals were between 3-4 years old and weighed between 63-90 kg. Limbs were immediately removed of skin, excess musculature, and amputated 135mm from the knee joint line on the tibia and 145mm from the joint line on the femur. Once dissected, with the knee joint synovial sac intact, limbs were frozen for later testing.

Prior to testing, joints were allowed to thaw overnight under refrigeration. The quadriceps complex and patella were peeled back exposing the stifle joint. The femoral attachment of the

lateral collateral ligament was located and a pilot hole drilled 6mm above the attachment. Subsequent enlargements were made until the through hole was 10.5mm in diameter. The tibial plateau and posterior aspect of the femoral condyles were used as guides with the direction of the tunnel running parallel to both. A second hole parallel to the first with an end diameter of 10.5mm was created in a similar fashion 80mm from the condyle hole centered in the femoral shaft. The second hole was created using accustom upper flexion fixture to ensure alignment. The limb was set to a flexion angle of 60 degrees and potted using Smooth Cast 321 (Smooth-On, Easton, PN). Polyethylene thread was tied around the dissected quadriceps complex providing an anchoring point for a 10lb weight to be used for patella tensioning.

7.2.2 Tekscan Calibration

Contact pressure and area were measured with thin film piezoelectric pressure sensors (K-scan model 4041, Tekscan, South Boston, MA, USA). These sensors are created by overlaying a series of rows and columns creating a matrix of intersecting points, or sensels. For the sensors, each of the two prongs has a total of ninety $1mm^2$ sensels from which temporal changes in electrical charge due to loading can be gathered and based on calibration back calculated for pressure readings. The choice of a calibration method for Tekscan sensors has been reported to affect the accuracy of readings[232,233], so a custom 12 point calibration curve was utilized along with sensitivity adjustments within the Tekscan software for each sensor independently. This calibration approach was found to result in the least amount of error. Sensors were placed stacked between two leather covered metal plates and loaded using a servohydraulic test system (Bionic Model 370.02 MTS Corp., Eden Prairie, MN) to their max pressure of 13.79MPa. All loads were removed from the sensor and then slowly reapplied until all sensels were reading load. In addition to this minimum pressure reading, readings were taken at

0.54MPa, and from there in increments of 1.08MPa up to 13.46MPa. Custom written Matlab (Mathworks, Natick, MA) code was then used to average all raw value sensel readings and create a calibration curve from a linear interpolation of the applied pressure vs average raw values. Raw values from subsequent *in situ* testing were applied to this curve to ascertain the apparent pressure at each individual sensel.

7.2.3 Testing Fixture

Limbs were tested in a custom fixture designed to fix flexion angle of the femur but allow for natural orientation of tibia with respect to the femur using a universal joint and platform with medial-lateral and anterior-posterior translations (Figure 7-1). Limbs were tested at 45°, 60°, and 75° which cover the active range of motion of a sheep during gait[234–236]. At each angle loads ranging from 0-181 kg were applied in increments of 22.7 kg effectively testing the unloaded condition through at least 2x bodyweight encompassing previously reported *in vivo* peak loading conditions[234,235,237]. To ensure positioning was consistent across testing conditions, location markers were used to maintain medial lateral translation, varus valgus rotation, and internal and external abduction compared to the native intact condition.

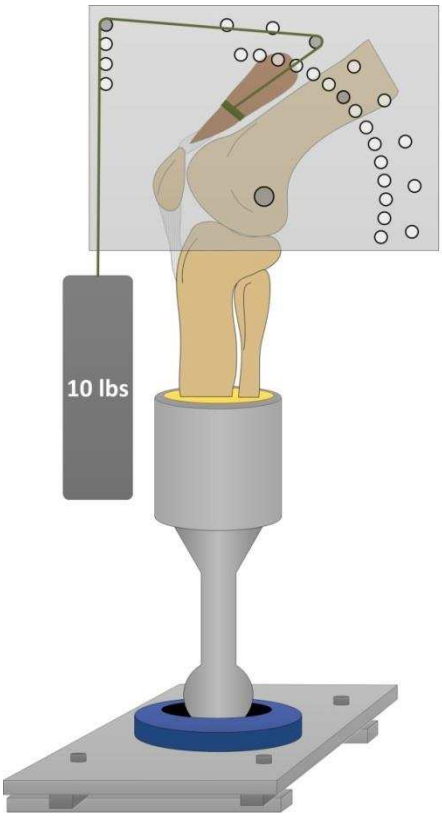

Figure 7-1: Custom testing fixture for Tekscan pressure distribution assessments with translation in the anterior-posterior and medial-lateral as well as universal joint

7.2.4 Tekscan Implantation

Sensors were covered with polypropylene film to prevent delamination due to moisture exposure. The lateral long digital extensor tendon was excised to allow sensor insertion. Likewise, the synovial capsule attachment to the menisci was severed such that sensors could be placed in both the medial and lateral hemijoints under the menisci on the articulating surface of the tibia. Polyethylene threads were passed through the joint space and used to pull sensors into place. Sensors were positioned such that the anterior medial aspect of each of the two prongs aligned with the anterior attachments of the menisci. Tekscan sensors remained within the joint during testing of each condition but were realigned between angels and removed and realigned between conditions. No additional sutures or adhesive were used to maintain sensor position.

7.2.5 Testing Conditions

All limbs were subjected to a total of 5 conditions: intact, medial meniscectomy, suture repair of the native excised medial meniscus, medial meniscus allograft transplant, and an implantation of our novel 3D TPE meniscal construct (Figure 7-2). For the meniscectomy condition, a scalpel blade was used to sever the native entheses as close to the insertion site as possible. Additional cuts were made to free the medial meniscus from the medial collateral ligament (MCL) while keeping the MCL fully intact. Following the meniscectomy testing condition, two bone tunnels 6 mm in diameter were created originating as near the native attachment sites as possible and exiting in the anteromedial aspect of the tibia. All treatment conditions were pulled around the femoral condyles from the posterior aspect between the MCL and joint space, the sutures were passed through the bone tunnels, and secured via suture knots on the anteromedial aspect of the tibia.

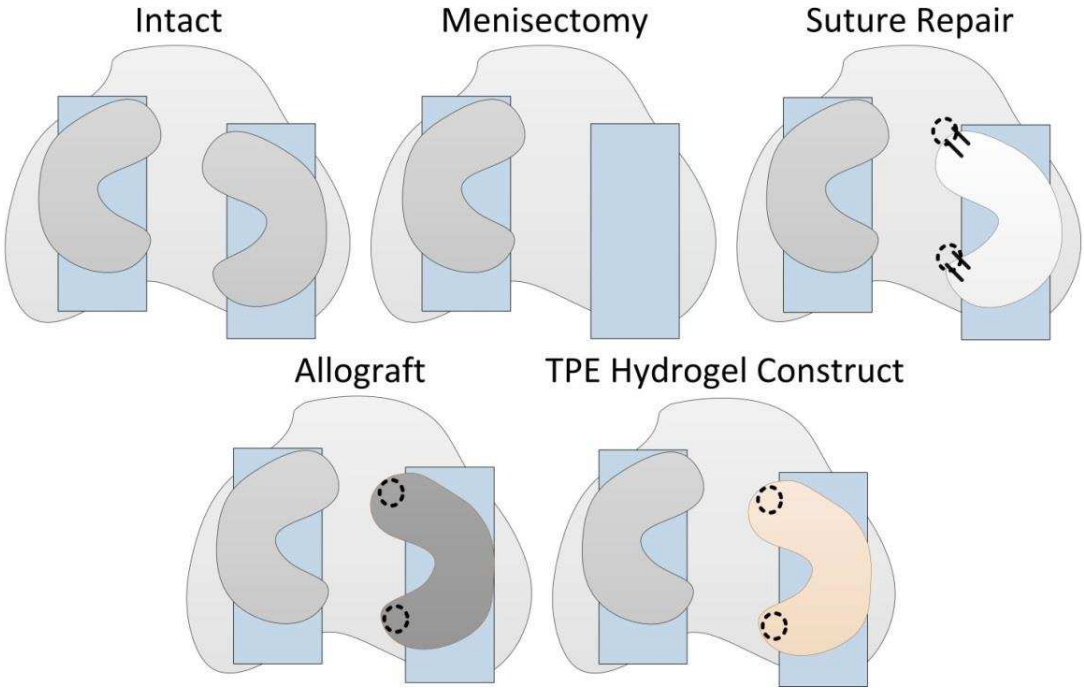

Figure 7-2: Representative diagrams of the five testing conditions as seen looking down on tibial plateau (light grey) with Tekscan under the menisci (blue).

Two sutures were passed through the anterior and posterior horns of the native excised medial meniscus for the suture repair condition. This condition represented the best case scenario as it is a perfect match for both geometry and size. The fourth condition, an allograft transplant was implanted using similar bone block methods to previous work[209,238]. Allografts with 5.9 mm in diameter bone blocks were harvested from separate ovine limbs. Three sizes categorized by overall length and width (small, medium, and large) were available for size matching to the native meniscus. Sutures were passed through the bone blocks and used for securing the allograft within the joint. The allograft transplant represents the "gold standard" for meniscal replacement treatments and represents a replacement that is generally sized and geometry matched. The final condition, TPE hydrogel construct, also followed the concepts of the bone bock methods. TPE hydrogel constructs with tabs extending from the main body were created using negative molding and 3D printing techniques. Molds were designed from a μCT image of a single ovine medial meniscus. Tabs of 5 mm in diameter were added to the solid meniscal body at 90° and 45° from the anterior and posterior horns respectively which allowed for insertion into the bone tunnels created for the other treatment conditions. Tabs were swollen into 6mm diameter plugs of polylactic acid (PLA) that were 3D printed hollow cylinders which provided a solid body for sutures to pass through and together these PLA plugs containing the TPE tabs acted as bone plugs (Figure 7-3). Similar to the allograft condition, the TPE constructs were created in small, medium and large sizes for a general size and geometry matched to be made after the native tissue was excised.

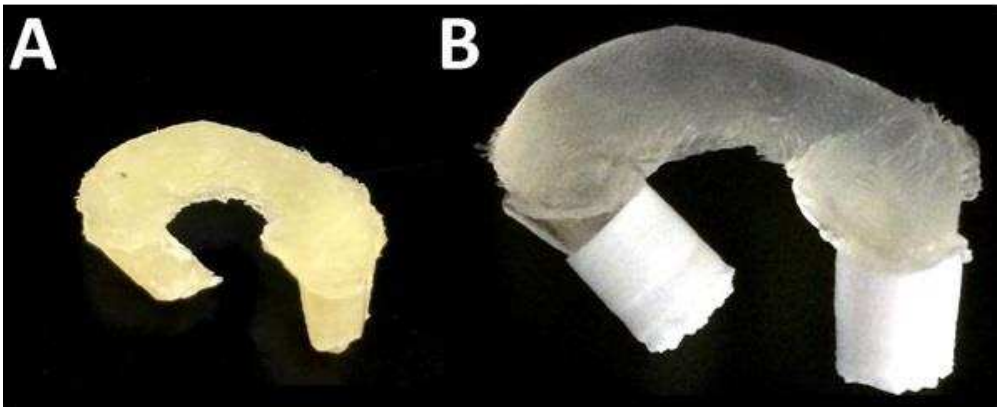

Figure 7-3: Example of TPE hydrogel construct A) melt pressed dry TPE construct B) swollen TPE hydrogel construct with tabs swollen into PLA cylinders

7.2.6 Analysis

Tekscan raw value readings were converted to pressures using the custom calibration curve previously described. Sensel raw values beyond the calibration curve were capped at the maximum of 13.79MPa to avoid inaccuracies of interpolation beyond the curve. Contact area, mean pressure, and max pressure were only calculated from the total number of sensels detecting pressure rather than the total number of sensels which make up the sensor. Since assessments were only made within a single angle and load, a repeated measures analysis of variance (ANOVA) with post hoc Tukey's test was used to determine if there were differences across conditions. This approach paired the data from a single limb whereby reducing errors that could arise from limb to limb variability.

7.3 Results

In the intact native condition, all limbs were able to be loaded to the max 181kg at all flexion angles (Figure 7-4). Contact areas were seen to increase in both the medial and lateral hemijoints between 0 and 45kg but reached a plateau around 68kg and little change was seen at higher loading regimes. A greater contact area was observed in the medial hemijoint compared to

the lateral across all angles, and the medial hemijoint had a consistent contact area cross flexion angles while the lateral hemijoint had a reduced contact area with increased flexion angle. On average, across all angles, for applied loads greater than 68kg, the medial hemijoint recorded a contact area 31±8% greater than the lateral hemijoint. As expected there was an increase in both maximum and mean contact pressures with increased loading. A linear fit of the maximum to mean pressure had a corresponding R^2 value of 0.82 indicating that there was a correlation between the two measures and thus generally a more uniform distribution of pressure. Pressures were also observed to shift from a higher lateral reading at lower flexion angles to greater medial readings at increased flexion angles. Medial vs lateral mean pressure readings were most similar at 60° flexion with only a 10% difference between the two compared to a 74% and 54% difference at flexion angles of 45° and 75° respectively.

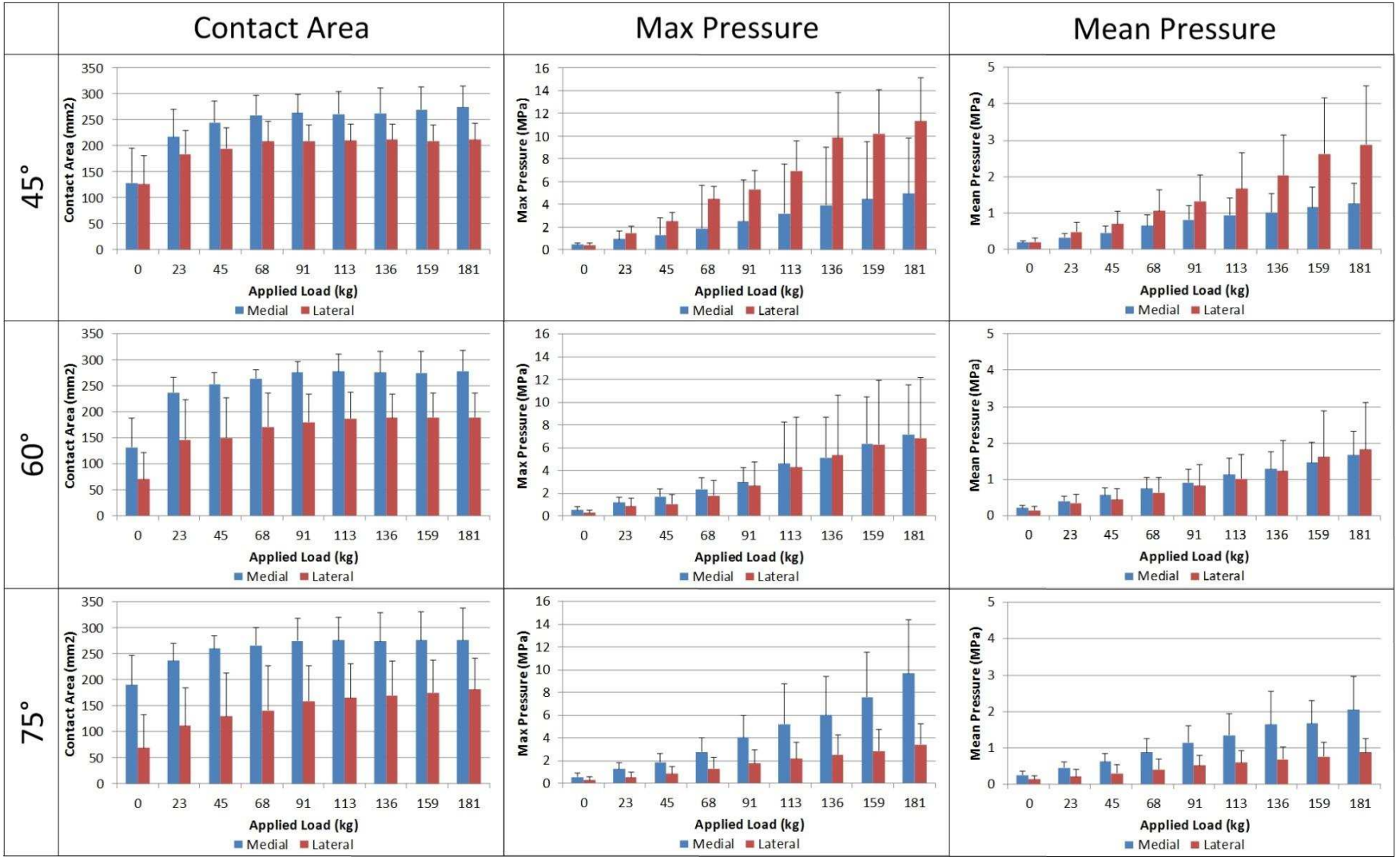

Figure 7-4: Results for the native condition contact area, max pressure, and mean pressure for both the medial and lateral hemijoints at all three flexion angles (45°, 60°, 75°) and all loads for n=7 joints

Removal of the meniscus and subsequent treatments resulted in increased instability of the joint in part due to the level of dissection necessary for sensor insertion. For this reason, there was an inability to consistently obtain results from all 9 loading conditions at all 3 loading angles in the meniscectomy and treatment conditions. Limbs were tested at each condition/angle/load until either all combinations were achieved or a combination was attempted three times without success. As a result, the total number of testing combinations varied across conditions and limbs. Results were grouped based on angle and load and samples were reduced such that within angle and load each individual limb had an equal sample size for all conditions. This effectively reduced the sample size of limbs tested to: n = 5 at 45° and loading conditions up to 113kg, n=7 at 60° and up to 159kg, and n=7 at 70° and up to 181kg.

All limbs had similar trends when comparing the meniscectomy and treatment conditions back to the native condition. Likewise, changes seen at lower loads were generally consistent but amplified with increased applied load (Figure 7-5). All results and significant differences can be seen in Tables 7-1-7-6. The greatest number of significant differences were observed at 60° and 75° (111 out of 480 comparisons and 132 out of 540 comparisons respectively), but these angles also represent the flexion angles where the greatest number of measurements were possible. There were a number of instances where the maximum pressure was at or exceeded the capacity of the sensors, and this was more frequently observed at higher applied loads and higher flexion angles.

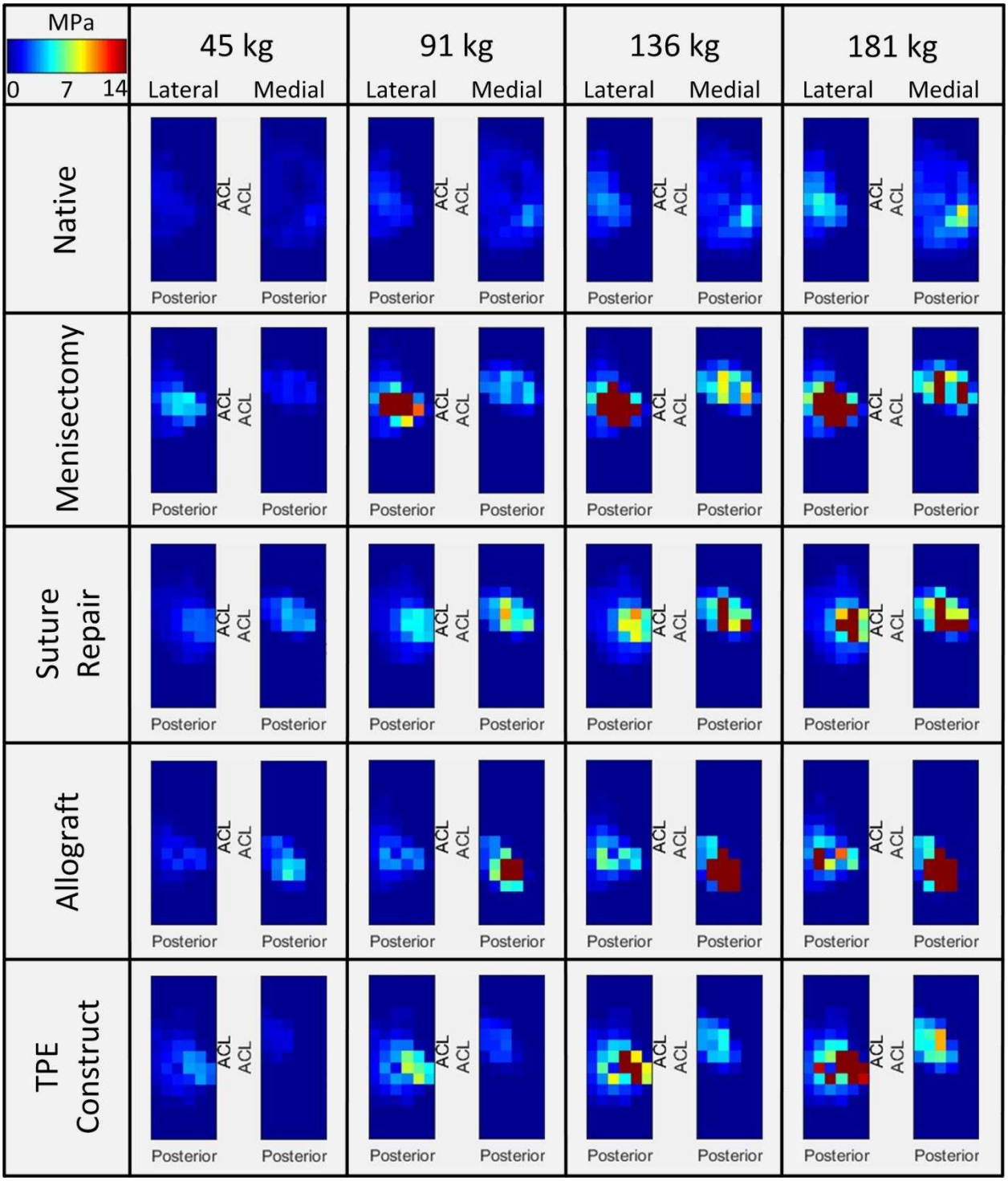

Figure 7-5: Representative results from Tekscan pressure sensors of one joint at 60° medial and lateral hemijoint, data is presented for loading conditions of 45, 91, 136, and 181 kg

Table 7-1: Results for medial contact area average ± std (grey shading indicates significant difference from native, [M] indicates significant difference from meniscectomy, [S] indicates significant difference from suture repair, [A] indicates significant difference from allograft)

Medial Contact Area (mm^2)						
Angle	**Load (kg)**	**Native**	**Menisectomy**	**Suture Repair**	**Allograft**	**TPE**
45°	**0**	130.0 ± 78.2	36.0 ± 26.4	33.4 ± 25.1	28.1 ± 20.3	23.7 ± 22.3
	23	205.5 ± 68.3	53.6 ± 32.2	72.9 ± 9.1	51.8 ± 15.3	39.5 ± 26.3
	45	230.1 ± 46.1	66.7 ± 21.8	79.0 ± 13.5	68.5 ± 9.1	41.3 ± 28.2
	68	252.1 ± 46.5	70.3 ± 21.3	88.7 ± 16.3	73.8 ± 14.7	51.8 ± 15.6
	91	254.7 ± 41.7	78.2 ± 23.1	95.7 ± 23.5	80.8 ± 13.0	56.2 ± 11.4
	113	262.6 ± 36.8	81.7 ± 18.5	101.9 ± 22.0	83.4 ± 15.8	58.0 ± 11.8 [S]
	136					
	159					
	181					
60°	**0**	134.9 ± 53.8	45.8 ± 22.1	55.2 ± 24.2	29.5 ± 21.5	24.5 ± 13.6
	23	245.9 ± 18.3	76.5 ± 17.4	95.4 ± 31.6	63.4 ± 28.8	47.7 ± 10.9 [S]
	45	259.7 ± 21.0	83.4 ± 17.2	111.0 ± 34.1	73.4 ± 30.0 [S]	55.8 ± 13.1 [S]
	68	266.6 ± 17.5	88.4 ± 18.9	121.1 ± 42.0	81.5 ± 31.1	61.5 ± 16.8 [S]
	91	275.4 ± 16.6	89.7 ± 18.9	122.3 ± 46.1	93.5 ± 21.5	63.4 ± 17.4 [S]
	113	281.7 ± 18.5	92.2 ± 17.9	125.5 ± 48.8	99.7 ± 23.7	64.0 ± 21.8 [S]
	136	282.9 ± 19.4	94.7 ± 16.6	125.5 ± 49.5	104.8 ± 29.0	68.4 ± 22.1 [S]
	159	281.0 ± 19.6	96.0 ± 16.1	128.0 ± 54.5	107.9 ± 28.1	70.3 ± 21.8 [S]
	181					
75°	**0**	187.7 ± 60.0	46.1 ± 22.8	45.6 ± 26.4	30.7 ± 17.7	30.2 ± 21.7 [S]
	23	236.6 ± 37.0	66.4 ± 12.1	93.9 ± 29.8	63.1 ± 18.3	52.1 ± 13.2 [S]
	45	261.8 ± 26.2	75.7 ± 15.3	107.6 ± 35.3	74.1 ± 18.4 [S]	57.6 ± 11.8 [S]
	68	273.3 ± 27.2	76.8 ± 13.9	115.3 ± 35.7 [M]	83.4 ± 23.6	56.0 ± 15.0 [S]
	91	284.9 ± 33.4	79.0 ± 13.5	122.4 ± 39.8 [M]	95.0 ± 30.9	58.7 ± 14.8 [S]
	113	286.5 ± 33.3	81.8 ± 15.0	130.6 ± 43.9 [M]	101.0 ± 33.4	60.4 ± 14.0 [S]
	136	289.3 ± 34.8	81.8 ± 15.6	131.2 ± 44.0 [M]	110.3 ± 36.2	60.9 ± 13.4 [S A]
	159	290.9 ± 36.0	81.2 ± 14.1	131.2 ± 40.8 [M]	119.1 ± 45.5	62.6 ± 15.0 [S A]
	181	293.1 ± 35.3	80.7 ± 12.8	135.6 ± 38.7 [M]	127.3 ± 56.2	64.2 ± 16.4 [S A]

Table 7-2: Results for medial max pressure average ± std (grey shading indicates significant difference from native, [M] indicates significant difference from meniscectomy, [S] indicates significant difference from suture repair, [A] indicates significant difference from allograft)

Medial Max Pressure (MPa)						
Angle	**Load (kg)**	**Native**	**Menisectomy**	**Suture Repair**	**Allograft**	**TPE**
45°	**0**	0.4 ± 0.3	0.4 ± 0.2	0.3 ± 0.2	0.2 ± 0.2	0.3 ± 0.3
	23	0.9 ± 0.7	1.9 ± 1.2	2.3 ± 1.8	1.9 ± 1.1	3.5 ± 5.0
	45	1.2 ± 1.0	4.2 ± 2.2	5.0 ± 5.0	3.1 ± 1.4	5.1 ± 5.2
	68	1.8 ± 1.4	8.3 ± 5.4	6.8 ± 4.4	5.2 ± 3.7	8.4 ± 5.9
	91	2.5 ± 2.1	9.5 ± 5.8	10.3 ± 4.5	8.6 ± 4.9	10.4 ± 5.6
	113	3.3 ± 3.3	11.9 ± 4.3	11.3 ± 3.7	11.9 ± 4.2	11.3 ± 5.6
	136					
	159					
	181					
60°	**0**	0.5 ± 0.2	0.4 ± 0.2	0.6 ± 0.4	0.3 ± 0.2	0.3 ± 0.4
	23	1.2 ± 0.4	1.9 ± 0.8	4.1 ± 4.6	3.5 ± 4.7	3.2 ± 4.8
	45	1.7 ± 0.7	4.3 ± 2.8	7.3 ± 5.4	4.9 ± 4.6	4.6 ± 4.3
	68	2.4 ± 1.0	7.3 ± 4.6	9.8 ± 5.1	7.8 ± 5.9	7.8 ± 5.0
	91	2.9 ± 1.1	10.4 ± 4.2	11.6 ± 3.9	10.4 ± 5.7	9.7 ± 5.3
	113	3.6 ± 1.2	11.5 ± 3.9	12.4 ± 3.7	11.9 ± 4.9	11.4 ± 4.1
	136	4.3 ± 1.5	13.2 ± 1.6	12.7 ± 3.0	11.9 ± 4.9	12.6 ± 3.2 [A]
	159	5.8 ± 3.3	13.8 ± 0.0	13.3 ± 1.4	12.0 ± 4.8	12.8 ± 2.6
	181					
75°	**0**	0.5 ± 0.3	0.8 ± 0.9	0.5 ± 0.4	0.5 ± 0.8	0.4 ± 0.3
	23	1.2 ± 0.5	3.2 ± 2.5	4.5 ± 4.0	4.2 ± 4.4	4.2 ± 4.0
	45	1.7 ± 0.7	10.0 ± 5.3	8.7 ± 5.0	7.6 ± 5.4	9.4 ± 4.4
	68	2.5 ± 1.0	12.1 ± 3.2	11.8 ± 3.7	11.5 ± 4.1	13.3 ± 1.1
	91	3.6 ± 1.6	13.8 ± 0.0	13.8 ± 0.0	12.5 ± 3.6	13.8 ± 0.0
	113	4.2 ± 1.6	13.8 ± 0.0	13.8 ± 0.0	12.7 ± 3.2	13.8 ± 0.0
	136	5.0 ± 2.0	13.8 ± 0.0	13.8 ± 0.0	13.2 ± 1.6	13.8 ± 0.0
	159	6.8 ± 3.4	13.8 ± 0.0	13.8 ± 0.0	13.8 ± 0.0	13.8 ± 0.0
	181	9.1 ± 4.7	13.8 ± 0.0	13.8 ± 0.0	13.8 ± 0.0	13.8 ± 0.0

Table 7-3: Results for medial mean pressure average ± std (grey shading indicates significant difference from native, [M] indicates significant difference from meniscectomy, [S] indicates significant difference from suture repair, [A] indicates significant difference from allograft)

Medial Mean Pressure (MPa)						
Angle	**Load (kg)**	**Native**	**Menisectomy**	**Suture Repair**	**Allograft**	**TPE**
45°	**0**	0.2 ± 0.1	0.3 ± 0.2	0.2 ± 0.1	0.2 ± 0.1	0.1 ± 0.2
	23	0.3 ± 0.1	1.0 ± 0.5	0.8 ± 0.4	1.1 ± 0.7	1.1 ± 1.0
	45	0.4 ± 0.3	1.7 ± 0.7	1.5 ± 1.1	1.4 ± 0.7	2.0 ± 1.4
	68	0.6 ± 0.4	2.7 ± 1.3	2.0 ± 1.2	2.0 ± 1.2	2.8 ± 1.6
	91	0.8 ± 0.5	4.0 ± 2.4	2.9 ± 1.8	2.8 ± 1.8	3.4 ± 1.7
	113	0.9 ± 0.6	4.9 ± 2.1	3.6 ± 2.1	3.5 ± 1.9	4.3 ± 2.1
	136					
	159					
	181					
60°	**0**	0.2 ± 0.1	0.2 ± 0.1	0.3 ± 0.2	0.2 ± 0.1	0.2 ± 0.2
	23	0.4 ± 0.1	0.9 ± 0.3	1.2 ± 0.8	0.9 ± 0.7	1.0 ± 0.8
	45	0.6 ± 0.2	1.6 ± 0.6	1.7 ± 0.9	1.5 ± 1.0	1.9 ± 1.3
	68	0.8 ± 0.3	2.6 ± 1.2	2.5 ± 1.3	2.0 ± 1.3	3.0 ± 1.7
	91	0.9 ± 0.4	3.7 ± 1.6	3.2 ± 1.5	2.6 ± 1.6	3.9 ± 1.9
	113	1.1 ± 0.4	4.4 ± 2.0	3.6 ± 1.5	3.3 ± 1.9	5.0 ± 1.9
	136	1.3 ± 0.5	4.9 ± 1.8	3.9 ± 1.5	3.5 ± 1.9	5.6 ± 1.8
	159	1.5 ± 0.6	5.7 ± 1.7	4.1 ± 1.6	3.6 ± 1.9	6.3 ± 1.9
	181					
75°	**0**	0.2 ± 0.1	0.4 ± 0.3	0.3 ± 0.2	0.3 ± 0.3	0.2 ± 0.1
	23	0.4 ± 0.2	1.3 ± 0.8	1.2 ± 0.9	1.2 ± 1.0	1.6 ± 1.5
	45	0.6 ± 0.2	3.2 ± 2.0	1.9 ± 1.1 [M]	1.8 ± 1.2 [M]	2.9 ± 1.3
	68	0.8 ± 0.4	4.6 ± 2.1	2.5 ± 1.3 [M]	2.5 ± 1.3 [M]	4.1 ± 1.0
	91	1.1 ± 0.4	5.2 ± 2.1	2.8 ± 1.1 [M]	3.0 ± 1.6 [M]	5.1 ± 1.2 [SA]
	113	1.2 ± 0.5	5.4 ± 1.9	3.0 ± 1.0 [M]	3.3 ± 1.2 [M]	5.5 ± 1.4 [SA]
	136	1.4 ± 0.6	6.0 ± 1.7	3.1 ± 0.9 [M]	3.3 ± 1.0 [M]	5.9 ± 1.5 [SA]
	159	1.6 ± 0.6	6.4 ± 1.7	3.3 ± 0.9 [M]	3.4 ± 1.2 [M]	6.1 ± 1.8 [SA]
	181	2.0 ± 1.0	6.6 ± 1.6	3.2 ± 0.8 [M]	3.6 ± 1.2 [M]	6.1 ± 1.6 [SA]

Table 7-4: Results for lateral mean pressure average ± std (grey shading indicates significant difference from native, [M] indicates significant difference from meniscectomy, [S] indicates significant difference from suture repair, [A] indicates significant difference from allograft)

Lateral Contact Area (mm^2)						
Angle	**Load (kg)**	**Native**	**Menisectomy**	**Suture Repair**	**Allograft**	**TPE**
45°	**0**	118.6 ± 57.9	115.9 ± 40.1	73.8 ± 61.3	85.2 ± 63.8	98.4 ± 68.4
	23	191.5 ± 46.7	150.2 ± 55.0	104.5 ± 69.2	119.4 ± 63.8	137.9 ± 63.8
	45	202.9 ± 36.9	163.3 ± 66.0	108.0 ± 73.8	123.8 ± 61.4	146.7 ± 61.2
	68	211.7 ± 39.6	167.7 ± 69.1	112.4 ± 73.1	127.3 ± 57.3	151.9 ± 62.5
	91	209.9 ± 27.5	172.1 ± 74.6	113.3 ± 70.4	129.1 ± 60.7	155.4 ± 62.2
	113	212.5 ± 30.2	178.3 ± 72.7	117.7 ± 69.7	135.2 ± 56.7	156.3 ± 61.3
	136					
	159					
	181					
60°	**0**	54.6 ± 45.5	100.4 ± 60.8	75.9 ± 77.9	65.9 ± 52.6	60.8 ± 57.0
	23	133.0 ± 82.6	131.1 ± 60.6	107.9 ± 78.4	112.9 ± 61.5	99.1 ± 60.3
	45	143.7 ± 83.0	144.3 ± 66.1	117.3 ± 82.2	129.9 ± 55.7	107.3 ± 59.3
	68	160.6 ± 71.1	154.9 ± 63.2	121.1 ± 71.0	134.2 ± 49.3	106.0 ± 61.4
	91	171.9 ± 60.3	169.4 ± 58.0	113.5 ± 70.0	136.8 ± 48.5	112.3 ± 57.3
	113	182.5 ± 56.3	171.9 ± 55.5	116.1 ± 66.6	141.1 ± 51.7	117.9 ± 54.9
	136	184.4 ± 52.1	176.3 ± 47.6	118.6 ± 66.8	145.5 ± 53.6	117.9 ± 53.7
	159	186.3 ± 52.6	183.8 ± 44.4	121.1 ± 65.0	150.6 ± 52.7	128.6 ± 53.8
	181					
75°	**0**	64.8 ± 67.0	100.4 ± 74.2	54.9 ± 57.9	49.9 ± 54.4	47.8 ± 50.1 [M]
	23	107.6 ± 76.6	124.0 ± 87.8	96.1 ± 65.7	93.9 ± 47.1	99.3 ± 58.6
	45	125.1 ± 88.0	135.0 ± 87.6	108.1 ± 71.1	107.0 ± 46.2	114.2 ± 65.6
	68	137.2 ± 92.7	138.9 ± 82.0	108.7 ± 64.5	127.3 ± 46.9	139.4 ± 56.6
	91	159.2 ± 73.7	149.8 ± 68.2	116.4 ± 61.8	136.7 ± 39.9	142.7 ± 61.9
	113	166.3 ± 71.0	160.3 ± 60.6	124.6 ± 62.8	146.0 ± 35.1	146.6 ± 61.2
	136	170.7 ± 70.1	169.6 ± 50.7	126.8 ± 64.2	149.3 ± 39.3	152.6 ± 59.4
	159	176.7 ± 68.1	178.4 ± 42.8	129.5 ± 62.8	153.7 ± 43.5	160.3 ± 57.7
	181	183.3 ± 63.6	180.0 ± 42.2	129.0 ± 59.7	147.7 ± 34.3	166.9 ± 56.2

Table 7-5: Results for lateral max pressure average ± std (grey shading indicates significant difference from native, [M] indicates significant difference from meniscectomy, [S] indicates significant difference from suture repair, [A] indicates significant difference from allograft)

Lateral Max Pressure (MPa)						
Angle	**Load (kg)**	**Native**	**Menisectomy**	**Suture Repair**	**Allograft**	**TPE**
45°	**0**	0.3 ± 0.2	0.7 ± 0.3	0.4 ± 0.2	0.4 ± 0.4	0.3 ± 0.2 [M]
	23	1.3 ± 0.7	1.7 ± 1.1	1.4 ± 1.1	1.6 ± 1.1	1.5 ± 0.9
	45	1.9 ± 1.0	3.2 ± 2.2	2.8 ± 2.9	2.6 ± 1.6	2.6 ± 1.6
	68	3.2 ± 1.8	7.1 ± 6.3	6.1 ± 7.0	3.9 ± 2.7	4.6 ± 3.2
	91	4.2 ± 2.4	7.5 ± 6.0	6.3 ± 6.9	8.1 ± 6.5	7.9 ± 6.0
	113	6.4 ± 4.8	9.5 ± 6.2	6.4 ± 6.8	8.8 ± 6.8	9.3 ± 6.4
	136					
	159					
	181					
60°	**0**	0.2 ± 0.2	0.6 ± 0.4	0.3 ± 0.2	0.3 ± 0.3	0.3 ± 0.2
	23	0.5 ± 0.4	1.7 ± 0.7	0.9 ± 0.7	1.2 ± 0.8	1.2 ± 1.0
	45	0.8 ± 0.5	3.2 ± 1.7	1.7 ± 1.1 [M]	1.9 ± 1.2 [M]	1.9 ± 1.5 [M]
	68	1.2 ± 0.8	7.7 ± 5.4	2.8 ± 1.8 [M]	3.9 ± 4.3	3.8 ± 4.7
	91	1.9 ± 1.8	9.2 ± 5.9	5.9 ± 5.6 [M]	5.7 ± 5.6	4.3 ± 4.8
	113	3.4 ± 4.6	9.4 ± 5.7	6.6 ± 5.4	6.5 ± 5.2	5.7 ± 5.7
	136	3.7 ± 4.5	9.5 ± 5.6	8.1 ± 5.6	7.2 ± 4.9	6.6 ± 5.9
	159	4.1 ± 4.4	10.7 ± 5.5	9.0 ± 6.1	8.9 ± 5.2	7.4 ± 6.1
	181					
75°	**0**	0.3 ± 0.3	0.4 ± 0.3	0.4 ± 0.3	0.2 ± 0.2	0.2 ± 0.2
	23	0.5 ± 0.4	1.1 ± 0.8	1.1 ± 0.8	0.6 ± 0.5	0.5 ± 0.3
	45	0.8 ± 0.7	2.2 ± 1.7	2.2 ± 1.7	1 .0 ± 0.9 [M]	0.8 ± 0.5
	68	1.2 ± 1.1	4.0 ± 4.3	4.0 ± 4.3	1.7 ± 1.4	1.5 ± 0.8
	91	1.7 ± 1.3	5.9 ± 5.3	5.9 ± 5.3	2.7 ± 2.0 [M]	2.2 ± 1.3 [M]
	113	2.2 ± 1.5	7.7 ± 5.7	7.7 ± 5.7	5.3 ± 5.4	3.9 ± 3.7
	136	2.6 ± 1.8	8.8 ± 5.6	8.8 ± 5.6	5.5 ± 5.4	4.8 ± 4.2
	159	2.9 ± 2.0	10.0 ± 5.5	10.0 ± 5.5	5.9 ± 5.3	6.6 ± 5.2
	181	3.4 ± 2.0	10.4 ± 5.2	10.4 ± 5.2	7.0 ± 5.7	8.3 ± 5.6

Table 7-6: Results for lateral mean pressure average ± std (grey shading indicates significant difference from native, [M] indicates significant difference from meniscectomy, [S] indicates significant difference from suture repair, [A] indicates significant difference from allograft)

Lateral Mean Pressure (MPa)						
Angle	**Load (kg)**	**Native**	**Menisectomy**	**Suture Repair**	**Allograft**	**TPE**
45°	**0**	0.2 ± 0.1	0.3 ± 0.1	0.2 ± 0.1	0.2 ± 0.1	0.2 ± 0.1 [M]
	23	0.5 ± 0.3	0.6 ± 0.3	0.5 ± 0.3	0.6 ± 0.4	0.5 ± 0.3
	45	0.6 ± 0.4	0.9 ± 0.6	0.7 ± 0.7	0.8 ± 0.5	0.8 ± 0.5
	68	0.9 ± 0.6	1.4 ± 1.0	1.2 ± 1.3	1.1 ± 0.8	1.1 ± 0.7
	91	1.2 ± 0.7	2.1 ± 1.8	1.7 ± 1.9	1.6 ± 1.3	1.4 ± 0.9
	113	1.5 ± 1.0	2.7 ± 2.1	2.0 ± 2.4	2.0 ± 1.7	1.9 ± 1.3
	136					
	159					
	181					
60°	**0**	0.1 ± 0.1	0.3 ± 0.1	0.2 ± 0.1 M	0.2 ± 0.1 [M]	0.2 ± 0.1 [M]
	23	0.3 ± 0.2	0.6 ± 0.3	0.4 ± 0.2 M	0.4 ± 0.2 [M]	0.4 ± 0.3 [M]
	45	0.4 ± 0.2	1.0 ± 0.5	0.6 ± 0.4 M	0.6 ± 0.4 [M]	0.6 ± 0.4 [M]
	68	0.5 ± 0.3	1.4 ± 1.0	0.8 ± 0.5 M	0.9 ± 0.7	0.8 ± 0.7 [M]
	91	0.6 ± 0.5	2.1 ± 1.5	1.2 ± 0.9	1.2 ± 0.9	1.0 ± 0.8 [M]
	113	0.8 ± 0.6	2.4 ± 1.6	1.4 ± 1.1	1.4 ± 1.0 [M]	1.3 ± 1.2 [M]
	136	0.9 ± 0.7	2.7 ± 1.9	1.7 ± 1.3	1.5 ± 1.0 [M]	1.7 ± 1.6
	159	1.2 ± 1.2	2.9 ± 1.9	2.0 ± 1.5	1.7 ± 1.1 [M]	1.8 ± 1.6
	181					
75°	**0**	0.1 ± 0.1	0.2 ± 0.1	0.1 ± 0.1	0.1 ± 0.1	0.2 ± 0.1
	23	0.2 ± 0.2	0.4 ± 0.3	0.3 ± 0.2	0.3 ± 0.1	0.3 ± 0.2
	45	0.3 ± 0.3	0.8 ± 0.5	0.4 ± 0.3	0.4 ± 0.2	0.5 ± 0.3
	68	0.4 ± 0.3	1.1 ± 0.7	0.6 ± 0.4	0.6 ± 0.3	0.6 ± 0.4
	91	0.5 ± 0.3	1.4 ± 1.0	0.8 ± 0.5	0.8 ± 0.4	0.7 ± 0.5 [M]
	113	0.6 ± 0.3	1.7 ± 1.0	1.1 ± 0.8	1.0 ± 0.5	0.9 ± 0.6
	136	0.7 ± 0.4	2.1 ± 1.2	1.3 ± 1.0	1.2 ± 0.7	1.2 ± 0.9
	159	0.7 ± 0.4	2.4 ± 1.3	1.4 ± 1.2	1.5 ± 0.9	1.5 ± 1.1
	181	0.8 ± 0.4	2.6 ± 1.4	1.6 ± 1.2	1.8 ± 1.0	1.7 ± 1.2

Due to limitations with stability and readings obtained within the range of the sensors, the best angle/load combination to compare conditions across angles is 91kg (Figure 7-6). This loading regime represents 1-1.5x body weight which is physiologically relevant. Overall, all

conditions resulted in a reduced contact area and increased maximum and mean pressures within the joint compared to the native intact condition. As expected, the greatest changes were observed in the medial compartment; however, there were a number of significant changes to the lateral hemijoint as well particularly in the meniscectomy condition.

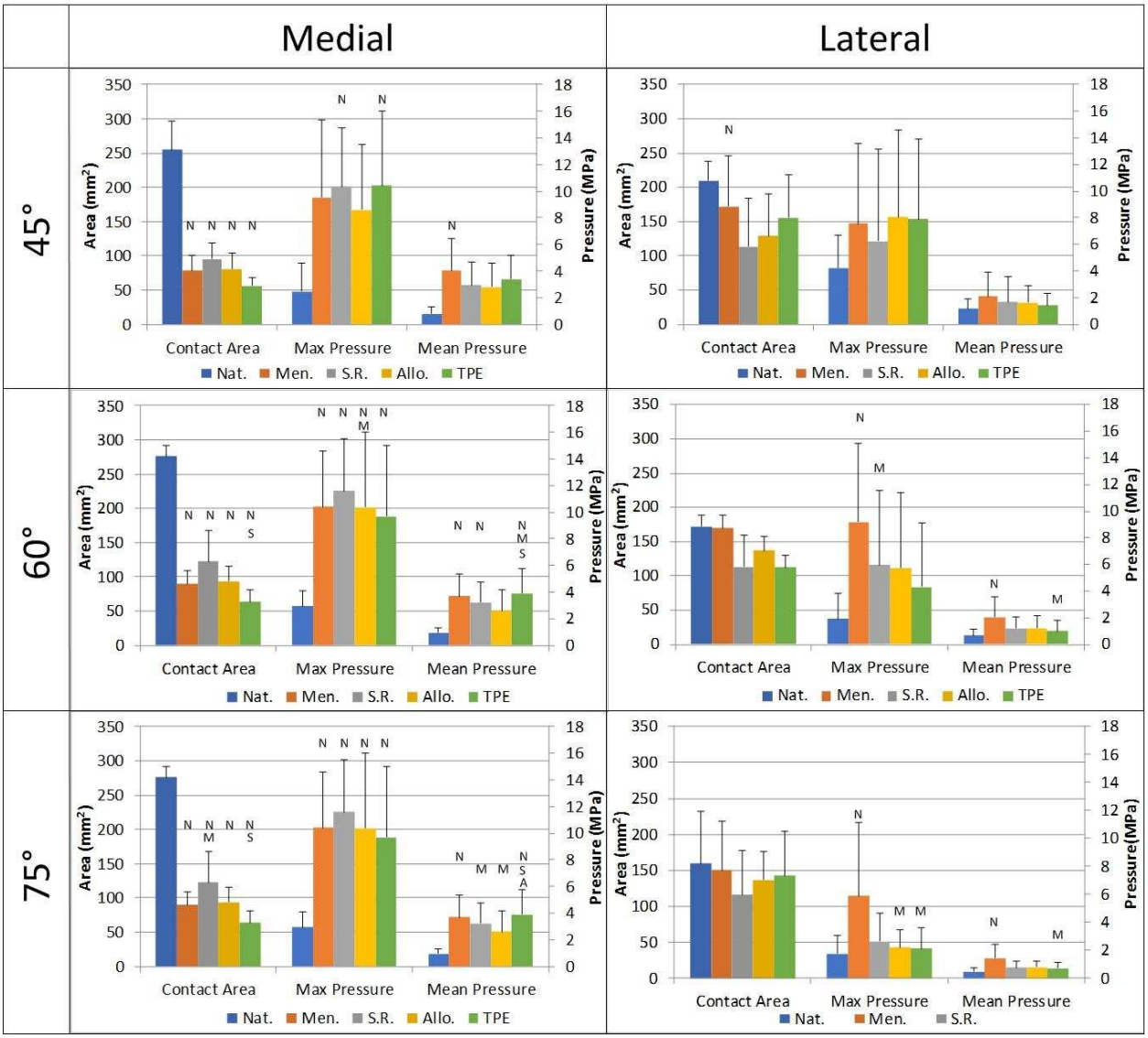

Figure 7-6: Results for the contact area, max pressure, and mean pressure for both the medial and lateral hemijoints at all three flexion angles (45°, 60°, 75°) with an applied load of 91kg average ± std. ^{N} indicates significant difference from native, ^{M} indicates significant difference from meniscectomy, ^{S} indicates significant difference from suture repair, ^{A} indicates significant difference from allograft

All conditions had a significantly lower medial contact area compared to the native condition at all loading regimes and at all flexion angles. At 75° flexion and at loads above 68kg the suture repair was able to significantly increase medial contact area compared to the meniscectomy condition but was still on average 50% lower than the native intact condition. At 60° and 75° flexion the suture repair was significantly better at maintaining contact area compared to the TPE construct, and at 75° and loads beyond 136kg, the allograft also outperformed the TPE construct with regards to maintaining medial contact area. The only contact area differences seen in the lateral hemijoint were between the meniscectomy condition and intact condition at 45° and 68-113kg.

Significant differences in medial maximum and mean pressures were identified at lower applied loads as flexion angle increased. At 45° the maximum and mean pressures were significantly increased in all conditions compared to the native at 113kg. Maximum pressure was significantly different in all conditions compared to the native at 91kg for 60° and 45kg at 75°. Mean pressure was generally significantly increased for all but the allograft condition at 60° and beyond 45kg, while at 75° both the suture repair and allograft prevented significant increases in mean pressure beyond 45kg. The suture repair and allograft conditions were also able to significantly lower medial mean pressures compared to the meniscectomy case at 75° beyond 68kg. The suture repair and allografts were also able to reduce mean pressures at 75° and beyond 91kg compared to the TPE construct.

The biggest improvements the treatment conditions offered compared to the meniscectomy condition were seen at the higher angles of 60° and 75° in the lateral hemijoint where maximum and mean pressures were reduced. At these angles, the TPE construct generally performed superior to the other treatments for maximum and mean pressure. While all treatment

conditions were not significantly different from the intact condition, mean and max pressures were still elevated. These elevated readings resulted in the treatments generally not being significantly different from the meniscectomy condition, although the TPE construct was most frequently significantly better than a meniscectomy suggesting it is both better than a meniscectomy and not statistically different from the intact condition.

7.4 Discussion

This study provided a more complete collection of pressure distribution data for an ovine model, as numerous angles and applied loads were reported as well as a broader comparison to multiple treatment options for meniscal injury including a novel 3D TPE hydrogel construct replacement. To the author's knowledge this the first study to report medial and lateral results following a complete meniscectomy and multiple treatment techniques. Results clearly indicate that a medial meniscectomy significantly alters the contact area and mean and maximum pressures not only within the medial hemijoint but also the lateral. None of the treatment conditions were able to fully repair the joints pressure distribution to the native condition, however, depending on the flexion angle and the applied load the treatment conditions were frequently better than the meniscectomy condition particularly at improving the lateral pressure distributions.

Two ovine studies, one at 91kg and 60° and one at 130kg and 6.5°, have previously accessed the native contact areas and peak pressures of both the medial and lateral hemijoints[239,240]. Both of these reported larger contact areas in the medial hemijoint which is consistent with the findings of this study's intact native condition. Directly comparing results from 60° and 91kg, the current study found average contact areas of 275mm^2 and 171mm^2 for

the medial and lateral hemijoints respectively compared to the previously reported 252 mm^2 and 240 mm^2. The two studies, however, have conflicting reports on maximum pressures as one reports the lateral hemijoint having a higher max pressure while the other reports the medial hemijoint. A gait study by Taylor et. al. concluded load was primarily distributed through the medial compartment which aligns with our findings as well as those by Lee Shee et. al. who found the medial hemijoint had a 42% greater contact area and 12% higher peak pressure[237,240].

Although only medial findings were reported, numerous studies have compared contact area, mean pressure, and maximum pressure for the ovine joint in the native intact condition and medial meniscectomy condition, but at limited flexion angles and low loading conditions (10-51kg) [216,241,242]. On average these reports observed a meniscectomy decreases medial contact area by 65±18% compared to the 70±2% seen in this current study for similar loads. The average increase in mean and maximum pressures found within this study are also comparable to those previously reported, with maximum pressure increasing 290±170% and mean pressure increasing 310±140% at an applied load of 45kg[216,242,243].

Overall, the decrease in contact area and increase in maximum and mean pressures seen with the meniscectomy condition were as expected. However, none of the treatment conditions restored these measures. At the higher flexion angles of 60°, the treatment conditions were beginning to outperform the meniscectomy condition but still showed significant increased medial contact area and pressures compared to the native intact condition. One exception to this was that no significant difference was found between the medial mean pressures of the native condition and the allograft. Similarly, while the medial contact area and maximum pressures of the treatment conditions were significantly different than the native intact condition both the suture repair and allograft prevented a significant increase in medial mean pressure at 75°. Many

of the differences seen between the meniscectomy condition and the treatment conditions were observed in the lateral hemijoint by way of restoring lateral maximum and mean pressures.

The suture repair and allografts were specifically chosen to assess the role of geometry and size. The suture repair represented a perfect match for both geometry and size, with the allograft size matched only on a scale of small, medium, and large and since it was donor tissue only a general match to the geometry of the excised native meniscus was achieved. Few significant differences were seen between these two conditions. In fact, the allograft had fewer significant differences across the board than the suture repair when compared to the native intact conditions. Suggesting that exact size and geometry may not play as significant a role as once thought, and that future replacements could perhaps proceed with a more general meniscus shape in a limited number of sizes (small, medium, large).

A large area of concern which is not addressed in this study is the role of attachment and specifically the attachment method. Although the allograft and TPE construct had bone blocks and solid cylindrical plugs respectively that were used for insertion compared to only sutures for the suture repair, all three conditions were limited in the degree to which they could be tensioned and pulled into the joint. The allograft also retained the soft to hard tissue gradient while the suture repair condition relied solely on the sutures pulled through the tissue to maintain its position relative the bone tunnels. This could account for the inability of any of the treatment conditions to restore contact area or pressures to the native condition. Clinically there is no consensus on the best fixation method for allografts[244], and further work is necessary to determine if using sutures pulled through bone tunnels is sufficient in anchoring meniscal replacements, or if screw fixation is preferable or necessary. Furthermore, additional

investigation is necessary to determine the extent to which the fixation method affected the current study.

Comparing the performance of the TPE construct, the only significant difference across the remaining treatment conditions occurred at 45° and less than 113kg of load where the TPE construct had a significantly lower medial contact area compared to the suture repair. At both 60° and 75° the TPE construct had decreased contact area compared to the suture repair and at 75° the TPE construct also had a significantly lower contact area compared to the allograft. However, for the most part, the measured change in contact area only resulted in a significant change in pressure readings at 75° and above 91kg where the TPE construct had an increased mean medial pressure compared to the suture repair and allograft conditions. This suggests there may be some potential extrusion of the TPE construct at higher flexion angles and loads, or the TPE construct was offloading to areas outside the scope of the sensor. The TPE hydrogel material in its current form is a homogeneous isotropic material and may not be able to withstand the hoop stresses created within the knee joint. It is less stiff than the native tissue and would be more likely to deform in the radial direction. Altering the material to have some anisotropy in the circumferential direction by incorporation of fibers could improve its in situ load distribution ability by helping it maintain its position within the joint.

This study is not without limitations. One limitation was the size, shape, and capacity of the sensors used. Significant dissection was required to fit the sensors within the joint which in turn destabilized the knee resulting in incomplete data sets. Additionally, the max capacity of the sensors was 13.79MPa which unfortunately meant that some of the peak loads were not able to be recorded under certain high loading conditions. Additionally, bone tunnels were drilled as near to the original attachment locations as possible but had to be shifted slightly to avoid

interfering with the anterior and posterior cruciate ligament tibial attachments. This not only reduced the footprint the sensors could occupy, but could also be a source of error when comparing all treatment conditions to the native intact condition.

In conclusion, a medial meniscectomy decreased contact area and increased the mean and maximum pressure reading for both the medial and lateral hemijoint. No treatment condition tested within this study was able to fully restore medial joint contact area and medial pressures to the native condition. To some degree, all repair and replacement conditions including a novel TPE hydrogel meniscal replacement were significantly better than a meniscectomy as they typically repaired all increases in lateral pressures. Although the TPE construct did not restore contact area and pressure distribution in the medial compartment as well as hoped, it performed as well as, if not better, than the other repair and replacement options at restoring lateral pressures. At high flexion angles and high loads, improvements to the TPE construct are necessary if it is to match the performance of the suture repair and allograft. Further work is also necessary to determine the best anchoring and attachment methods.

CHAPTER 8:
CONCLUSIONS

8.1 Importance of Work

Meniscal injuries are thought to be the most common knee injury occurring in 60-70 cases per 100,000 persons[245]. In the United States alone an estimated 500,000 surgical procedures were performed on the meniscus in 2006[181]. Meniscal injuries are in part such a widespread issue as they affect both the younger healthier populations as well as the older populations and can lead to degradation of neighboring tissues and the onset of osteoarthritis. The rate of degenerative meniscal tears is 68-90% in patients with radiographic osteoarthritis[246], but the peak incidence of meniscal injuries in males is between 31-40 years old and for females, the peak incidence is between 11-20 years old[247]. Many of these tears in younger individuals are sports-related injuries, and it has been found that individuals are 15 times more likely to eventually need a total knee replacement due to OA after a meniscal injury[248].

Clinically there remain few options for individuals suffering from meniscal injuries. Even though it has been proven to lead to early onset osteoarthritis one of the most common approaches is a partial meniscectomy. These are performed in an effort to limit the total damage and acute pain caused by meniscal tear propagation. Some surgeons suture the damaged meniscal portions together as an attempted repair but without sufficient blood supply, the tissue will not heal. Only a handful of products are clinically available as meniscal scaffolds or inert replacements and all are limited in their performance and under what conditions they can be implanted. There exists a clinical need for a meniscal replacement that is more mimetic of the native tissue and can be implemented regardless of meniscal damage.

8.2 Summary of Findings and Future Work

This work provided an investigation into the use of a thermoplastic elastomer hydrogel (polystyrene-polyethylene oxide diblock copolymer) as a potential material for an inert artificial meniscal replacement. The material properties of a 72 mol% triblock TPE hydrogel blend were investigated and compared to both human and ovine native meniscus. Both the compressive and tensile elastic moduli were assessed as well as the shear modulus, dynamic modulus, fatigue resistance, and cyclical relaxation. Overall the TPE hydrogel material is a promising material for a meniscal replacement. It had an equilibrium and shear modulus similar to the native human meniscus as well as a cyclical relaxation comparable to higher cycle numbers. It also had a higher fatigue resistance compared to more traditional hydrogels. However, the instantaneous stiffness, rate and degree of relaxation, and tensile modulus all differed significantly from the native meniscus. Thus, further incorporation of a secondary network particularly in the circumferential direction may be necessary to achieve a more mimetic tensile modulus.

A novel method for creating a negative mold based on high-resolution imaging of the native tissue as well as creation and implantation methods of a 3D TPE meniscal construct into an ovine joint were presented. The molding process described does have some limitations including the resolution at which it can recreate features, but is far more accurate at recapitulating the native meniscal geometry compared to the generic crescent wedge shapes used by other tissue engineered scaffolds. The method could also be implemented for patient-specific molding or personalized replacement creation. Molds were created using an unmodified low-cost 3D printer and open source software which reduces overall cost particularly if scaled to mass production. Alternative printing technology is available if a higher resolution mold is desired. Furthermore, due to the thermoplastic elastomer nature of this material, it could be created into a

printable filament and used to direct 3D print a dry TPE meniscal construct. This would reduce overall cost and time by eliminating the need for a negative mold. Elimination of the mold would also allow for a higher resolution print. Another aspect of the construct worth future investigation is the use of the extension tabs and the solid PLA plugs. If that method is found to be the best, the plugs could easily be created in nearly any material in order to be biocompatible, but an alternative method is also possible. The construct itself was a homogeneous isotropic material, and the sharper transitions to these extension tabs created stress concentrations on the construct which served as locations for failure. A smoother transition, such as the creation of a gradient, from the softer main body of the TPE hydrogel, construct to the ends of the tabs could help reduce those stress concentrations and increase the possibilities for fixation. Additional work could improve upon the implantation method. All implantations were performed in cadaver limbs which were highly dissected and removed of excess musculature. Surgical techniques will likely need to be adjusted when moving to an *in vivo* large animal model.

The pressure distribution study presented represents the most encompassing study to date using an ovine model. Multiple angles and loads were assessed and data collected for both the medial and lateral hemijoints for a number of treatment conditions. The 3D TPE meniscal constructs were compared to the native tissue as well as a meniscectomy, suture repair of the native tissue, and allograft transplant. Overall all conditions decreased contact area and increased mean and max pressures in the medial hemijoint. Compared the meniscectomy condition all the treatment conditions improved the mean and max pressure changes to the lateral hemijoint and slightly improved the pressures in the medial hemijoint but none of the treatments were able to restore medial contact areas or pressures to the native condition. Nevertheless, the 3D TPE hydrogel construct remains a promising meniscal replacement option. Additional work is

necessary to improve upon the fixation method of the 3D TPE hydrogel construct. Simple sutures and endotabs were used for the in situ testing performed within this study, but a fixation method which would allow better initial tensioning/placement of the construct within the joint as well as limit the relaxation following implantation would be ideal. Incorporation of fibers running through the construct or a transition from soft to hard material at the tabs of the construct would greatly increase the fixation options which could be explored.

This work presented the first steps in the creation of a new inert artificial meniscal replacement more mimetic in material properties as well as shape and geometry compared to any other replacement or scaffold currently available. The findings provided material properties for this novel TPE hydrogel material compared to human tissues, as well new information as to how the TPE hydrogel, as well as human and ovine meniscal tissue, respond under certain dynamic loading conditions. The molding techniques could be applied to any thermoplastic elastomer material in order to create more unique and complex meniscal constructs. The pressure distribution study suggests there is still much which can be improved upon for not only our TPE hydrogel construct but for other surgical treatments as well. Overall this work provides a launching pad for the continued investigation of this TPE hydrogel material as a potential meniscal replacement, as well as a guide for other potential replacements.

REFERENCES

1. Heegaard, J., Leyvraz, P. F., Curnier, A., Rakotomanana, L. & Huiskes, R. The biomechanics of the human patella during passive knee flexion. *J. Biomech.* **28,** 1265–1279 (1995).
2. Butler, D. L., Noyes, F. R. & Grood, E. S. Ligamentous restraints to anterior-posterior drawer in the human knee. A biomechanical study. *J. Bone Joint Surg. Am.* **62,** 259–70 (1980).
3. Amis, A. A. *et al.* Biomechanics of the PCL and related structures: posterolateral, posteromedial and meniscofemoral ligaments. *Knee Surgery, Sport. Traumatol. Arthrosc.* **11,** 271–281 (2003).
4. Wymenga, A. B., Kats, J. J., Kooloos, J. & Hillen, B. Surgical anatomy of the medial collateral ligament and the posteromedial capsule of the knee. *Knee Surgery, Sport. Traumatol. Arthrosc.* **14,** 229–234 (2006).
5. LaPrade, R. F., Ly, T. V, Wentorf, F. a & Engebretsen, L. The posterolateral attachments of the knee: a qualitative and quantitative morphologic analysis of the fibular collateral ligament, popliteus tendon, popliteofibular ligament, and lateral gastrocnemius tendon. *Am. J. Sports Med.* **31,** 854–860 (2003).
6. Schmidt, T. a, Gastelum, N. S., Nguyen, Q. T., Schumacher, B. L. & Sah, R. L. Boundary lubrication of articular cartilage: role of synovial fluid constituents. *Arthritis Rheum.* **56,** 882–91 (2007).
7. Lenoch, F. Disturbance of nourishment of the articular cartilage and its relation to the development of osteoarthrosis. *Rev. Czech. Med.* **16,** 113–7 (1970).
8. Fithian, D. C., Kelly, M. A. & Mow, V. C. Material properties and structure-function relationships in the menisci. *Clin. Orthop. Relat. Res.* 19–31 (1990).
9. Walker, P. S. & Erkman, M. J. The role of the menisci in force transmission across the knee. *Clin. Orthop. Relat. Res.* **109,** 184–92 (1975).
10. Kurosawa, H., Fukubayashi, T. & Nakajima, H. Load-bearing mode of the knee joint: physical behavior of the knee joint with or without menisci. *Clin. Orthop. Relat. Res.* 283–90 (1980).
11. Ahmed, A. M. & Burke, D. L. In-vitro measurement of static pressure distribution in synovial joints--Part I: Tibial surface of the knee. *J. Biomech. Eng.* **105,** 216–25 (1983).
12. Shrive, N. G., O'Connor, J. J. & Goodfellow, J. W. Load-bearing in the knee joint. *Clin. Orthop. Relat. Res.* **NA;,** 279–87 (1978).
13. Krause, W. R., Pope, M. H., Johnson, R. J. & Wilder, D. G. Mechanical changes in the knee after meniscectomy. *J. Bone Joint Surg. Am.* **58,** 599–604 (1976).
14. Mow, V. C., Arnoczky, S. P. & Jackson, D. W. *Knee meniscus: basic and clinical foundations*. (Raven Press, 1992).
15. Upton, M. L. *et al.* Biaxial strain effects on cells from the inner and outer regions of the meniscus. *Connect. Tissue Res.* **47,** 207–14 (2006).
16. MacCONAILL, M. A. The movements of bones and joints; the synovial fluid and its assistants. *J. Bone Joint Surg. Br.* **32–B,** 244–52 (1950).
17. McNicol, D. & Roughley, P. J. Extraction and characterization of proteoglycan from human meniscus. *Biochem. J.* **185,** 705–13 (1980).

18. Petersen, W. & Tillmann, B. Age-related blood and lymph supply of the knee menisci. A cadaver study. *Acta Orthop. Scand.* **66,** 308–312 (1995).
19. Clark, C. R. & Ogden, J. A. Development of the menisci of the human knee joint. Morphological changes and their potential role in childhood meniscal injury. *J. Bone Joint Surg. Am.* **65,** 538–47 (1983).
20. Abraham, A. C. & Haut Donahue, T. L. From Meniscus to Bone: A Quantitative Evaluation of Structure and Function of the Human Meniscal Attachments. *Acta Biomater.* (2013). doi:10.1016/j.actbio.2013.01.031
21. Messner, K. & Gao, J. The menisci of the knee joint. Anatomical and functional characteristics, and a rationale for clinical treatment. *J. Anat.* **193 (Pt 2,** 161–78 (1998).
22. Kohn, D. & Moreno, B. Meniscus insertion anatomy as a basis for meniscus replacement: A morphological cadaveric study. *Arthrosc. J. Arthrosc. Relat. Surg.* **11,** 96–103 (1995).
23. Keene, G. C., Bickerstaff, D., Rae, P. J. & Paterson, R. S. The natural history of meniscal tears in anterior cruciate ligament insufficiency. *Am. J. Sports Med.* **21,** 672–9 (1988).
24. Hough, A. J. & Webber, R. J. Pathology of the Meniscus. *Clin. Orthop. Relat. {...}* **252,** 32–40 (1990).
25. Englund, M. *et al.* Incidental meniscal findings on knee MRI in middle-aged and elderly persons. *N. Engl. J. Med.* **359,** 1108–15 (2008).
26. McNicholas, M. J. *et al.* Total meniscectomy in adolescence. A thirty-year follow-up. *J. Bone Joint Surg. Br.* **82,** 217–21 (2000).
27. Fairbank, T. J. Knee joint changes after meniscectomy. *J. Bone Joint Surg. Br.* **30B,** 664–70 (1948).
28. McDermott, I. D. & Amis, a a. The consequences of meniscectomy. *J. Bone Joint Surg. Br.* **88,** 1549–56 (2006).
29. Peterfy, C. G. *et al.* Whole-Organ Magnetic Resonance Imaging Score (WORMS) of the knee in osteoarthritis. *Osteoarthritis Cartilage* **12,** 177–90 (2004).
30. Felson, D. T. & Neogi, T. Osteoarthritis: is it a disease of cartilage or of bone? *Arthritis Rheum.* **50,** 341–4 (2004).
31. McGonagle, D., Tan, A. L., Carey, J. & Benjamin, M. The anatomical basis for a novel classification of osteoarthritis and allied disorders. *J. Anat.* **216,** 279–91 (2010).
32. Hunter, D. J. *et al.* The association of meniscal pathologic changes with cartilage loss in symptomatic knee osteoarthritis. *Arthritis Rheum.* **54,** 795–801 (2006).
33. Sharma, L. *et al.* Relationship of meniscal damage, meniscal extrusion, malalignment, and joint laxity to subsequent cartilage loss in osteoarthritic knees. *Arthritis Rheum.* **58,** 1716–26 (2008).
34. Greis, P. E., Bardana, D. D., Holmstrom, M. C. & Burks, R. T. Meniscal injury: I. Basic science and evaluation. *J. Am. Acad. Orthop. Surg.* **10,** 168–176 (2002).
35. Brindle, T., Nyland, J. & Johnson, D. L. The meniscus: review of basic principles with application to surgery and rehabilitation. *J. Athl. Train.* **36,** 160–9 (2001).
36. Felson, D. T., Anderson, J. J., Naimark, a, Walker, a M. & Meenan, R. F. Obesity and knee osteoarthritis. The Framingham Study. *Ann. Intern. Med.* **109,** 18–24 (1988).
37. Lee, R. & Kean, W. F. Obesity and knee osteoarthritis. *Inflammopharmacology* **20,** 53–8 (2012).
38. Muthuri, S. G., McWilliams, D. F., Doherty, M. & Zhang, W. History of knee injuries and knee osteoarthritis: a meta-analysis of observational studies. *Osteoarthritis Cartilage* **19,** 1286–93 (2011).

39. Lohmander, L. S., Ostenberg, a, Englund, M. & Roos, H. High prevalence of knee osteoarthritis, pain, and functional limitations in female soccer players twelve years after anterior cruciate ligament injury. *Arthritis Rheum.* **50,** 3145–52 (2004).
40. Neogi, T. & Zhang, Y. Epidemiology of osteoarthritis. *Rheum. Dis. Clin. North Am.* **39,** 1–19 (2013).
41. Bhattacharyya, T. *et al.* The clinical importance of meniscal tears demonstrated by magnetic resonance imaging in osteoarthritis of the knee. *J. Bone Joint Surg. Am.* **85–A,** 4–9 (2003).
42. Katz, J. N. & Martin, S. D. Meniscus--friend or foe: epidemiologic observations and surgical implications. *Arthritis Rheum.* **60,** 633–5 (2009).
43. Morgan, C. D., Wojtys, E. M., Casscells, C. D. & Casscells, S. W. Arthroscopic meniscal repair evaluated by second-look arthroscopy. *Am J Sport. Med* **19,** 632–638 (1991).
44. Warren, R. F. Arthroscopic meniscus repair. *Arthroscopy* **1,** 170–172 (1985).
45. Hanks, G. A., Gause, T. M., Sebastianelli, W. J., O'Donnell, C. S. & Kalenak, A. Repair of peripheral meniscal tears: Open versus arthroscopic technique. *Arthrosc. J. Arthrosc. Relat. Surg.* **7,** 72–77 (1991).
46. Scott, G. A., Jolly, B. L. & Henning, C. E. Combined posterior incision and arthroscopic intra-articular repair of the meniscus. An examination of factors affecting healing. *J. Bone Joint Surg. Am.* **68,** 847–61 (1986).
47. DeHaven, K. E., Black, K. P. & Griffiths, H. J. Open meniscus repair. Technique and two to nine year results. *Am. J. Sports Med.* **17,** 788–95
48. Buckwalter, J. a. Sports, joint injury, and posttraumatic osteoarthritis. *J. Orthop. Sports Phys. Ther.* **33,** 578–88 (2003).
49. Englund, M., Roos, E. M. & Lohmander, L. S. Impact of type of meniscal tear on radiographic and symptomatic knee osteoarthritis: a sixteen-year followup of meniscectomy with matched controls. *Arthritis Rheum.* **48,** 2178–87 (2003).
50. Roos, E. M., Ostenberg, a, Roos, H., Ekdahl, C. & Lohmander, L. S. Long-term outcome of meniscectomy: symptoms, function, and performance tests in patients with or without radiographic osteoarthritis compared to matched controls. *Osteoarthritis Cartilage* **9,** 316–24 (2001).
51. Goble, E. M., Kohn, D., Verdonk, R. & Kane, S. M. Meniscal substitutes--human experience. *Scand. J. Med. Sci. Sports* **9,** 146–57 (1999).
52. Rath, E., Richmond, J. C., Yassir, W., Albright, J. D. & Gundogan, F. Meniscal allograft transplantation. Two- to eight-year results. *Am. J. Sports Med.* **29,** 410–4 (2001).
53. Stollsteimer, G. T., Shelton, W. R., Dukes, a & Bomboy, a L. Meniscal allograft transplantation: a 1-to 5-year follow-up of 22 patients. *Arthrosc. J. ...* **16,** 343–347 (2000).
54. Crook, T. B., Ardolino, A., Williams, L. A. P. & Barlow, I. W. Meniscal allograft transplantation: A review of the current literature. *Ann. R. Coll. Surg. Engl.* **91,** 361–365 (2009).
55. Lee, S. R., Kim, J. G. & Nam, S. W. The tips and pitfalls of meniscus allograft transplantation. *Knee Surg. Relat. Res.* **24,** 137–45 (2012).
56. Chen, Y. *et al.* Current advances in the development of natural meniscus scaffolds: innovative approaches to decellularization and recellularization. *Cell Tissue Res.* 1–12 (2017). doi:10.1007/s00441-017-2605-0
57. Yuan, Z. *et al.* AMECM/DCB scaffold prompts successful total meniscus reconstruction in a rabbit total meniscectomy model. *Biomaterials* **111,** 13–26 (2016).

58. Sandmann, G. H. *et al.* Generation and characterization of a human acellular meniscus scaffold for tissue engineering. *J. Biomed. Mater. Res. A* **91,** 567–74 (2009).
59. Pabbruwe, M. B. *et al.* Repair of meniscal cartilage white zone tears using a stem cell/collagen-scaffold implant. *Biomaterials* **31,** 2583–2591 (2010).
60. Monllau, J. C. *et al.* Outcome after partial medial meniscus substitution with the collagen meniscal implant at a minimum of 10 years' follow-up. *Arthrosc. - J. Arthrosc. Relat. Surg.* **27,** 933–943 (2011).
61. Zaffagnini, S. *et al.* Prospective Long-Term Outcomes of the Medial Collagen Meniscus Implant Versus Partial Medial Meniscectomy. *Am. J. Sports Med.* **39,** 977–985 (2011).
62. Leroy, A. *et al.* Actifit®polyurethane meniscal scaffold: MRI and functional outcomes after a minimum follow-up of 5 years. *Orthop. Traumatol. Surg. Res.* **103,** 609–614 (2017).
63. van Tienen, T. G., Hannink, G. & Buma, P. Meniscus replacement using synthetic materials. *Clin. Sports Med.* **28,** 143–56 (2009).
64. Park, S. H., Kim, T. G., Kim, H. C., Yang, D. Y. & Park, T. G. Development of dual scale scaffolds via direct polymer melt deposition and electrospinning for applications in tissue regeneration. *Acta Biomater.* **4,** 1198–1207 (2008).
65. Baek, J. *et al.* Meniscus Tissue Engineering Using a Novel Combination of Electrospun Scaffolds and Human Meniscus Cells Embedded within an Extracellular Matrix Hydrogel. *J. Orthop. Res.* (2015). doi:10.1002/jor.22802
66. Guarino, V., Gloria, A., De Santis, R. & Ambrosio, L. in *Biomedical Applications of Hydrogels Handbook* **c,** 227–245 (Springer New York, 2010).
67. Wu, J. *et al.* An injectable extracellular matrix derived hydrogel for meniscus repair and regeneration. *Acta Biomater.* (2015). doi:10.1016/j.actbio.2015.01.027
68. Elsner, J. J. *et al.* Design of a Free-Floating Polycarbonate-Urethane Meniscal Implant Using Finite Element Modeling and Experimental Validation. *J. Biomech. Eng.* **132,** 95001 (2010).
69. Vrancken, A. C. T. *et al.* In Vivo Performance of a Novel, Anatomically Shaped, Total Meniscal Prosthesis Made of Polycarbonate Urethane: A 12-Month Evaluation in Goats. *Am. J. Sports Med.* 36354651771368 (2017). doi:10.1177/0363546517713687
70. Kobayashi, M., Toguchida, J. & Oka, M. Preliminary study of polyvinyl alcohol-hydrogel (PVA-H) artificial meniscus. *Biomaterials* **24,** 639–47 (2003).
71. Holloway, J. L., Lowman, A. M. & Palmese, G. R. Mechanical evaluation of poly(vinyl alcohol)-based fibrous composites as biomaterials for meniscal tissue replacement. *Acta Biomater.* **6,** 4716–4724 (2010).
72. Martinek, V. *et al.* Second generation of meniscus transplantation: In-vivo study with tissue engineered meniscus replacement. *Arch. Orthop. Trauma Surg.* **126,** 228–234 (2006).
73. Gwinner, C. *et al.* Biomechanical performance of a collagen meniscus implant with regard to suture material and irrigation fluid. *Knee* **24,** 726–732 (2017).
74. Reguzzoni, M., Manelli, A., Ronga, M., Raspanti, M. & Grassi, F. A. Histology and ultrastructure of a tissue-engineered collagen meniscus before and after implantation. *J. Biomed. Mater. Res. - Part B Appl. Biomater.* **74,** 808–816 (2005).
75. Steadman, J. R. & Rodkey, W. G. Tissue-engineered collagen meniscus implants: 5- To 6-year feasibility study results. *Arthrosc. - J. Arthrosc. Relat. Surg.* **21,** 515–525 (2005).
76. Welsing, R. T. C. *et al.* Effect on tissue differentiation and articular cartilage degradation

of a polymer meniscus implant: A 2-year follow-up study in dogs. *Am. J. Sports Med.* **36,** 1978–89 (2008).
77. Chiari, C. *et al.* A tissue engineering approach to meniscus regeneration in a sheep model. *Osteoarthritis Cartilage* **14,** 1056–65 (2006).
78. Bouyarmane, H. *et al.* Polyurethane scaffold in lateral meniscus segmental defects: Clinical outcomes at 24months follow-up. *Orthop. Traumatol. Surg. Res.* **100,** 153–157 (2014).
79. Papalia, R. *et al.* Scaffolds for partial meniscal replacement: An updated systematic review. *Br. Med. Bull.* **107,** 19–40 (2013).
80. Zur, G. *et al.* Chondroprotective effects of a polycarbonate-urethane meniscal implant: Histopathological results in a sheep model. *Knee Surgery, Sport. Traumatol. Arthrosc.* **19,** 255–263 (2011).
81. Majd, S. E. *et al.* An in vitro study of cartilage-meniscus tribology to understand the changes caused by a meniscus implant. *Colloids Surf. B. Biointerfaces* **155,** 294–303 (2017).
82. Kobayashi, M., Toguchida, J. & Oka, M. Development of an artificial meniscus using polyvinyl alcohol-hydrogel for early return to, and continuance of, athletic life in sportspersons with severe meniscus injury. I: mechanical evaluation. *Knee* **10,** 47–51 (2003).
83. Holloway, J. L., Spiller, K. L., Lowman, A. M. & Palmese, G. R. Analysis of the in vitro swelling behavior of poly(vinyl alcohol) hydrogels in osmotic pressure solution for soft tissue replacement. *Acta Biomater.* **7,** 2477–2482 (2011).
84. Suciu, A. N., Iwatsubo, T., Matsuda, M. & Nishino, T. A Study upon Durability of the Artificial Knee Joint with PVA Hydrogel Cartilage. *JSME International Journal Series C* **47,** 199–208 (2004).
85. Kelly, B. T. *et al.* Hydrogel meniscal replacement in the sheep knee: preliminary evaluation of chondroprotective effects. *Am. J. Sports Med.* **35,** 43–52 (2007).
86. Petrini, P., Farè, S., Piva, A. & Tanzi, M. C. Design, synthesis and properties of polyurethane hydrogels for tissue engineering. *J. Mater. Sci. Mater. Med.* **14,** 683–686 (2003).
87. Guo, C. & Bailey, T. S. Highly distensible nanostructured elastic hydrogels from AB diblock and ABA triblock copolymer melt blends. *Soft Matter* **6,** 4807 (2010).
88. Guo, C. & Bailey, T. S. Tailoring mechanical response through coronal layer overlap in tethered micelle hydrogel networks. *Soft Matter* **11,** 7345–55 (2015).
89. Bates, F. S. & Fredrickson, G. H. Block copolymers -- designer soft materials. *Phys. Today* **52,** 32–38 (1999).
90. Cochran, E. W., Garcia-Cervera, C. J. & Fredrickson, G. H. Stability of the gyroid phase in diblock copolymers at strong segregation. *Macromolecules* **39,** 2449–2451 (2006).
91. Park, K. *et al.* Preparation and characterization of self-assembled nanoparticles of heparin-deoxycholic acid conjugates. *Langmuir* **20,** 11726–11731 (2004).
92. Bromberg, L. Scaling of Rheological Properties of Hydrogels from Associating Polymers. *Macromolecules* **31,** 6148–6156 (1998).
93. Fujiwara, T. *et al.* Novel thermo-responsive formation of a hydrogel by stereo-complexation between PLLA-PEG-PLLA and PDLA-PEG-PDLA block copolymers. *Macromol. Biosci.* **1,** 204–208 (2001).
94. Gong, J. P., Katsuyama, Y., Kurokawa, T. & Osada, Y. Double-network hydrogels with

extremely high mechanical strength. *Adv. Mater.* **15,** 1155–1158 (2003).
95. Kamata, H., Akagi, Y., Kayasuga-Kariya, Y., Chung, U. -i. & Sakai, T. 'Nonswellable' Hydrogel Without Mechanical Hysteresis. *Science (80-.).* **343,** 873–875 (2014).
96. Li, W. *et al.* Hydrophobically associated hydrogels based on acrylamide and anionic surface active monomer with high mechanical strength. *Soft Matter* **8,** 5078 (2012).
97. Henderson, K. J., Zhou, T. C., Otim, K. J. & Shull, K. R. Ionically cross-linked triblock copolymer hydrogels with high strength. *Macromolecules* **43,** 6193–6201 (2010).
98. Sun, J.-Y. *et al.* Highly stretchable and tough hydrogels. *Nature* **489,** 133–6 (2012).
99. Brown, A. E. X., Litvinov, R. I., Discher, D. E., Purohit, P. K. & Weisel, J. W. Multiscale Mechanics of Fibrin Polymer: Gel Stretching with Protein Unfolding and Loss of Water. *Science (80-.).* **325,** 741–744 (2009).
100. Bin Imran, A. *et al.* Extremely stretchable thermosensitive hydrogels by introducing slide-ring polyrotaxane cross-linkers and ionic groups into the polymer network. *Nat. Commun.* **5,** 5124 (2014).
101. Ito, K. Novel Cross-Linking Concept of Polymer Network: Synthesis, Structure, and Properties of Slide-Ring Gels with Freely Movable Junctions. *Polym. J.* **39,** 489–499 (2007).
102. Sakai, T. *et al.* Highly elastic and deformable hydrogel formed from tetra-arm polymers. *Macromol. Rapid Commun.* **31,** 1954–1959 (2010).
103. Sakai, T. *et al.* Design and fabrication of a high-strength hydrogel with ideally homogeneous network structure from tetrahedron-like macromonomers. *Macromolecules* **41,** 5379–5384 (2008).
104. Andrews, S., Shrive, N. & Ronsky, J. The shocking truth about meniscus. *Journal of Biomechanics* **44,** 2737–2740 (2011).
105. Wagenseil, J. E. & Mecham, R. P. Vascular Extracellular Matrix and Arterial Mechanics. *Physiol. Rev.* **89,** 957–989 (2009).
106. El Fray, M., Prowans, P., Puskas, J. E. & Altstädt, V. Biocompatibility and fatigue properties of polystyrene-polyisobutylene-polystyrene, an emerging thermoplastic elastomeric biomaterial. *Biomacromolecules* **7,** 844–850 (2006).
107. Miller, A. T., Safranski, D. L., Smith, K. E., Guldberg, R. E. & Gall, K. Compressive cyclic ratcheting and fatigue of synthetic, soft biomedical polymers in solution. *J. Mech. Behav. Biomed. Mater.* **54,** 268–82 (2016).
108. Puskas, J. E. *et al.* Fatigue testing of implantable specimens: Effect of sample size and branching on the dynamic fatigue properties of polyisobutylene-based biomaterials. *Polymer (Guildf).* **50,** 591–597 (2009).
109. Puskas, J. E. *et al.* Dynamic stress relaxation of thermoplastic elastomeric biomaterials. *Polymer (Guildf).* **50,** 245–249 (2009).
110. Zhao, X. Multi-scale multi-mechanism design of tough hydrogels: building dissipation into stretchy networks. *Soft Matter* **10,** 672–687 (2014).
111. Long, R. & Hui, C.-Y. Fracture toughness of hydrogels: measurement and interpretation. *Soft Matter* **12,** 8069–8086 (2016).
112. Naficy, S., Brown, H. R., Razal, J. M., Spinks, G. M. & Whitten, P. G. Progress Toward Robust Polymer Hydrogels. *Aust. J. Chem.* **64,** 1007 (2011).
113. Freutel, M. *et al.* Medial meniscal displacement and strain in three dimensions under compressive loads: MR assessment. *J. Magn. Reson. Imaging* **40,** 1181–1188 (2014).
114. Spencer Jones, R. *et al.* Direct measurement of hoop strains in the intact and torn human

medial meniscus. *Clin. Biomech.* **11,** 295–300 (1996).
115. Tissakht, M. & Ahmed, a M. Tensile stress-strain characteristics of the human meniscal material. *J. Biomech.* **28,** 411–22 (1995).
116. Costi, J. J. *et al.* Direct measurement of intervertebral disc maximum shear strain in six degrees of freedom: Motions that place disc tissue at risk of injury. *J. Biomech.* **40,** 2457–2466 (2007).
117. Stokes, I. A. Surface strain on human intervertebral discs. *Journal of orthopaedic research : official publication of the Orthopaedic Research Society* **5,** 348–355 (1987).
118. Armstrong, C. G., Bahrani, A. S. & Gardner, D. L. In vitro measurement of articular-cartilage deformations in the intact human hip-joint under load. *J. Bone Jt. Surgery-American Vol.* **61,** 744–755 (1979).
119. Guterl, C. C. *et al.* Two-dimensional strain fields on the cross-section of the human patellofemoral joint under physiological loading. *J. Biomech.* **42,** 1275–1281 (2009).
120. Guo, C., Lewis, J. T., Scalfani, V. F., Schwartz, M. M. & Bailey, T. S. Dangling-End Double Networks: Tapping Hidden Toughness in Highly Swollen Thermoplastic Elastomer Hydrogels. *Chem. Mater.* **28,** 1678–1690 (2016).
121. Wijayasekara, D. B. *et al.* Elastic free-standing RTIL composite membranes for CO2/N2 separation based on sphere-forming triblock/diblock copolymer blends. *J. Memb. Sci.* **511,** 170–179 (2016).
122. Allen, K. D. & Golightly, Y. M. Epidemiology of osteoarthritis: state of the evidence. *Curr. Opin. Rheumatol.* **27,** 276–283 (2015).
123. Fujiwara, A. *et al.* The relationship between facet joint osteoarthritis and disc degeneration of the lumbar spine: an MRI study. *Eur. Spine J.* **8,** 396–401 (1999).
124. Sharma, L. Osteoarthritis year in review 2015: clinical. *Osteoarthr. Cartil.* **24,** 36–48 (2016).
125. Beveridge, J. E., Shrive, N. G. & Frank, C. B. Meniscectomy causes significant in vivo kinematic changes and mechanically induced focal chondral lesions in a sheep model. *J. Orthop. Res.* **29,** 1397–405 (2011).
126. Butler, D., Trafimow, J. H., Andersson, G. B., McNeill, T. W. & Huckman, M. S. Discs degenerate before facets. *Spine (Phila. Pa. 1976).* **15,** 111–3 (1990).
127. Sophia Fox, A. J., Bedi, A. & Rodeo, S. A. The Basic Science of Articular Cartilage: Structure, Composition and Function. *Orthopaedics* **1,** 461–468 (2009).
128. Roberts, S., Eisenstein, S. M., Menage, J., Evans, E. H. & Ashton, I. K. Mechanoreceptors in intervertebral discs. Morphology, distribution, and neuropeptides. *Spine (Phila. Pa. 1976).* **20,** 2645–51 (1995).
129. Karuppal, R. Current concepts in the articular cartilage repair and regeneration. *J. Orthop.* **14,** A1–A3 (2017).
130. Verdonk, P. C. M. *et al.* Transplantation of Viable Meniscal Allograft. *J. Bone Jt. Surg.* **87–A,** 715–724 (2005).
131. Urban, J. P. G. & Roberts, S. Degeneration of the intervertebral disc. *Arthritis Res. Ther.* **5,** 120–130 (2003).
132. Ghiselli, G., Wang, J. C., Bhatia, N. N., Hsu, W. K. & Dawson, E. G. Adjacent segment degeneration in the lumbar spine. *J. Bone Joint Surg. Am.* **86–A,** 1497–503 (2004).
133. Hilibrand, A. S. & Robbins, M. Adjacent segment degeneration and adjacent segment disease: The consequences of spinal fusion? *Spine J.* **4,** 190–194 (2004).
134. Nguyen, Q. T., Hwang, Y., Chen, A. C., Varghese, S. & Sah, R. L. Cartilage-like

mechanical properties of poly (ethylene glycol)-diacrylate hydrogels. *Biomaterials* **33,** 6682–90 (2012).
135. Baker, M. I., Walsh, S. P., Schwartz, Z. & Boyan, B. D. A review of polyvinyl alcohol and its uses in cartilage and orthopedic applications. *J. Biomed. Mater. Res. B. Appl. Biomater.* **100,** 1451–7 (2012).
136. Xiao, Y., Friis, E. A., Gehrke, S. H. & Detamore, M. S. Mechanical testing of hydrogels in cartilage tissue engineering: beyond the compressive modulus. *Tissue Eng. Part B. Rev.* **19,** 403–12 (2013).
137. Jones, E. M. C., Silberstein, M. N., White, S. R. & Sottos, N. R. In Situ Measurements of Strains in Composite Battery Electrodes during Electrochemical Cycling. *Exp. Mech.* **54,** 971–985 (2014).
138. Abraham, A. C., Edwards, C. R., Odegard, G. M. & Donahue, T. L. H. Regional and fiber orientation dependent shear properties and anisotropy of bovine meniscus. *J. Mech. Behav. Biomed. Mater.* **4,** 2024–30 (2011).
139. Fischenich, K. M., Boncella, K., Lewis, J. T., Bailey, T. S. & Haut Donahue, T. L. Dynamic compression of human and ovine meniscal tissue compared with a potential thermoplastic elastomer hydrogel replacement. *J. Biomed. Mater. Res. A* **105,** 1–7 (2017).
140. Chia, H. N. & Hull, M. L. Compressive moduli of the human medial meniscus in the axial and radial directions at equilibrium and at a physiological strain rate. *J. Orthop. Res.* **26,** 951–6 (2008).
141. Moyer, J. T., Priest, R., Bouman, T., Abraham, A. C. & Haut Donahue, T. L. Indentation properties and glycosaminoglycan content of human menisci in the deep zone. *Acta Biomater.* 1–6 (2013). doi:10.1016/j.actbio.2012.12.033
142. Bursac, P., York, A., Kuznia, P., Brown, L. M. & Arnoczky, S. P. Influence of donor age on the biomechanical and biochemical properties of human meniscal allografts. *Am. J. Sports Med.* **37,** 884–889 (2009).
143. Hayes, W. C. & Mockros, L. F. Viscoelastic properties of human articular cartilage. *J. Appl. Physiol.* **31,** 562–568 (1971).
144. Wilson, W., Huyghe, J. M. & van Donkelaar, C. C. A composition-based cartilage model for the assessment of compositional changes during cartilage damage and adaptation. *Osteoarthr. Cartil.* **14,** 554–560 (2006).
145. Julkunen, P. *et al.* Stress-relaxation of human patellar articular cartilage in unconfined compression: Prediction of mechanical response by tissue composition and structure. *J. Biomech.* **41,** 1978–1986 (2008).
146. Cloyd, J. M. *et al.* Material properties in unconfined compression of human nucleus pulposus, injectable hyaluronic acid-based hydrogels and tissue engineering scaffolds. *Eur. Spine J.* **16,** 1892–1898 (2007).
147. Umehara, S. *et al.* Effects of degeneration on the elastic modulus distribution in the lumbar intervertebral disc. *Spine* **21,** 811–819; discussion 820 (1996).
148. Klisch, S. M. & Lotz, J. C. A special theory of biphasic mixtures and experimental results for human annulus fibrosus tested in confined compression. *J Biomech Eng* **122,** 180–188 (2000).
149. Iatridis, J. C. *et al.* Degeneration affects the anisotropic and nonlinear behaviors of human anulus fibrosus in compression. *J. Biomech.* **31,** 535–544 (1998).
150. Wilson, W., van Donkelaar, C. C., van Rietbergen, B., Ito, K. & Huiskes, R. Stresses in the local collagen network of articular cartilage: a poroviscoelastic fibril-reinforced finite

element study. *J. Biomech.* **37,** 357–66 (2004).
151. Moyer, J. T., Abraham, A. C. & Haut Donahue, T. L. Nanoindentation of human meniscal surfaces. *J. Biomech.* **45,** 2230–2235 (2012).
152. Danso, E. K. *et al.* Characterization of site-specific biomechanical properties of human meniscus-Importance of collagen and fluid on mechanical nonlinearities. *J. Biomech.* **48,** 1499–1507 (2015).
153. Bursac, P., Arnoczky, S. & York, A. Dynamic compressive behavior of human meniscus correlates with its extra-cellular matrix composition. *Biorheology* **46,** 227–37 (2009).
154. Joshi, M. D., Suh, J. K., Marui, T. & Woo, S. L. Interspecies variation of compressive biomechanical properties of the meniscus. *J. Biomed. Mater. Res.* **29,** 823–8 (1995).
155. Martin Seitz, A., Galbusera, F., Krais, C., Ignatius, A. & Dürselen, L. Stress-relaxation response of human menisci under confined compression conditions. *J. Mech. Behav. Biomed. Mater.* **26,** 68–80 (2013).
156. Sweigart, M. a *et al.* Intraspecies and interspecies comparison of the compressive properties of the medial meniscus. *Ann. Biomed. Eng.* **32,** 1569–79 (2004).
157. Jurvelin, J. S., Buschmann, M. D. & Hunziker, E. B. Mechanical anisotropy of the human knee articular cartilage in compression. *Proc. Inst. Mech. Eng. Part H J. Eng. Med.* **217,** 215–219 (2003).
158. Sokoloff, L. Elasticity of aging cartilage. *Fed. Proc.* **25,** 1089–95 (1966).
159. Shepherd, D. E. & Seedhom, B. B. The 'instantaneous' compressive modulus of human articular cartilage in joints of the lower limb. *Rheumatology (Oxford).* **38,** 124–32 (1999).
160. Tanaka, E. *et al.* Dynamic compressive properties of the mandibular condylar cartilage. *J. Dent. Res.* **85,** 571–5 (2006).
161. Fortis, A. P., Kostopoulos, V., Panagiotopoulos, E., Tsantzalis, S. & Kokkinos, A. Viscoelastic properties of cartilage-subchondral bone complex in osteoarthritis. *J. Med. Eng. Technol.* **28,** 223–6 (2004).
162. Akizuki, S. *et al.* Tensile properties of human knee joint cartilage: I. Influence of ionic conditions, weight bearing, and fibrillation on the tensile modulus. *J. Orthop. Res.* **4,** 379–92 (1986).
163. Chen, S. S., Falcovitz, Y. H., Schneiderman, R., Maroudas, A. & Sah, R. L. Depth-dependent compressive properties of normal aged human femoral head articular cartilage: Relationship to fixed charge density. *Osteoarthr. Cartil.* **9,** 561–569 (2001).
164. Son, M. *et al.* Regional variation in T1ρ and T2 times in osteoarthritic human menisci: correlation with mechanical properties and matrix composition. *Osteoarthritis Cartilage* **21,** 796–805 (2013).
165. Párraga Quiroga, J. M., Emans, P., Wilson, W., Ito, K. & van Donkelaar, C. C. Should a native depth-dependent distribution of human meniscus constitutive components be considered in FEA-models of the knee joint? *J. Mech. Behav. Biomed. Mater.* **38,** 242–250 (2014).
166. Newell, N. *et al.* Biomechanics of the human intervertebral disc: A review of testing techniques and results. *J. Mech. Behav. Biomed. Mater.* **69,** 420–434 (2017).
167. Iatridis, J. C., Kumar, S., Foster, R. J., Weidenbaum, M. & Mow, V. C. Shear mechanical properties of human lumbar annulus fibrosus. *J. Orthop. Res.* **17,** 732–7 (1999).
168. Fujita, Y., Wagner, D. R., Biviji, A. A., Duncan, N. A. & Lotz, J. C. Anisotropic shear behavior of the annulus fibrosus: Effect of harvest site and tissue prestrain. *Med. Eng. Phys.* **22,** 349–357 (2000).

169. Hori, R. Y. & Mockros, L. F. Indentation tests of human articular cartilage. *J. Biomech.* **9,** 259–268 (1976).
170. Setton, L. a, Mow, V. C. & Howell, D. S. Mechanical behavior of articular cartilage in shear is altered by transection of the anterior cruciate ligament. *J. Orthop. Res.* **13,** 473–82 (1995).
171. Markovic, M. *et al.* Hybrid Tissue Engineering Scaffolds by Combination of Three-Dimensional Printing and Cell Photoencapsulation. *J. Nanotechnol. Eng. Med.* **6,** 0210011–0210017 (2015).
172. Skaggs, D. L., Weidenbaum, M., Iatridis, J. C., Ratcliffe, A. & Mow, V. C. Regional variation in tensile properties and biochemical composition of the human lumbar anulus fibrosus. *Spine (Phila. Pa. 1976).* **19,** 1310–9 (1994).
173. Lechner, K., Hull, M. L. & Howell, S. M. Is the circumferential tensile modulus within a human medial meniscus affected by the test sample location and cross-sectional area? *J. Orthop. Res.* **18,** 945–51 (2000).
174. Huang, C. Y., Stankiewicz, A., Ateshian, G. A. & Mow, V. C. Anisotropy, inhomogeneity, and tension-compression nonlinearity of human glenohumeral cartilage in finite deformation. *J. Biomech.* **38,** 799–809 (2005).
175. Allen, A. A., Caldwell, G. L. J. & Fu, F. H. Anatomy and biomechanics of the meniscus. *Oper. Tech. Orthop.* **5,** 2–9 (1995).
176. Nakano, T., Dodd, C. M. & Scott, P. G. Glycosaminoglycans and proteoglycans from different zones of the porcine knee meniscus. *J. Orthop. Res.* **15,** 213–20 (1997).
177. Valiyaveettil, M., Mort, J. S. & McDevitt, C. a. The concentration, gene expression, and spatial distribution of aggrecan in canine articular cartilage, meniscus, and anterior and posterior cruciate ligaments: a new molecular distinction between hyaline cartilage and fibrocartilage in the knee joint. *Connect. Tissue Res.* **46,** 83–91 (2005).
178. Leslie, B. W., Gardner, D. L., McGeough, J. a. & Moran, R. S. Anisotropic response of the human knee joint meniscus to unconfined compression. *Proc. Inst. Mech. Eng. H.* **214,** 631–5 (2000).
179. Fischenich, K. M., Lewis, J., Kindsfater, K. a., Bailey, T. S. & Haut Donahue, T. L. Effects of degeneration on the compressive and tensile properties of human meniscus. *J. Biomech.* **48,** 1407–11 (2015).
180. Fox, A. J. S., Wanivenhaus, F., Burge, A. J., Warren, R. F. & Rodeo, S. a. The human meniscus: A review of anatomy, function, injury, and advances in treatment. *Clin. Anat.* **0,** (2014).
181. Kim, S., Bosque, J., Meehan, J. P., Jamali, A. & Marder, R. Increase in outpatient knee arthroscopy in the United States: a comparison of National Surveys of Ambulatory Surgery, 1996 and 2006. *J. Bone Joint Surg. Am.* **93,** 994–1000 (2011).
182. Renström, P. & Johnson, R. J. Anatomy and biomechanics of the menisci. *Clin. Sports Med.* **9,** 523–38 (1990).
183. Kobayashi, M., Chang, Y.-S. & Oka, M. A two year in vivo study of polyvinyl alcohol-hydrogel (PVA-H) artificial meniscus. *Biomaterials* **26,** 3243–8 (2005).
184. Messner, K. Meniscal substitution with a Teflon-periosteal composite graft: a rabbit experiment. *Biomaterials* **15,** 223–230 (1994).
185. Kelly, B. T. *et al.* Meniscal allograft transplantation in the sheep knee: evaluation of chondroprotective effects. *Am. J. Sports Med.* **34,** 1464–77 (2006).
186. Gruchenberg, K. *et al.* In vivo performance of a novel silk fibroin scaffold for partial

meniscal replacement in a sheep model. *Knee Surgery, Sport. Traumatol. Arthrosc.* **23,** 2218–2229 (2014).
187. Vrancken, a. C. T. *et al.* Functional biomechanical performance of a novel anatomically shaped polycarbonate urethane total meniscus replacement. *Knee Surg. Sports Traumatol. Arthrosc.* (2015). doi:10.1007/s00167-015-3632-6
188. Tienen, T. G. *et al.* A porous polymer scaffold for meniscal lesion repair--a study in dogs. *Biomaterials* **24,** 2541–2548 (2003).
189. Tienen, T. G. *et al.* Replacement of the knee meniscus by a porous polymer implant: a study in dogs. *Am. J. Sports Med.* **34,** 64–71 (2006).
190. Cristino, S. *et al.* Analysis of mesenchymal stem cells grown on a three-dimensional HYAFF 11??-based prototype ligament scaffold. *J. Biomed. Mater. Res. - Part A* **73,** 275–283 (2005).
191. Kon, E. *et al.* Tissue engineering for total meniscal substitution: animal study in sheep model--results at 12 months. *Tissue Eng. Part A* **18,** 1573–82 (2012).
192. Takroni, T., Laouar, L., Adesida, A., Elliott, J. A. W. & Jomha, N. M. Anatomical study: comparing the human, sheep and pig knee meniscus. *J. Exp. Orthop.* **3,** 35 (2016).
193. Chevrier, A., Nelea, M., Hurtig, M. B., Hoemann, C. D. & Buschmann, M. D. Meniscus structure in human, sheep, and rabbit for animal models of meniscus repair. *J. Orthop. Res.* **27,** 1197–203 (2009).
194. Choi, B. C. K., Pak, A. W. P., Choi, J. C. L. & Choi, E. C. L. Daily step goal of 10,000 steps: A literature review. *Clinical and Investigative Medicine* **30,** 146–151 (2007).
195. Woo, S. L., Gomez, M. A. & Akeson, W. H. The time and history-dependent viscoelastic properties of the canine medical collateral ligament. *J. Biomech. Eng.* **103,** 293–8 (1981).
196. Doehring, T. C., Carew, E. O. & Vesely, I. The effect of strain rate on the viscoelastic response of aortic valve tissue: A direct-fit approach. *Ann. Biomed. Eng.* **32,** 223–232 (2004).
197. Nicolle, S., Vezin, P. & Palierne, J. F. A strain-hardening bi-power law for the nonlinear behaviour of biological soft tissues. *J. Biomech.* **43,** 927–932 (2010).
198. Galley, N. K. *et al.* Frictional properties of the meniscus improve after scaffold-augmented repair of partial meniscectomy: A pilot study. *Clin. Orthop. Relat. Res.* **469,** 2817–2823 (2011).
199. Sanchez-Adams, J., Willard, V. P. & Athanasiou, K. a. Regional variation in the mechanical role of knee meniscus glycosaminoglycans. *J. Appl. Physiol.* **111,** 1590–6 (2011).
200. Felson, D. T. *et al.* The prevalence of knee osteoarthritis in the elderly. The Framingham Osteoarthritis Study. *Arthritis Rheum.* **30,** 914–8 (1987).
201. Maletius, W. & Messner, K. Eighteen- to twenty-four-year follow-up after complete rupture of the anterior cruciate ligament. *Am. J. Sports Med.* **27,** 711–7 (1999).
202. Englund, M. Meniscal tear--a feature of osteoarthritis. *Acta Orthop. Scand. Suppl.* **75,** 1–45, backcover (2004).
203. Stärke, C., Kopf, S., Petersen, W. & Becker, R. Meniscal repair. *Arthroscopy* **25,** 1033–44 (2009).
204. Haut Donahue, T. L., Hull, M. L., Rashid, M. M. & Jacobs, C. R. The sensitivity of tibiofemoral contact pressure to the size and shape of the lateral and medial menisci. *J. Orthop. Res.* **22,** 807–14 (2004).
205. Haut Donahue, T. L., Hull, M. L., Rashid, M. M. & Jacobs, C. R. A Finite Element Model

of the Human Knee Joint for the Study of Tibio-Femoral Contact. *J. Biomech. Eng.* **124,** 273 (2002).
206. Fischenich, K. M., Lewis, J. T., Bailey, T. S. & Donahue, T. L. H. Mechanical Viability of a Thermoplastic Elastomer Hydrogel as a Soft Tissue Replacement Material. *J. Mech. Behav. Biomed. Mater.* **79,** 341–347 (2018).
207. Cole, B. J., Carter, T. R. & Rodeo, S. A. Allograft meniscal transplantation: background, techniques, and results. *Instr. Course Lect.* **52,** 383–396 (2003).
208. McNickle, A. G., Wang, V. M., Shewman, E. F., Cole, B. J. & Williams, J. M. Performance of a sterile meniscal allograft in an ovine model. *Clin. Orthop. Relat. Res.* **467,** 1868–1876 (2009).
209. Shelton, W. R. & Dukes, A. D. Meniscus replacement with bone anchors: a surgical technique. *Arthroscopy* **10,** 324–7 (1994).
210. von Lewinski, G., Kohn, D., Wirth, C. J. & Lazovic, D. The influence of nonanatomical insertion and incongruence of meniscal transplants on the articular cartilage in an ovine model. *Am. J. Sport. Med.* **36,** 841–850 (2008).
211. Zhang, Z.-Z. *et al.* 3D-Printed Poly(ε-caprolactone) Scaffold Augmented With Mesenchymal Stem Cells for Total Meniscal Substitution. *Am. J. Sports Med.* 36354651769151 (2017). doi:10.1177/0363546517691513
212. Szojka, A. *et al.* Biomimetic 3D printed scaffolds for meniscus tissue engineering. *Bioprinting* **8,** 1–7 (2017).
213. Ballyns, J. J., Wright, T. M. & Bonassar, L. J. Effect of media mixing on ECM assembly and mechanical properties of anatomically-shaped tissue engineered meniscus. *Biomaterials* **31,** 6756–63 (2010).
214. Yang, F., Tadepalli, V. & Wiley, B. J. 3D Printing of a Double Network Hydrogel with a Compression Strength and Elastic Modulus Greater than those of Cartilage. *ACS Biomater. Sci. Eng.* **3,** 863–869 (2017).
215. Lee, S. J. *et al.* Tibiofemoral Contact Mechanics After Serial Medial Meniscectomies in the Human Cadaveric Knee. *Am. J. Sports Med.* **34,** 1334–1344 (2006).
216. von Lewinski, G., Stukenborg-Colsman, C., Ostermeier, S. & Hurschler, C. Experimental measurement of tibiofemoral contact area in a meniscectomized ovine model using a resistive pressure measuring sensor. *Ann. Biomed. Eng.* **34,** 1607–14 (2006).
217. Padalecki, J. R. *et al.* Biomechanical consequences of a complete radial tear adjacent to the medial meniscus posterior root attachment site: in situ pull-out repair restores derangement of joint mechanics. *Am J Sport. Med* **42,** 699–707 (2014).
218. Tapper, E. M. & Hoover, N. W. Late results after meniscectomy. *J. Bone Joint Surg. Am.* **51,** 517–26 passim (1969).
219. Paxton, E. S., Stock, M. V. & Brophy, R. H. Meniscal repair versus partial meniscectomy: A systematic review comparing reoperation rates and clinical outcomes. *Arthrosc. - J. Arthrosc. Relat. Surg.* **27,** 1275–1288 (2011).
220. Scotti, C., Hirschmann, M., Antinolfi, P., Martin, I. & Peretti, G. Meniscus repair and regeneration: review on current methods and research potential. *Eur. Cells Mater.* **26,** 150–170 (2013).
221. Koukoulias, N., Dimitriadis, T., Germanou, E., Papavasileiou, A. & Sinopidis, C. Meniscal Scaffolds : a Mini Review. *J. Surg. Surg. Res.* **1,** 11–14 (2015).
222. Buma, P., Ramrattan, N. N., van Tienen, T. G. & Veth, R. P. H. Tissue engineering of the meniscus. *Biomaterials* **25,** 1523–32 (2004).

223. Sun, J., Vijayavenkataraman, S. & Liu, H. An overview of scaffold design and fabrication technology for engineered knee meniscus. *Materials (Basel).* **10,** 1–19 (2017).
224. Alhalki, M. M., Howell, S. M. & Hull, M. L. How three methods for fixing a medial meniscal autograft affect tibial contact mechanics. *Am. J. Sports Med.* **27,** 320–8 (1999).
225. Chen, M. I., Branch, T. P. & Hutton, W. C. Is it important to secure the horns during lateral meniscal transplantation? A cadaveric study. *Arthroscopy* **12,** 174–181 (1996).
226. Paletta, G. A., Manning, T., Snell, E., Parker, R. & Bergfeld, J. The effect of allograft meniscal replacement on intraarticular contact area and pressures in the human knee. A biomechanical study. *Am. J. Sports Med.* **25,** 692–8
227. Radin, E. L., de Lamotte, F. & Maquet, P. Role of the menisci in the distribution of stress in the knee. *Clin. Orthop. Relat. Res.* 290–4 (1984).
228. Fukubayashi, T. & Kurosawa, H. The contact area and pressure distribution pattern of the knee: A study of normal and osteoarthrotic knee joints. *Acta Orthop.* **51,** 871–879 (1980).
229. Allen, M. J., Houlton, J. E., Adams, S. B. & Rushton, N. The surgical anatomy of the stifle joint in sheep. *Vet. Surg.* **27,** 596–605 (1998).
230. Proffen, B. L., McElfresh, M., Fleming, B. C. & Murray, M. M. A comparative anatomical study of the human knee and six animal species. *Knee* **19,** 493–9 (2012).
231. Harris, M. L., Morberg, P., Bruce, W. J. M. & Walsh, W. R. An improved method for measuring tibiofemoral contact areas in total knee arthroplasty: A comparison of K-scan sensor and Fuji film. *J. Biomech.* **32,** 951–958 (1999).
232. Brimacombe, J. M., Wilson, D. R., Hodgson, A. J., Ho, K. C. T. & Anglin, C. Effect of Calibration Method on Tekscan Sensor Accuracy. *J. Biomech. Eng.* **131,** 34503 (2009).
233. Herregodts, S., Baets, P. De, Victor, J. & Verstraete, M. A. Use of Tekscan Pressure Sensors for Measuring Contact Pressures in the Human Knee Joint. 8–10
234. Taylor, W. R. *et al.* Tibio-femoral joint contact forces in sheep. *J. Biomech.* **39,** 791–798 (2006).
235. Tapper, J. E. *et al.* Dynamic in vivo kinematics of the intact ovine stifle joint. *J. Orthop. Res.* **24,** 782–92 (2006).
236. Darcy, S. P. *et al.* A comparison of passive flexion-extension to normal gait in the ovine stifle joint. *J. Biomech.* **41,** 854–860 (2008).
237. Taylor, W. R. *et al.* The medial-lateral force distribution in the ovine stifle joint during walking. *J. Orthop. Res.* **29,** 567–571 (2011).
238. Woodmass, J. M., Johnson, N. R., Levy, B. A., Stuart, M. J. & Krych, A. J. Lateral Meniscus Allograft Transplantation: The Bone Plug Technique. *Arthrosc. Tech.* (2017). doi:10.1016/j.eats.2017.04.016
239. Heckelsmiller, D. J. *et al.* Changes in Joint Contact Mechanics in a Large Quadrupedal Animal Model After Partial Meniscectomy and a Focal Cartilage Injury. *J. Biomech. Eng.* **139,** 54501 (2017).
240. Lee-Shee, N. K., Dickey, J. P. & Hurtig, B. Contact mechanics of the ovine stifle during simulated early stance in gait: An in vitro study using robotics. *Vet. Comp. Orthop. Traumatol.* **20,** 70–72 (2007).
241. Brophy, R. H. *et al.* Implantation of a synthetic meniscal scaffold improves joint contact mechanics in a partial meniscectomy cadaver model. *J. Biomed. Mater. Res. A* **92,** 1154–61 (2010).
242. Cottrell, J. M. *et al.* A new technique to measure the dynamic contact pressures on the Tibial Plateau. *J. Biomech.* **41,** 2324–2329 (2008).

243. Brophy, R. H., Zeltser, D., Wright, R. W. & Flanigan, D. Anterior cruciate ligament reconstruction and concomitant articular cartilage injury: incidence and treatment. *Arthroscopy* **26,** 112–20 (2010).
244. Rijk, P. C. Meniscal allograft transplantation - Part I: Background, results, graft selection and preservation, and surgical considerations. *Arthrosc. - J. Arthrosc. Relat. Surg.* **20,** 728–743 (2004).
245. Hede, A., Jensen, D. B., Blyme, P. & Sonne-Holm, S. Epidemiology of meniscal lesions in the knee. 1,215 open operations in Copenhagen 1982-84. *Acta Orthop. Scand.* **61,** 435–7 (1990).
246. Makris, E. a, Hadidi, P. & Athanasiou, K. a. The knee meniscus: structure-function, pathophysiology, current repair techniques, and prospects for regeneration. *Biomaterials* **32,** 7411–31 (2011).
247. Poehling, G. G., Ruch, D. S. & Chabon, S. J. The landscape of meniscal injuries. *Clin. Sports Med.* **9,** 539–49 (1990).
248. Khan, T. *et al.* ACL and meniscal injuries increase the risk of primary total knee replacement for osteoarthritis: a matched case-control study using the Clinical Practice Research Datalink (CPRD). *Br. J. Sports Med.* bjsports-2017-097762 (2018). doi:10.1136/bjsports-2017-097762
249. Mchenry, J. A. Nitric Ozide Production of Meniscal Explants Following Dynamic Compression. (Michigan Technological University, 2005).
250. Remley, K. Determining the Efficacy of Poloxamer 188 (P188) in Meniscal Damage Prevention. (2016).
251. ASTM. Standard Test Method for Cyclic Fatigue Testing of Metal Tibial Tray Components of. *Astm* **i,** 1–6 (2015).
252. Walker, P. S. *et al.* A knee simulating machine for performance evaluation of total knee replacements. *J. Biomech.* **30,** 83–9 (1997).
253. Desjardins, J. D., Walker, P. S., Haider, H. & Perry, J. The use of a force-controlled dynamic knee simulator to quantify the mechanical performance of total knee replacement designs during functional activity. *J. Biomech.* **33,** 1231–1242 (2000).
254. Burgess, I. C., Kolar, M., Cunningham, J. L. & Unsworth, A. Development of a six station knee wear simulator and preliminary wear results. *Proc. Inst. Mech. Eng. Part H J. Eng. Med.* **211,** 37–47 (1997).
255. Barnett, P. I. *et al.* Investigation of wear of knee prostheses in a new displacement/force-controlled simulator. *Proc. Inst. Mech. Eng. Part H J. Eng. Med.* **216,** 51–61 (2002).

APPENDIX A:
HALF MILLION CYCLICAL TESTING

A previously validated bioreactor was used to test the fatigue resistance of the SOS72 TPE hydrogel material[249]. Loading was performed in this custom validated bioreactor that was designed to allow simultaneous axial displacement of up to six samples while maintaining hydration. The system consisted of a linear actuator (Ultra Motion Bug) driven by a motor (SM1720 Ultramotion, Mattituck, NY) and equipped with a load transducer (1210AF-300, Interface, Inc. Scottsdale, AZ). Motor control was accomplished through a custom LabVIEW graphical user interface (GUI) [250].

Eighteen plugs of SOS72 were synthesized and melt pressed as previously described. After a 24hr swelling period, dimensions of the plugs were 5mm in nominal diameter with an average thickness of 2.9 ± 0.09mm. Samples were grouped by three for a total of n=6 groups and subjected to 500,000 continuous cycles at 12% strain and 1Hz. Periodically throughout the testing regime samples were rehydrated with phosphate buffered saline solution. Data were collected at two periods, the initial 1000 cycles and the final 1000 cycles (Figure A-1).

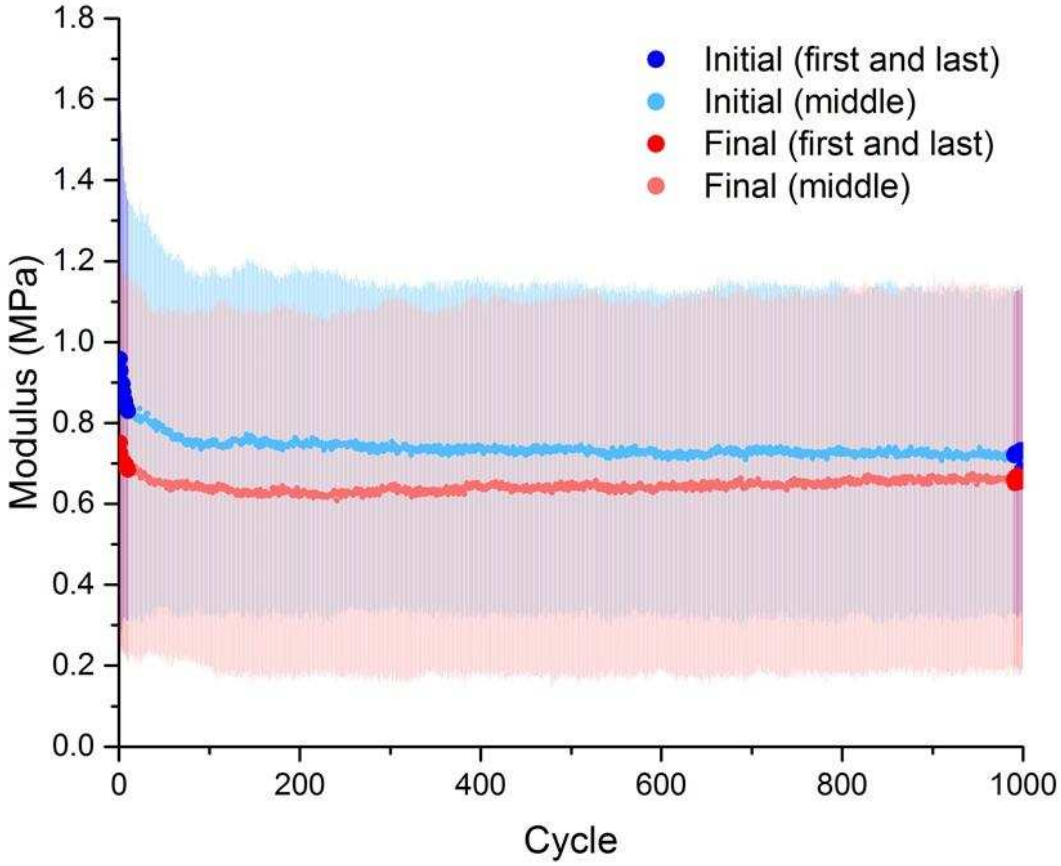

Figure A-1. Average and std of each of the 1000 cycle loading periods

For each individual period, the displacement and average force across the 3 samples were collected. Stress was calculated assuming constant contact area and strain was calculated from displacement and initial average thickness data. Elastic modulus was determined from a linear fit of the loading portion of the stress-strain data for each individual cycle for the entire 1,000 cycle period. The first and last 10 cycles from these periods were averaged for each set of samples for statistical analysis (Figure A-2).

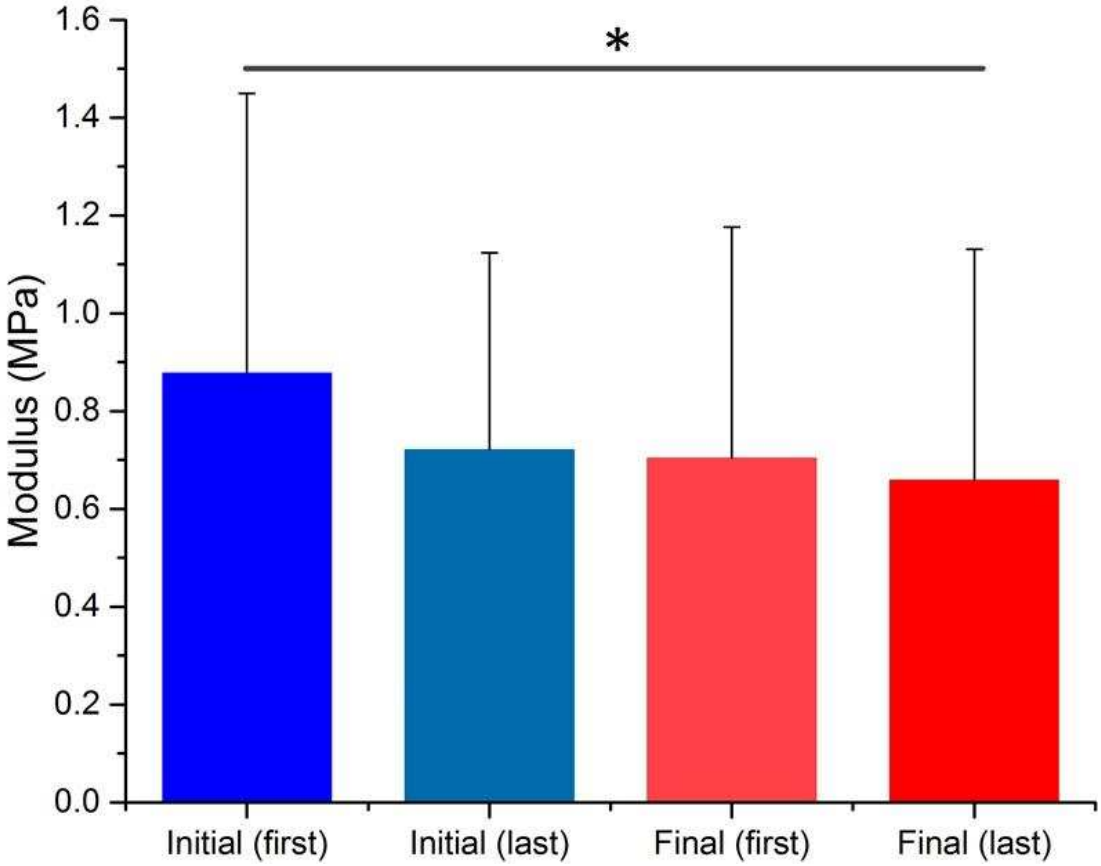

Figure A-2. Average and std for the first and last 10 cycles of the initial and final loading periods
* denotes significant difference

A paired t-test was performed to assess the difference between the first 10 cycles of the initial period and the last 10 cycles of the final period and a statistical difference ($p<0.05$) was found. However, no statistical differences were seen between the first 10 data cycles and the last 10 cycles from the first period or between the first 10 from the first period and the first 10 of the final period suggesting a slow relaxation of the TPE hydrogel. Likewise, no significant difference was seen between the first 10 and last 10 cycles of the final period. Across the 500,000 cycles, there was an average decrease in modulus of 26 ± 16%. This apparent decrease in modulus is likely a result of the inability of the material to recover 100% of its initial water content during the 0.5 seconds between max compression and reloading from the subsequent cycle.

Future work should focus on the wear resistance of the material in addition to extended fatigue. With an average step count of only approximately 5500 steps per day for many Americans[194], it is common for implants to undergo at least 1 million cycles for every year of simulated *in vivo* usage. Furthermore, standards which exist for components of a total knee replacement state a minimum of 10 million cycles should be performed to test resistance to failure[251]. Thus additional testing should consider a greater number of cycles for assessing both failure and wear. In addition to increasing the cycle count, future work should consider a more complex loading mechanism or knee simulator as has been previously done for total knee replacements to assess the wear of the construct rather than the fatigue of the bulk material[252–255]. While the current test provided valuable preliminary insight, the more complex loading regime will highlight the ability of the TPE hydrogel material to withstand conditions more mimetic of the native loading environment.